Surface chemistry of Burrup Rock art at the Yara monitoring sites September 2021

Report for Yara Pilbara Nitrates by CBG Solutions

Prepared by Dr Ian D MacLeod
Heritage Conservation Solutions

Version 1.7

15 December 2021

Figure 1: View of the TAN plant from site from site 22

Contents

Executive Summary

- Measurements in September 2021 were conducted on gabbro sites (7, 22 & 23) and granophyre sites (4, 5, 6 & 21) with the locations determined through the CSIRO monitoring program. Monitoring of the culturally significant Climbing Man site and of the adjacent split rock was also assessed.
- Replicate rock washing experiments were made at each site. Normally duplicate data sets agree to within a 5% range of soluble cations and anions.
- The surface pH and chloride and the redox voltages were measured at all sites and the Pourbaix plots (voltage vs. pH) confirmed the decay mechanisms are dominated by manganese solution chemistry and, in some cases, by iron solution equilibria.
- In contrast to 2020, half the fourteen rock washing data returned measurable concentrations of iron in solution. Sites 6, 7 & 22 continued to be below the iron detection limit.
- The colour difference between the engravings and the host rock correlated well with the minimum pH recorded in 2021.
- Sites 5, 7, 23 and the Climbing Man split rock gave no detectable boron, indicating no loss of chlorite. The mean concentration of boron in the wash solutions was 5.9 ± 0.1 x 10^{-7} M and was independent of the mean surface acidity. The ratio of chloride to boron indicated most of the boron comes from sea salts.
- The absence of major cyclonic rainfall events saw an accumulation of chloride salts on many of the exposed rock surfaces, with surface spot readings up to several hundred ppm. The solution washing data shows much lower concentrations at 2.1 ± 1.1 ppm at 11 of the duplicate eight sites. Sites 6, 21 and 23 had a mean chloride level of 44 ±10 ppm.
- The mean nitrate concentration in wash solutions in 2021 was higher at 0.31 ± 0.27 ppm than the 2021 value of 0.17 ± 0.10 ppm. The 2021 nitrate was approximately half the value of 0.7 ± 0.6 during 2017- 2019.
- There is a strong correlation between both the mean and the minimum pH, and the surface nitrate concentrations found on the rocks.
- The mean sulphate concentration for moderate to low chloride ion activity was 0.9 ±0.6 ppm. Three high sulphate sites (6, 21 & 23) showed correspondingly high chloride activity, all of which is controlled by deposition of sea salts.
- Most sites show uniform horizontal pH profiles across the rock surfaces. Acidity generally increases down the rock surface in response to higher levels of moisture and micronutrients.
- Data from the new ASD spectrophotometer readings are accessible through the CSIRO team at Kensington. The mineralogy of the surfaces is comparable to the earlier studies.
- Data from the Konica Minolta chromameter has been independently audited and reviewed by Australian Microfading Services.

Background

To comply with the regulations concerning retention of its operating licence, EPBC 2008/4546, Yara Pilbara Nitrates engaged CGB Solutions to develop appropriate methodologies to conduct colour monitoring measurements on the six sites surrounding the ammonia and ammonium nitrate plants in the Burrup. The lead consultant (Warren Fish) conducted meetings with the management team from Yara to develop the timetable and to engage with key community members of the Murujuga Aboriginal Corporation for permission to come to country in September 2021 to repeat the colour measurements done in previous years by the CSIRO team. A training refamiliarization session was undertaken by MacLeod with Dr Ian Lau, of CSIRO Kensington, to ensure that the spectral and colour measurements would be compliant and would provide relevant data for the assessment of the condition of the rock engravings. MacLeod retired from the Western Australian Museum in 2016 and is now the Principal of Heritage Conservation Solutions and has published peer-reviewed papers on the conservation of Aboriginal rock art and has 40-years' experience in materials conservation (Appendix I).

During the first phase (2003-2004) of research into the condition of the rock surfaces in the Burrup, several engraved rocks in the "Museum Compound" were examined regarding their acidity (as measured with a surface pH electrode), water-soluble minerals on the rock surfaces and the microbiological activity. Samples of the rock surface were swabbed with sterile culture material and placed into prepared phials. The biological material was stored at zero degrees before being taken to laboratories in Perth (Department of Agriculture) for characterisation. Other reference measurements were conducted on Gidley and Dolphin Islands in the Dampier Archipelago to act as reference points away from industrial activities associated with the Woodside gas plant and iron ore shipping out of Dampier ports.

Analysis of the solution chemistry collected between 2003 and 2004 provided strong indications of a possible link between the amount of nitrate on the rocks and the level of microbiological activity. The acidic metabolites from the organisms appeared to be contributing to the overall acidification of the rock surfaces and mobilisation of key minerals containing both iron and manganese, as well as copper and nickel. To assess any potential impacts that emissions from the Pilbara Nitrates plant might have, solution sampling on the rock surfaces on the six CSIRO approved sites within the 2 km radius of the Pilbara Nitrates plant were conducted. The rock irrigation data was done in conjunction with surface measurements of the pH, chloride ion activity and the redox potential of the rock surfaces at the same locations. The wash solutions were analysed for sulphate, sulphite, nitrate, and nitrite ions, ammonia and ammonium ions as well as for a wide range of metal cations. The electrical conductivity of the wash solutions was also measured as a guide to the overall nature of the soluble minerals and salts that were mobilised during the five minutes of sample collection.

Field work was conducted on the six monitoring stations around the Yara plant in September 2021 and at the additional site 4, which is close to the service road near the Woodside old flare tower. This report includes commentary on the interpretation of the colour measurements from the Konica Minolta Chromameter. The Yara sites were part of the CSIRO colour and mineralogy monitoring of the Burrup that has been undergoing continuous evaluation for the past 15 years. In addition to conducting the required ASD spectrophotometer readings, used to determine the mineralogy of the rock surfaces and that of the associated engravings, and the chromameter measurements, a series of pH, chloride and redox potential readings were taken directly on the rocks themselves or at sites adjacent to the CSIRO monitoring points. In the light of operational complexities in 2020 with the original machine, the new ASD spectrophotometer and driving laptop were taken in 2021 and worked seamlessly. Data from the flat surface pH, chloride electrodes and redox potentials was combined with analyses from distilled water irrigation of the rocks. These analyses included all metal ions and chloride, nitrate, nitrite, oxalate, and sulphate anions. The refrigerated samples were

stored off site until they were transported by air to the Bentley based laboratories of the ChemCentre for independent NATA accredited chemical analyses.

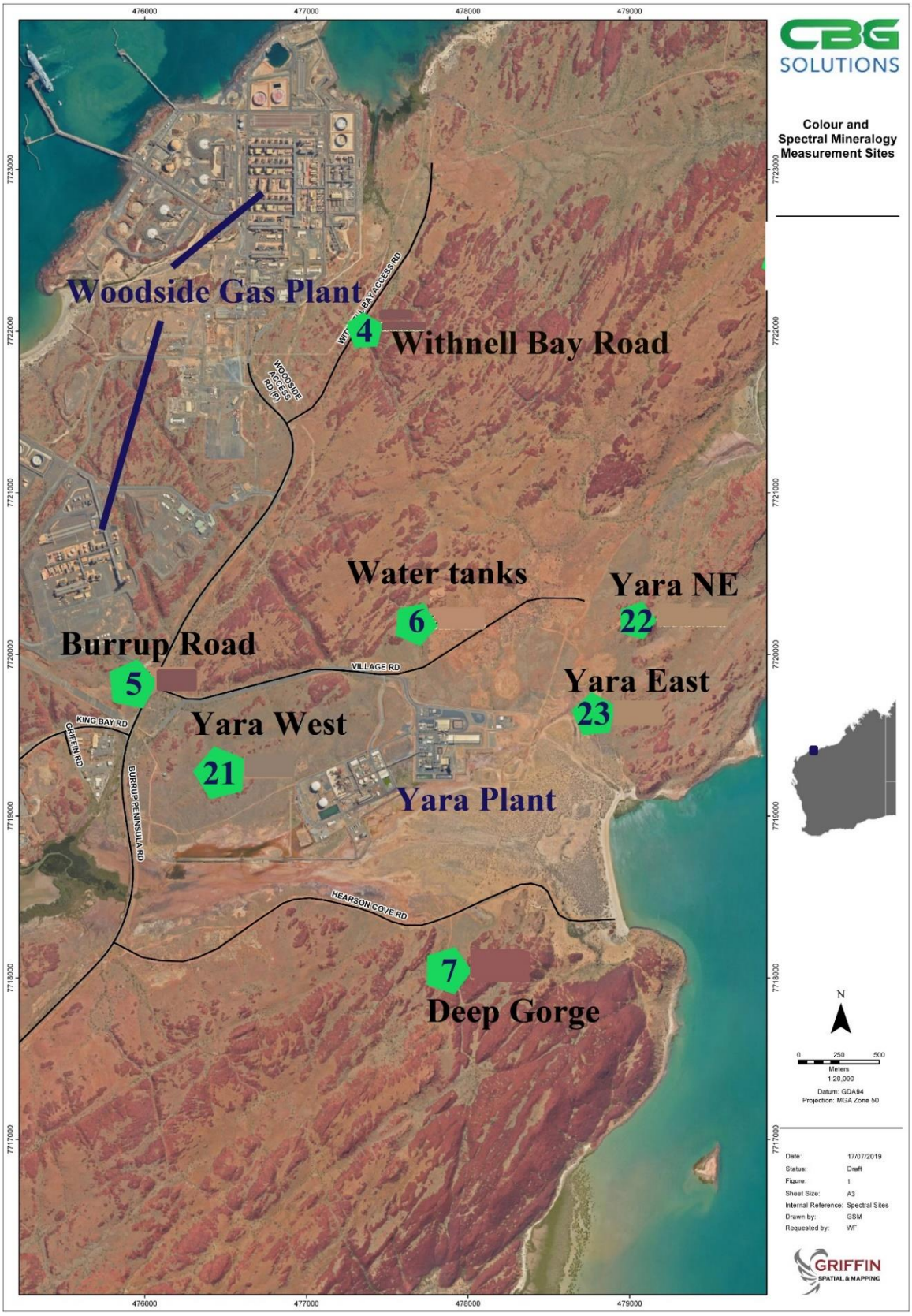

Figure 2: View of the main Yara monitoring points in the Burrup peninsular

This report examines in detail the solution chemistry and provides a synthesis on the historical data relating to two sets of solution and surface pH measurements conducted in 16-17 years before the present work was conducted. The Yara referenced sites of interest included granophyre at the Burrup Road (5), the Water Tanks (6) and Yara West (21) sites, while gabbro rocks were found on sites at Deep Gorge (7), Yara North East (22) and Yara East (23). All these sites lie within a 2 km radius of the present operational sites of the ammonia plant and the Technical Ammonium Nitrate (TAN) site. The additional site that was chemically assessed was number 4, adjacent to the Woodside plant about two hundred metres from the flare tower (see Figure 2). Apart from the CSIRO colour coded and recorded sites, the split rock adjacent to the Climbing Man in the eponymously named gully, at the head of which site 4 is located, was also recorded for comparative purposes.

Measurement of pH and chloride activity and redox potentials

The pH and chloride ion measurements taken on rocks adjacent to the CSIRO reference engraved sites in cases where concern was held regarding potential impact of the pH, chloride, and redox measurements. Other than for sites 6, 7 all measurements were done directly on the CSIRO rocks. The pH data was recorded using a flat surface pH electrode which had been calibrated each morning using standard pH buffers at pH 4 and pH 7 before the field measurements commenced. The pH meter was temperature compensated using a thermocouple connected to the TPS Aqua pH meter (pH/ORP/^{o}C) and the glass electrode was a VWR model no W7567287. Readings of the surface pH were standardised by recording the values after an elapsed interval of one minute. If the surface was more responsive and the pH reading stabilised in 40 seconds, then that value was recorded and keeping the probe in position did not alter the steady value that had been noted. Owing to the porous nature of the rock substrate prolonged equilibration times can result in pH values that are not reflective of the local microenvironment. A small amount of water is needed to keep the bulb wet and the solution in contact with the internal reference electrode. The electrical circuit of the pH electrode is completed through connecting the internal Ag/AgCl reference electrode through two fine wicks which are situated at 180^{o} to each other on either side of the glass membrane and held in place by the soft plastic ring fitting inside the 12-mm external diameter solid epoxy body.

The chloride ion activity was measured using a TPS WP-90 ion-pH-mV-^{o}C meter coupled with an Orion Thermo 1609-186881 chloride ion specific electrode. The rocks were wetted with two drops (0.08 ml) of a 0.05 molar sodium nitrate solution to provide an electrolyte to stabilise the liquid junction between the sensing head and the rock surface. Stable readings of the chloride activity were obtained within a minute. The electrode was calibrated daily with a 1,000 and a 100-ppm chloride reference solution before any field measurements were made.

The redox potential or voltage was recorded with a high impedance digital voltmeter, Testo 760-2 TRMS Multimeter on the auto ranging DC voltage setting. A sponge rubber pad had a cross cut in the surface through which the 2 mm od platinum electrode protruded and a TPS single junction AgCl reference electrode, filled with a gel based 3 M KCl solution to connect the internal salt bridge, was placed alongside the platinum electrode. The reference electrode (TPS 1808-246960) was calibrated at +0.210 mV vs. the standard hydrogen electrode using a saturated quinhydrone solution in a pH 4.0 buffer solution. The reference electrode voltage was regularly checked and remained stable for the duration of the measurement season.

Analysis of sea borne salts on the rocks

The amounts of surface chloride detected on the rock surfaces provide direct evidence of the impact of the marine environment and indicate that salt weathering of rocks, with extensive dehydration and rehydration cycles plays a significant role in the local environment. The wash solutions from the rock surfaces showed up a range of ions commonly associated with sea water, namely Na^{+}, K^{+}, Mg^{2+}, Ca^{2+}, Cl^{-} and SO_4^{2-}. Analysis of the way in which the concentrations varied across the Burrup was

consistent with known weather patterns of prevailing winds and proximity to the sea. Another noticeable factor is the location of the reference washing rocks in terms of being in a wind-shadow of larger rocks, which protect the surfaces from significant salt deposition. When the wash concentrations of sulphate are plotted as a function of the chloride, most of the data follow a linear relation that reflects the common ratios of the anions that are found in seawater. Data from the most recent irrigation experiments obtained in September 2021 is shown in Table 1. When significant differences from the normal ratios found in seawater are recorded for rock surfaces in the Burrup, these can be explained in terms of specific interaction of electrolytes with the surface minerals found on the rocks. Examples of this type of interaction are when higher ratios of $\{^{Cl}/_{SO4}\}$ are due to specific interaction of sulphate ions with calcareous microfossils, leading to loss of sulphate through the formation of gypsum, $CaSO_4.2H_2O$.

The microenvironment of the rocks was assessed through a combination of surface chloride (Orion Thermo combination Cl electrode) and surface pH (WVR flat electrode) measurements on the rock surfaces. The first round of measurements was made using a 0.05 M $NaNO_3$ solution in distilled water electrolyte was used for chloride measurements and the pH was recorded after equilibration with two to three drops (0.04-0.06 ml) of distilled water on the rock surface. The Chemistry Centre of WA determined the soluble nitrate, nitrite, sulphate, chloride, oxalate concentrations on the rock surfaces by ion chromatography from the distilled water washings which covered a 200 cm^2 area. Metal ions in the wash solutions were determined by inductively coupled plasma–mass spectrometric (ICP–MS) methods. This study is based on an initial survey in June 2003 (winter) of relocated engraved rocks which was then extended in August 2003 (spring) to include several sites located at a distance from known emission sources was concluded in February 2004 (summer) with repeated measurements on the Burrup.

Table 1: Ratio of salts in sea water and in the rock washings around the Yara plant

	Rock	Cl^-/Na^+	Cl^-/SO_4^{2-}	Cl^-/Ca^{2+}	Ca^{2+}/K^+	Ca^{2+}/Ba^{2+}	Mg^{2+}/Ca^2	Na^+/K^+
Sea water		**1.8**	**7.1**	**47**	**1**	**8,000**	**3.1**	**27**
Site 4 a	Granophyre	1.1	2.5	4.7	2.3	184	0.14	10
Site 4 b		3.5	9.3	9.3	0.8	375	Mg^{2+} BDL	2
Site 5 a	Granophyre	1.7	4.6	11.5	1	191	0.5	6.8
Site 5 b		1	1.9	1.2	3.3	765	Mg^{2+} BDL	3.8
Site 6 a	Granophyre	25.8	2.4	123	0.7	400	0.5	3.2
Site 6 b		2.3	2.3	8.3	3	300	0.33	11
Site 7a	Gabbro	1.4	2.7	4.5	0.9	500	0.33	2.9
Site 7b		1.8	2.3	4.7	1	333	Mg^{2+} BDL	2.7
Site 21 a	Granophyre	1.3	3.4	5.4	2.5	345	0.2	10.8
Site 21 b		3.5	3.4	15	3.7	250	0.5	15.2
Site 22 a	Gabbro	0.6	6.5	4.3	0.2	231	0.67	1.4
Site 22 b		0.8	3.3	2.6	1	312	0.2	3.2
Site 23 a	Gabbro	0.8	2.6	3.3	1.3	333	Mg^{2+} BDL	5.3
Site 23 b		22.2	3.3	64	2	444	0.25	5.8
CMs a*	Granophyre	6.2	4.2	6.6	2.8	518	0.14	3
CMs b		0.7	2.7	2	0.8	364	Mg^{2+} BDL	2.4

*CMs relates to the large split rock, approximately 3 metres to the left of the main Climbing Man panel. BDL: below detection limit of 0.1 ppm.

Data obtained for the 2017-2021 measurements for cations measurements were made on 200 ml samples and anions in 200 ml sample bottles collected over an area of approximately 500 cm^2. The main difference in the data collection method was that for the second time, two adjacent rocks were washed with ultra-pure water to test the reproducibility of the measurements. The results of the general test of electrical conductivity of the wash solutions, gave agreement within the range of ± 5% of the values, which is remarkably close agreement (Appendix III). Where the deviations on specific anions and cations were noted, the differences were understood in terms of the local microenvironment of the rock e.g., if it was more exposed or sheltered than the other one tested.
Studies by the CSIRO mineralogy team have shown that one of the common weathering minerals from both the gabbro and the granophyre rocks is kaolinite, $Al_2Si_2O_5(OH)_4$ and many other clay-like minerals. The only sites with measurable aluminium ions in the washing solutions were at the granophyre sites 4 and at the Climbing Man split rock and at site 5.

Ratios of chloride to sodium

Very high $\{^{Cl}/_{Na}\}$ ratios of 24.0 ±2.6, compared with the expected sea salt value of 1.8 were reported on one of the rocks at site 6 and at site 23. In both cases the high chloride to sodium ratios are associated with a mean chloride level of 50± 1 ppm in the washings. On site 23 the high chloride ratio test site was 8.5 metres further west up the gully and the "normal" ratio site at rock "b" was 40 cm distant from test rock "a". One area of the measured surface chloride activity on CSIRO rock 23 was very high, with a maximum of 161 ppm on the bottom row and at the mid-point. The least salty part of site 23 gave a chloride reading of 28 ppm on the second row of measurements towards the more sheltered left-hand side. Inspection of the rock at a raking angle showed up sparkles of halite (NaCl crystals) on the surface. A comparable situation occurred at site 6, the water tanks, where the reference rocks were within 40 cm of each other but the site with the high chloride activity (rock 6a) was associated with a natural depression in the rock. A similar surface topography describes reference rock 23b and so there appears to be specific adsorption phenomena associated with these weathered rocks, in which sodium cations are absorbed through an ion-exchange process. Future monitoring measurements will avoid rocks with this topography, to get a more representative surface that better reflects the nature of the engraved surfaces, rather than consideration of the ease of collecting the washing samples. Fourteen other samples which had gentle sloping and easy drainage surface topographies, the mean $\{^{Cl}/_{Na}\}$ ratio was 2.9 ± 2.4 for the balance of the washed rocks.

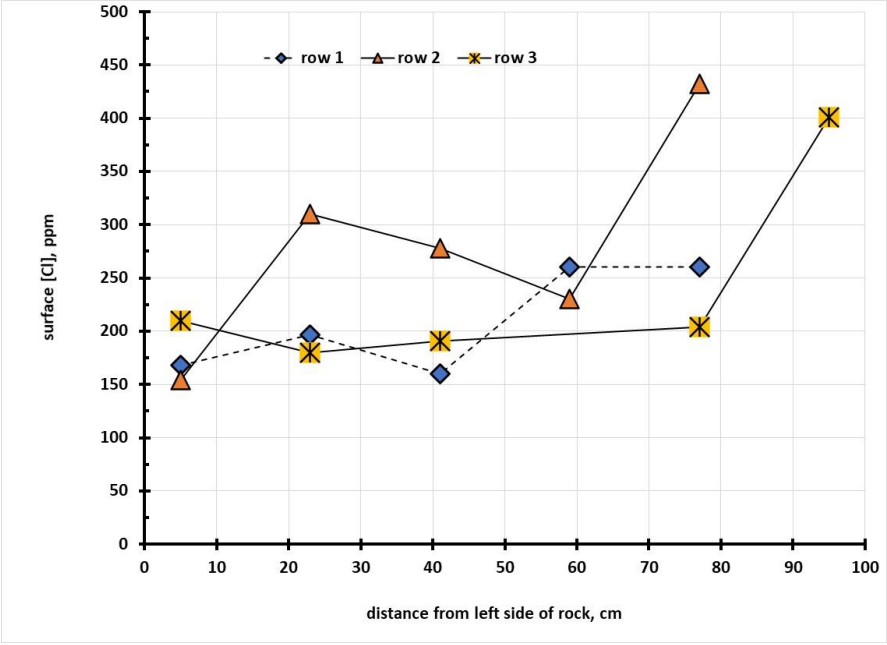

Figure 3: Chloride distribution plot along the x-axis of site 6, moving from left to right

Site 6 showed an extreme example of how the wind shadow areas of the monitoring rock surfaces can reflect the impact of wind-borne sea salt deposition. In moving from the left side of the rock towards the sheltered end, the chloride ion concentration increased, as seen schematically in Figure 3 and in the image of the rock itself in Figure 4. The shadow of the higher rocks to the right-hand side of the measurement sites creates a microenvironment where accumulation of salts occurs because of the combination of being in a wind and sunshine shadow from the prevailing westerly direction up the gully, from whence the wind-borne sea salts come to land on the site and increase the surface alkalinity.

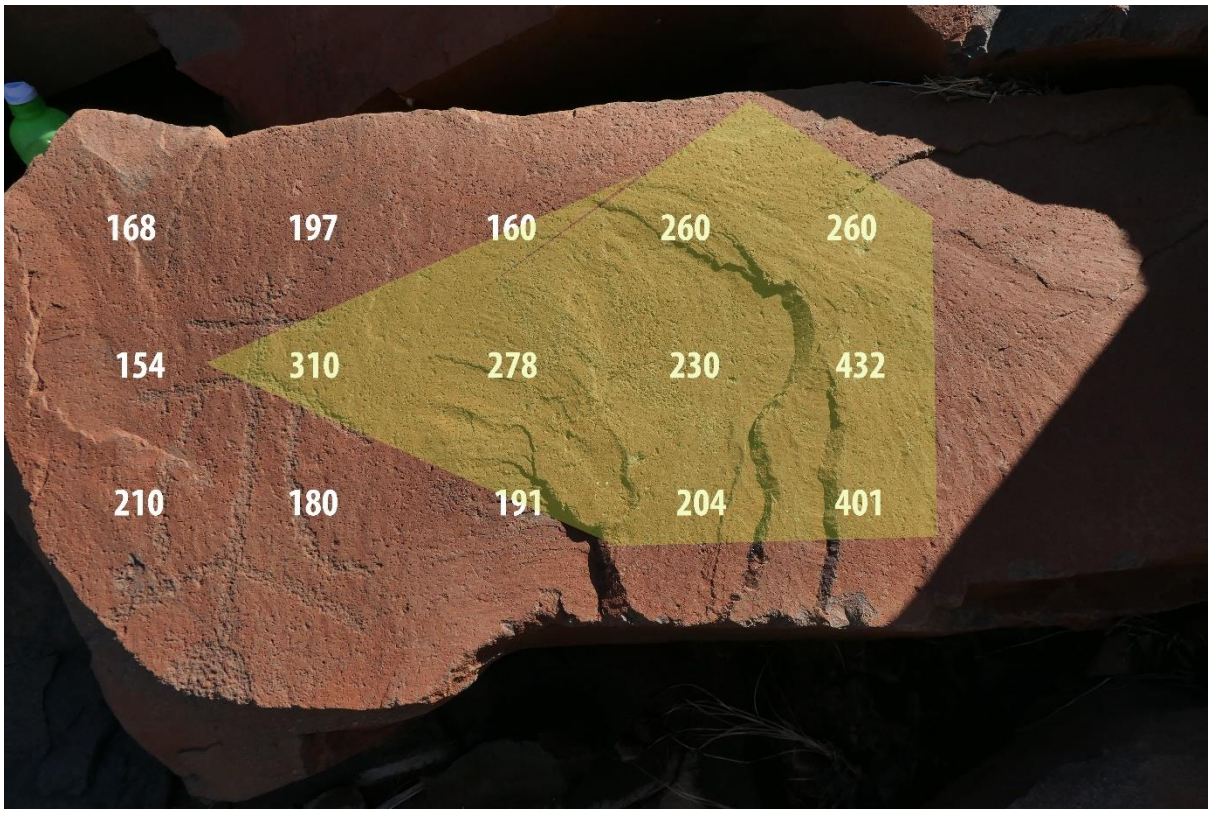

Figure 4: Site 6 surface Cl^- readings (ppm) and effect of the green wind shadow

Ratios of chloride to sulphate

The normal analytical ratio of chloride ions to sulphate in 36 ppt sea water is 7.1 (Table 1) and this ratio was approached at site 4 rock "b", and site 5 "a" along with site 22 "a" on top of the ridge, which is exposed to ocean breezes and for these the mean ratio $\{^{Cl}/_{SO4}\}$ was 6.8 ± 2.4 – halite crystals could be seen sparkling in the sun on all the above sites. For all the other rocks the $\{^{Cl}/_{SO4}\}$ ratio was 3.0 ± 0.6 which indicates that there is more than twice as much sulphate present as would be expected for the oxyanion coming from maritime salt spray. Site 4 is close to the flare tower of the NW Shelf gas plant, site 5 is close to the Pluto flare tower, site 6 is in the lee of the hills behind the old Woodside gas plant and site 7 is exposed to emissions from the Woodside plant. In general, there appears to be elevated sulphate on the rocks in many of the monitoring sites.

The mean concentration of sulphate in the wash solutions covered sites 4, 5, 6 b, 7, 21a, 22, 23a and at the Climbing Man site and was 0.87 ± 0.59 ppm, which is an indication that for these rocks there was not much sulphate present. However, for sites 6a, 21b and 23b the mean sulphate concentration was 15.0 ± 5.5 ppm which is significantly higher than those found on the other sampling sites. There has been little focus in the past decade on the potential impact of sulphates on

the acidification of the Burrup rock art sites, as the main interrogation has been on the concentration of soluble nitrates, which are a primary determinant in the overall biologically controlled deterioration of rock surfaces. To assess any potential impact of the sulphate on the acidification of the sites, a plot of the minimum pH on the monitoring sites was made against the measured sulphate in the wash solutions. Just as the mechanisms of adsorption of NO_x and SO_x onto the moistened rock surfaces are yet to be unequivocally established, the presence of a direct relationship between the concentration of sulphate in the wash solutions with the underlying acidity can be regarded as a de-facto correlation.

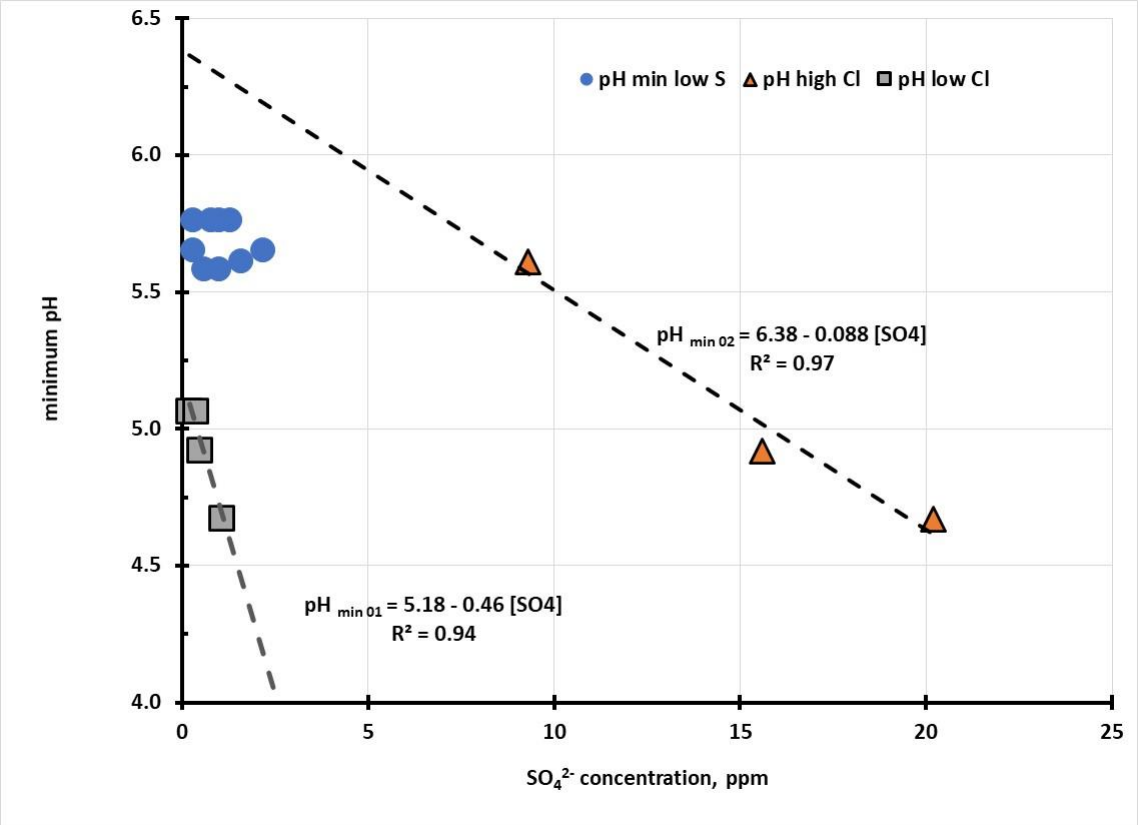

Figure 5: Plot of minimum pH with sulphate concentration on the rocks

The data can be conveniently split into the pH for high chloride ion activities and those for low saltiness of the washed rocks. The regression line for the high salt background materials gave Equation 1, viz.,

$$pH_{min\ 02} = 6.38 - 0.088\ [SO_4^{2-}] \quad \text{.....(1)}$$

For this regression analysis the R^2 was 0.97 and the intercept value was 6.38 ± 0.24 pH, which is typical of the alkaline nature of rock surfaces heavily "contaminated" with sea salt. In the presence of significant chloride concentration, it takes 11.4 ± 0.5 ppm of sulphate to bring about a pH change of one or a ten-fold increase in acidity. The pH_{min} sensitivity or slope was -0.088 ± 0.015 pH/ppm SO_4^{2-}. For the lower chloride rocks the pH intercept at zero sulphate was 5.18 ± 0.05 and the regression equation no 2 had an R^2 of 0.94,

$$pH_{min\ 01} = 5.18 - 0.46\ [SO_4^{2-}] \quad \text{.....(2)}$$

The minimum pH at zero sulphate is typical of the natural range of pH of the Burrup rocks in the absence of specific microbial activity. The reason why the second equation has just over five times the sensitivity to sulphate is simply due to the much lower buffer capacity of the salt solutions to acidic metabolites when bacteria are utilising sulphate as an energy source. The five other sites that show no clear relationship of pH with sulphate ion concentration in the range 0.3-2.2 ppm had a

mean pH_{min} of 5.68 ± 0.08 and for these sites there appears to be no specific response by the microflora to the presence of sulphate ions.

Ratio of chloride to calcium

For all but two of the 16 rock washing samples the mean $\{^{Cl}/_{Ca}\}$ ratio was 5.9 ± 3.8 which is very much lower than the ratio found in sea water, which is 47 times, owing to the lower solubility of calcium in sea water due to the balance between the pH and sulphate causing common-ion effects which enhance precipitation of calcium carbonates in the marine environment. The $\{^{Cl}/_{Ca}\}$ ratio was 123 for rock 6"a" and 64 for rock 23"b" and these two sites had very similar quite high chloride washing concentrations of 49 ppm and 51 ppm respectively. A more detailed analysis of the $\{^{Cl}/_{Ca}\}$ ratios shows that they are quite different for gabbro with a mean value of 3.9 ± 0.9 while the value of $\{^{Cl}/_{Ca}\}$ for the granophyre rock sites was 7.1 ± 4.4, which is consistent with the much higher calcium content of the gabbro rock crust, 10.9±1.9% CaO lowering the $\{^{Cl}/_{Ca}\}$ ratio from 7.1 to 3.9. It is noted that the granophyre crust has 1.4±0.8 % CaO (Ramanaidou and Fonteneau, 2017)

Ratio of calcium to potassium

In normal sea water the ratio of $\{^{Ca}/_{K}\}$ is 1:1 and this was observed for all three gabbro sites (7, 22 & 23) where the mean value of $\{^{Ca}/_{K}\}$ was 1.1 ± 0.6, with the high calcium oxide concentration in the gabbro rocks providing a form of buffering for the balance between potassium and calcium, which will be key elements for maintaining the health of the microflora living on the rock surfaces. For the five granophyre sites the $\{^{Ca}/_{K}\}$ ratio was 1.2 ± 1.1 but for sites 4a, 5b, 6b and the Climbing Man "a" rock the mean value was 2.9 ± 0.4; for these sites a possible reason behind the elevated of $\{^{Ca}/_{K}\}$ value is the low potassium levels found on these reference washing rocks, as the values are close to the limit of detection. Thus, there is no hidden or sinister reason why half of the granophyre rocks had apparently elevated of $\{^{Ca}/_{K}\}$ ratios.

Ratio of calcium to barium

The low solubility of barium in seawater is due to their relative abundances in the earth's crust underlying the oceans. All the washings from the Burrup rock art sites showed $\{^{Ca}/_{Ba}\}$ significantly depressed ratios, compared with the sea water value of 8,000. Inspection of the concentrations of calcium show normal values and so the twenty-fold drop in the ratio is a strong indicator of mobilisation of barium minerals from the rock surface are the reason for the change. The mean gabbro ratio for $\{^{Ca}/_{Ba}\}$ was 359 ± 97 while the granophyre rocks showed a higher standard deviation of the mean value of 369 ± 172. The lower background concentration of calcium in granophyre rocks means that there will be more random variations in their distribution across the weathered rock surfaces. Plots of $p[Ba^{2+}]$ against the mean surface pH showed no systematic trend, which indicates that the surface mineralogy of barium does not contain significant concentrations of barium oxide. In a similar vein, plots of $p[Ca^{2+}]$ against the mean pH of the eight sites studied showed no response of solubility with the range of mean pH values observed on the sites. The mean barium concentration in the wash solutions was 1.7×10^{-8} M which, when combined with the mean sulphate concentration of 7.3×10^{-5} M, gave a mean ionic product of 1.2×10^{-12} which is below the solubility product of 1.1×10^{-10}, which is why the data for sites 4, 6, 21 and Climbing Man (all granophyre sites) showed a steady decrease in the concentration of free barium with increasing sulphate concentration in the wash solution.

Ratio of magnesium to calcium

The maximum magnesium in the wash solutions was at the granophyre site 21 "b" at 1.1 ppm which is associated with the high chloride salt levels and so can be seen as just a reflection on the higher sea salt surface concentration. With the mean $\{^{Mg}/_{Ca}\}$ ratio for the gabbro rocks was 0.36 ± 0.21 being statistically identical with the granophyre ratio of 0.34 ± 0.17 this ratio is not able to discriminate between the surface chemistry of the gabbro and granophyre rocks. The mean value of

the $\{^{Mg}/_{Ca}\}$ ratio for all the Burrup rocks of 0.35 ± 0.17 is nine times less than the ratio found in seawater and this is just a reflection of the average calcium content of the host gabbro and granophyre rocks.

Ratio of sodium to potassium

The mean ratio of $\{^{Na}/_{K}\}$ for the 16 washing samples was 5.6 ± 4.1 or roughly one-fifth of the ratios found in normal seawater. This is consistent with the weathered crusts on the rock containing minerals with a high potassium content, rather than being due to a decreased sodium content. The ratios showed some differentiation with rock type but the differences in the mean values of the gabbro rock at $\{^{Na}/_{K}\}$ of 3.5 ± 1.7 and those of the granophyre cohort at 6.8 ± 4.6 were not statistically significant as the scatter of the data for the latter rock type was larger than the difference between the two mean values.

Environmental monitoring by Yara at weather stations

In conjunction with its normal environmental procedures Yara has three environmental monitoring stations at Burrup Road (site 5), the Water Tanks (site 6) and at Deep Gorge (site 7) for which data on the nature of the electrolytes and the pH of rainfall is recorded (Figure 6). The water is analysed for nitrite, nitrate, chloride, and sulphate, among other species and traditional variable such as hardness, which acts as an indicator of contributions from sea salts.

Figure 6: Location of the environmental monitoring stations around Yara plants

Key observations from the five sets of records for the water tanks (site 6) and Deep Gorge (site 7) but no rainfall was recorded at site 5 for the whole period of the monitoring locations between January and June 2021 – there is no data available for the period of June to September 2021 as there has been no rainfall events during that time. Site 5 seems to be regularly in a rain shadow area.

Rainwater at the Water Tanks, site 6

For the water tanks site, which was noted for the very high salt deposition areas in the wind shadow created by adjacent rocks, the pH of the rain water was linearly dependent on the sodium concentration, as shown in Equation 3.

$$^{\text{site 6: Na}}\text{pH}_{\text{rain}} = 6.29 + 0.19\ [Na^+]_{\text{ppm}} \quad (3)$$

The intercept value is within the range of normal CO_2 saturated water at a value of 6.29± 0.10 and the slope of equation 3 i.e., the pH dependence on the sodium ion concentration, was 0.19 ± 0.08 which is steeper than in 2020. There were only three points on the regression line (R^2 0.83) so not too much can be read into the specific slope and intercept values.

There was a simple relationship between the pH of the rainfall and the amount of nitrate in the rain, as shown in equation 4. The slope or pH dependence on the nitrate concentration was 1.98 ± 0.45 pH/ppm [NO_3] and not unexpectedly, the intercept pH was 0.5 greater than for the sodium dependence value of pH.

$$^{\text{site 6: NO3}}\text{pH}_{\text{rain}} = 6.78 - 1.98\ [NO_3^-]_{\text{ppm}} \quad \text{.....(4)}$$

The regression equation had an R^2 value of 0.91 and the associated errors with the intercept are ± 0.10 and the slope is ± 0.45, which represent errors of 1.4% and 22.8% respectively. The air monitoring station data showed that there was a 1:1 equivalence of the NO_x in the air which was converted into NO_3^- soluble nitrate in solution.

The environmental monitoring also reports the total nitrogen content, as determined by the Kjeldahl method (TK), which includes all forms of nitrogen (organic and inorganic) and for the Water Tanks site the regression analysis (equation 5) had an R^2 of 0.88 and the intercept was 6.76 ± 0.11, which is the same as for plots of pH with just nitrate, as shown by equation 4.

$$^{\text{site 6: N\_TK}}\text{pH}_{\text{rain}} = 6.76 - 1.36\ [N_{\text{total K}}]_{\text{ppm}} \quad \text{.....(5)}$$

Using data on the organic and inorganic nitrogen contents of the rain showed less of a pH dependence than with the nitrate alone as the slope was -1.36 ± 0.36 which is not statistically significant, owing to the relative scatter of data.

Although there was no reported SO_x levels, the sulphate concentration was plotted against the pH of the rain water and the three data points showed a linear decrease in pH with increasing sulphate ion concentration, as shown in Equation 6, for which the R^2 was 0.96, with errors of ± 0.12 in the intercept and ± 0.43 in the slope of equation 6,

$$^{\text{site 6: SO4}}\text{pH}_{\text{rain}} = 7.00 - 2.25\ [SO_4^{-2}]_{\text{ppm}} \quad \text{.....(6)}$$

The slopes of equations 4 and 6 were experimentally the same but in the absence of data on gaseous sulphur oxides it is not possible to draw any more conclusions. However, there are indications that the presence of sulphates does contribute to the acidity of the rainfall.

Rainwater at Deep Gorge, site 7

The 2021 data came from the relocated monitoring station at Deep Gorge, which is now on the other side of the ridge and closer to Hearson's Cove. To provide a comparison of the saltiness of the rainfall at site 6 with site 7, the pH of the rain was plotted against the sodium ion concentration, to provide the regression equation no 7, for which the R^2 was 0.96.

$$^{\text{site 7: Na}}\text{pH}_{\text{rain}} = 6.68 + 0.19\ [Na^+]_{\text{ppm}} \quad \text{.....(7)}$$

The same slope of 0.19 ± 0.03 pH/ppm Na^+ was found as at site 6, but the intercept was more alkaline at a pH value of 6.68 ± 0.08, compared with 6.29 for site 6. The more alkaline intercept value of the pH is due to the higher bicarbonate concentration in the rain water at site 7 (5.3 ppm HCO_3^-) compared with site 6 (3.5 ppm HCO_3^-).

There was a linear relationship between the pH of the rainfall and the amount of nitrate in the rain, as shown in equation 8, which had an R^2 value of 0.91, which indicates a good fit. The slope or pH dependence on the nitrate concentration was 3.29 ± 0.51 pH/ppm [NO_3] and the intercept pH was 6.67 ± 0.11 greater than for the sodium dependence value of pH.

$$^{\text{site 7: NO3}}\text{pH}_{\text{rain}} = 6.67 - 3.29\ [NO_3^-]_{\text{ppm}} \quad \text{.....(8)}$$

The intercept pH (the rainfall pH at zero nitrate concentration) was the same as found for the Water Tanks site 6 location. The mean concentration of sulphate in the rain water at Deep Gorge was 0.50 ppm which is higher than at site 6, where the mean value was 0.27 ppm. The higher concentration of sulphate at site 7 is consistent with the apparent greater sensitivity of the rain water pH to the nitrate concentration i.e., the slope $\{^{site\ 7}/_{site\ 6}\}$ ratio was 1.7 and the sulphate concentration ratios were 1.8, which indicates a strong connection between the two anions and the observed pH sensitivity. The air monitoring station data showed the same 1:1 equivalence of the NO_x in the air which was converted into NO_3^- soluble nitrate in solution on site 7 as initially observed at site 6.

The environmental monitoring also reports the total nitrogen content, as determined by the Kjeldahl method (TK), which includes all forms of nitrogen (organic and inorganic) and for the Deep Gorge site the regression analysis had an R^2 of 0.99 and the intercept was 6.42 ± 0.03, which is the same as for plots of pH with just nitrate, as shown by equation 4.

$$^{site\ 7:\ N\_TK}pH_{\ rain} = 6.42 - 2.02\ [N_{\ total\ K}]_{\ ppm} \quad \text{.....(9)}$$

Using data on the organic and inorganic nitrogen contents of the rain showed less of a pH dependence than with the nitrate alone as the slope was -2.02 ± 0.11 and the two slopes are statistically significantly different. For both site 6 and site 7 the dependence of pH on the total nitrogen is approximately 60% of the straight inorganic nitrate concentrations.

Although the direct influence of sulphate ions on the rainwater pH cannot be readily separated as to what is a sea salt contribution and what may have been derived from adsorption processes converting SO_x into SO_4^{2-} ions

$$^{site\ 7:\ SO4}pH_{\ rain} = 6.50 - 0.76\ [SO_4^{-2}]_{\ ppm} \quad \text{.....(10)}$$

The closeness of the fit of pH with the sulphate concentration was not as good as at site 6, with an R^2 value of 0.89 and so the slope had an error of ± 0.19 or 25% which is still significantly different to the slope of the pH with sulphate found on site 6. The intercept value for equation 10 was 6.50± 0.12 which is more acidic than the 7.00 value for site 6 and this is consistent with site 10 having a higher mean sulphate concentration.

Production management and site integrity improvements have had their impact on the amount of ammonia being found in the rainwater at the air monitoring sites. The only recorded NH_3 concentration was 0.1 ppm in week 9 at the Water Tanks site and 0.37 ppm NH_3 at Deep Gorge. The differences between the two sites may be due to the direction of the prevailing wind. It was noted that in 2018 only site 7 may have been affected by an accidental loss of ammonia or other industrial emissions in the airshed.

The background NO_x emissions are around 15 mg/m^3 from the plant while the package boiler contributes between 170-90 mg/m^3. Site 6 is 1.1 km from the main plants while sites 5 and 7 are equidistant at 1.4 km. The Bureau of Meteorology records for Karratha for the 12-months preceding the site measurements at total of 381.8 mm of rain fell and there were rainfall events in the period covered by the environment reports from Yara where the mean precipitation was 33.7 ± 21.6 mm. These periods of rainfall were picked up on the monitoring stations, which also had seven rain events in the seven monitoring months. There is a high chance of very polarised rainfall in the region (MacLeod and Fish, 2021).

Records from the plant operations indicate that there are short-term elevated NO_x emissions associated with the start-up of the TAN plant which are regulated under the sites operating licence. This data is valuable in that it shows the direct interaction of anthropogenically sourced gases with exposed surfaces, such as rocks and monitoring stations. Future monitoring work may involve sampling of rocks and soils adjacent to the Yara monitoring stations to develop a conversion

parameter that will enable emissions (mg/m^3) into solution concentrations of mg/litre so that acid loads, in terms of milliequivalents, can be calibrated across the monitoring stations.

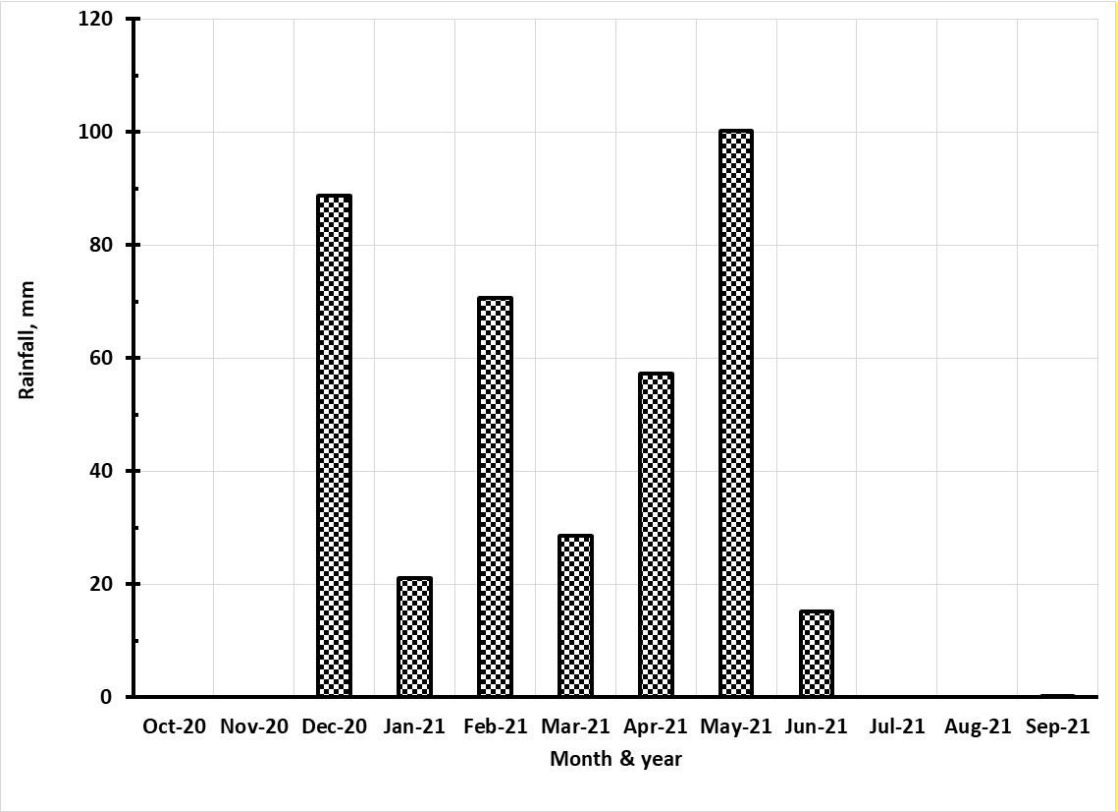

Figure 7: Distribution of rainfall at Karratha airport for one year prior to Sept 21.

Electrolytes and conductivity of wash solutions

Support for the aerosols from the ocean being deposited on the Burrup rocks as being the primary sources of naturally alkaline materials comes from examination of the electrical conductivity of the filtered wash solutions. The data collected in 2021 provides compelling evidence supporting this view, since there are sixteen sets of measurements across the eight sites, as shown in Figure 8. Since chloride is the dominant anion in seawater, it is appropriate to plot the electrical conductivity against the chloride concentration and only two of the sixteen sites deviated from a linear relationship, shown in Equation 10, and shown in Figure 8

$$\text{Electrical Conductivity} = 0.46 + 0.457\ [Cl] \quad \text{.....(11)}$$

The one point, at 32 ppm chloride, which lies below the general regression line is from site 21"b", which lies on top of a small hill just to the west of the Yara plant. This location also has high calcium and magnesium and sulphate ion, due to the sea salt spray and microfossils in the rock. This leads to lower conductivity due to ion-pairing effects in the weak electrolyte system. The R^2 for the relationship between conductivity and chlorinity is very high at 0.996 and this gives a slope error of ± 0.006 or 1.4%. However, the error in the intercept is 23% at ± 0.11 mS/metre which is associated with the variations in the wash solutions of other anions and cations that are not solely due to the presence, or absence, of sea water evaporites.

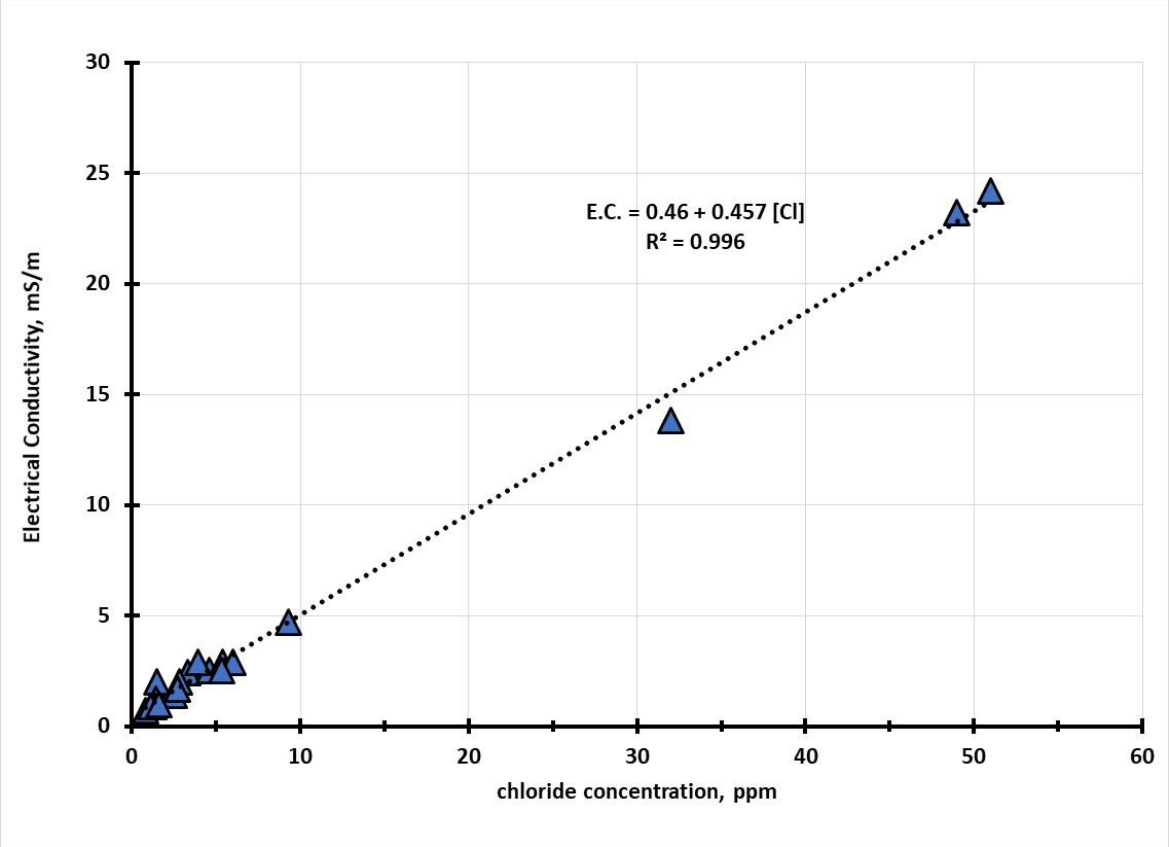

Figure 8: Plot of September 2021 electrical conductivity versus chloride in washed rocks

Interpretation of solution chemistry and cation mobilisation

Because the concentrations of cations in the wash solutions are low, it is more convenient to use a logarithmic value, expressed as pM, in the same format as pH represents the hydrogen ion activity. Higher pM values mean less metal ion activity since pM is equal to the log of the inverse of the metal ion concentration i.e., -log[M^{n+}]. When mineralisation (rock corrosion) products from the weathering of the rock crusts are dissolved the process involves neutralisation of either oxides or hydroxides of metal ions. When metal hydroxides are mobilized by acid dissolution the generic dissolution reaction can be written in the form show in Equation 12,

$$M(OH)_n + n\ H^+ \text{ —> } Mn^{n+} + n\ H_2O \quad \text{..... (12)}$$

In equation 12 the *n* value is the oxidation state of the metal, typically 2 and 3 for iron and mixtures of 2, 3, 4 etc. for manganese. The concentration of the metal ions is derived from the general equilibrium constant for the dissolution of a metal hydroxide into the component elements. Thus $K_{sp} = [OH^-]^n \times [M^{n+}]$, is mathematically the same if we rewrite the expression using the reciprocal values i.e.,

$$^1/K_{sp} = \{^1/_{[OH^-]^n}\} \times \{^1/_{[M^{n+}].}\} \quad \text{.....(13)}$$

Since the logarithm of $\{^1/_x\}$ is pX, then equation 13 can be expressed by the formula

$$pK_{sp} = n\ p[OH] + pM_{OH} \quad \text{..... (14)}$$

The formula, $p[OH] = pK_w - pH$, can be substituted into equation 14 then rearranged to give equation no 15, remembering that the self-ionisation constant of water, pK_w has a value of 14.

$$pM_{\ hydroxides} = pK_{sp} + n(pH\text{-}14) \quad \text{..... (15)}$$

Thus, for plots of the pM values for metal ions the intercept at zero pH is equal to (pK_{sp} -14 *n*). For metal oxides of the general formula M_xO_y dissolving to give metal ions and water, the concentration of the metal is given by Equation 16,

$$pM_{oxides} = {}^1/x\ \{pK_{sp}\} + 2\{y/x\}\ pH \quad \text{..... (16)}$$

When the pM values are plotted as a function of pH it is theoretically possible to determine if the dissolution process involves a hydroxide, which has a slope of *n* for the pM vs. pH plot. If the product dissolving is a mixed valency oxide, the slope of the pM vs. pH plot is $2^{y}/_{x}$, if the soluble ion is an un-complexed free metal ion.

Mobilisation of calcium and barium

Calcium solubility from 2003-2021

The most significant difference in the behaviour observed at the beginning of the monitoring program is that for the February 2004 data there was a change of mechanism of solubilisation of calcium as the slope of the p [Ca] vs pH plots changed from one (Equation 17) to two in 2004 (see Table 2). To bring about a change in dissolution mechanism implies that the surface chemistry of the rocks has undergone a notable change. The most likely mechanism is that for a 1:1 reaction it is the dissolution of calcium carbonate to form a soluble bicarbonate complex,

$$CaCO_3 + H^+ \rightarrow Ca(HCO_3)^+ \quad (17)$$

This is the reaction that dominates the solution processes for the 2003 and the results from 2017-2020. Owing to the changed microenvironmental conditions the mechanism changed to a 1:2 reaction for February 2004 in which the calcium carbonate would have dissolved fully as the disassociated bicarbonate, as shown in Equation 18.,

$$CaCO_3 + 2\,H^+ \rightarrow Ca^{2+} + H_2CO_3 \quad (18)$$

The most likely reason for the change in mechanism is due to the increasing acidity of the local environment, as the mean pH changed by - 0.7 or an increase in acidity by a factor of five, as seen in Table 2 below. For calcium minerals, the slope in 2017, 2018, 2019 and again in 2020 is for dissolution as the bicarbonate. The dramatic difference for the 2021 season of measurements is that the plots of p[Ca] vs. the mean surface pH values had a zero-order slope i.e., the calcium concentration was pH independent and constant at pM of 4.77 ± 0.21 or 1.69 ± 0.07 x 10^{-5} molar.

The mean pH values recorded for all the sites in 2021 was 5.96 ± 0.29 which is significantly more alkaline than in previous years. The change in mean surface pH is consistent with the accumulation of sea salts on the rock surfaces and this acts as a natural buffer to acidity arising from metabolites from the microflora. So, apart from an excursion during the acidic period in February 2004, the original slope or pH dependence of calcium solubility as observed in August 2003, the slope has remained as a 1:1 for the impact of pH on the mobilisation of calcium on the rock surfaces. The mean slope moved upwards to 1.5 (a mixture of reactions involving equations 17 and 18 on a 1:1 basis) in August 2019 when the acidity moved back towards the February 2004 values. With the impact of cyclone Damien in February 2020, the mean pH increased by 0.6 i.e., the acidity decreased by a factor of five times and the stoichiometry of the mobilisation of calcium minerals moved back to equation 17 or loss via formation of the soluble calcium bicarbonate.

Table 2: Solution properties of calcium and barium washings on the Burrup rocks

Date	mean pH	mean p[Ca]	mean p[Ba]	slope p[Ca]/pH	slope p[Ba]/pH
August ‘03	5.0 ± 0.5	3.6 ±0.4	6.6 ± 0.2	1.0 ± 0.1	0.4±0.2
February ‘04	4.3 ± 0.5	4.1 ± 0.6	7.2 ± 0.4	2.0 ± 0.2	2
November ‘17	5.7 ± 0.5	2.0 ± 0.6	5.2 ± 0.3	1.3 ± 0.3	0.5±0.1
Sept. ‘18	5.5 ± 0.8	3.3 ± 0.2	7.9 ± 3.2	1.3 ± 0.5	0.2 ± 0.1
August ‘19	4.6 ± 0.3	4.4 ± 0.6	7.5 ± 6.3	1.5 ± 0.2	2.4 ± 0.7
October ‘20	5.2 ± 0.5	4.5 ± 4.1	7.7 ± 4.7	1.2 ± 0.2	1.1 ± 0.2
September ‘21	6.0 ± 0.3	4.8 ± 0.2	7.8 ± 0.3	-0.3 ± 0.2	0.1 ± 0.3

The data presented in Table 2 is shown graphically in Figure 9 where there is a clear correlation between the increasing acidity of the sites and the number of protons involved in the mobilisation of calcium ions. The trend in decreasing slope with increasing pH ceased for the years 2017, 2018 and 2020 and stayed constant at a 1:1 slope, consistent with mobilisation involving uptake of a single proton.

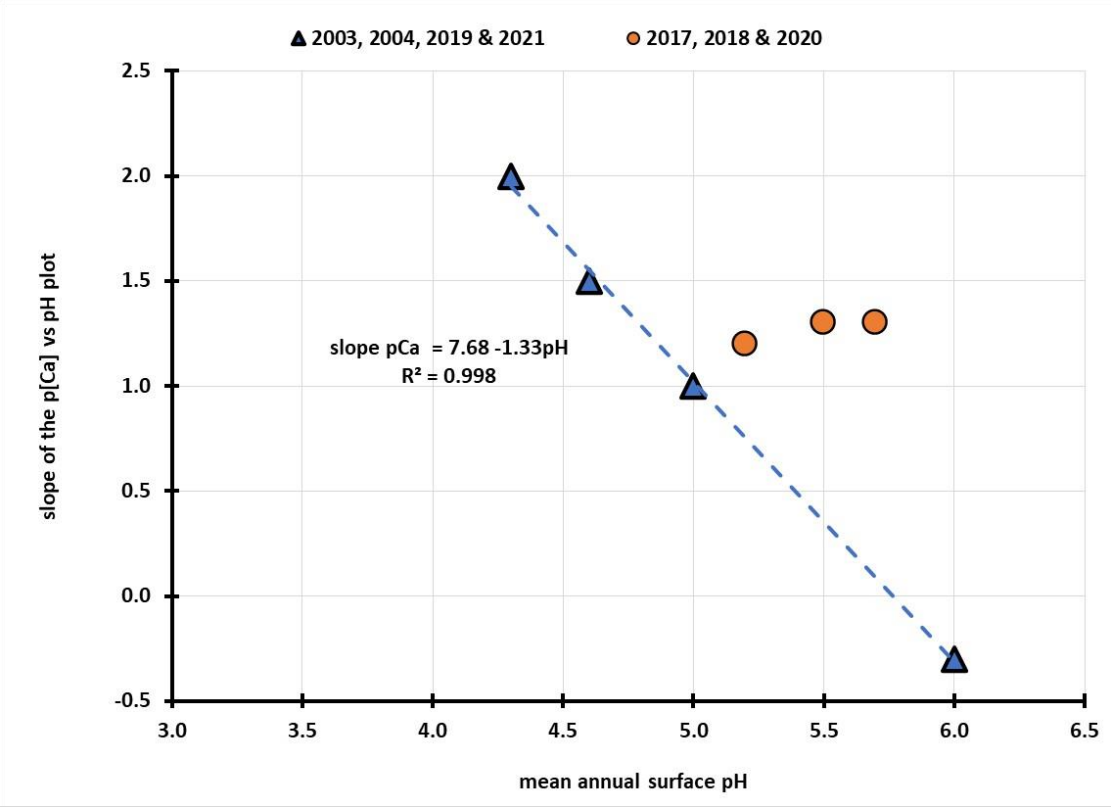

Figure 9: Plot of the seasonal variation in slope of p[Ca^{2+}] vs. pH 2003-2021

The impact of the release of ammonia, which acts as a pH buffer on the rocks, and of cyclonic rainfall is shown by the three points from August 2003, February 2004 and August 2019 form the regression line shown in Figure 9 and equation 19,

$$\text{Slope p [Ca]/pH}_{\text{seasonal}} = 7.68 - 1.33\ \text{pH} \quad \text{..... (19)}$$

The measurements from 2017, 2018 and 2020 lie as the orange circles off the regression line as these reflect the impact of cyclonic rainfall resetting the acidity clock on the rocks. It is now readily apparent that the solubility of calcium on the rock surfaces is directly affected by the mean acidity of the environment.

The chemical analysis done by CSIRO on the mineralogy of the rock crusts' weathered zones did not show up any significant amounts of barium, so it is considered likely that the presence of varying amounts of this heavy alkaline earth metal came from the sea. The chemistry of the barium minerals was considered a likely candidate to see if there was any systematic change in the rock chemistry from the time of the original measurements made in 2003 and the present round of data collected in 2020. Plots of the p[Ba^{2+}] versus pH did not follow any monotonic trend but for the more acidic years in 2004 and 2019, the slopes had a 2:1 stoichiometry which is consistent with acid dissolution of barium oxide, Equation 20, viz.,

$$BaO + 2\ H^{+} \rightarrow Ba^{2+} + H_2O \quad \text{..... (20)}$$

A similar stoichiometry would be obtained for the acid dissolution of barium carbonate. With the more alkaline mean pH values observed in November 2017 (5.7 ±0.5) and ten months later in

September 2018 (5.5 ± 0.8) the slope is 1.5, which means that there is a mixture of barium dissolving as a bicarbonate and a free barium ion. The mean ionic product of barium and sulphate for the 2021 wash solutions was 1.2 x 10^{-12} and barite or $BaSO_4$ has a pK_s of 9.6, which gives an ionic product of 1.1 x 10^{-10} which is more than 110 times higher than the mean ionic product for the wash solutions measured in 2021.

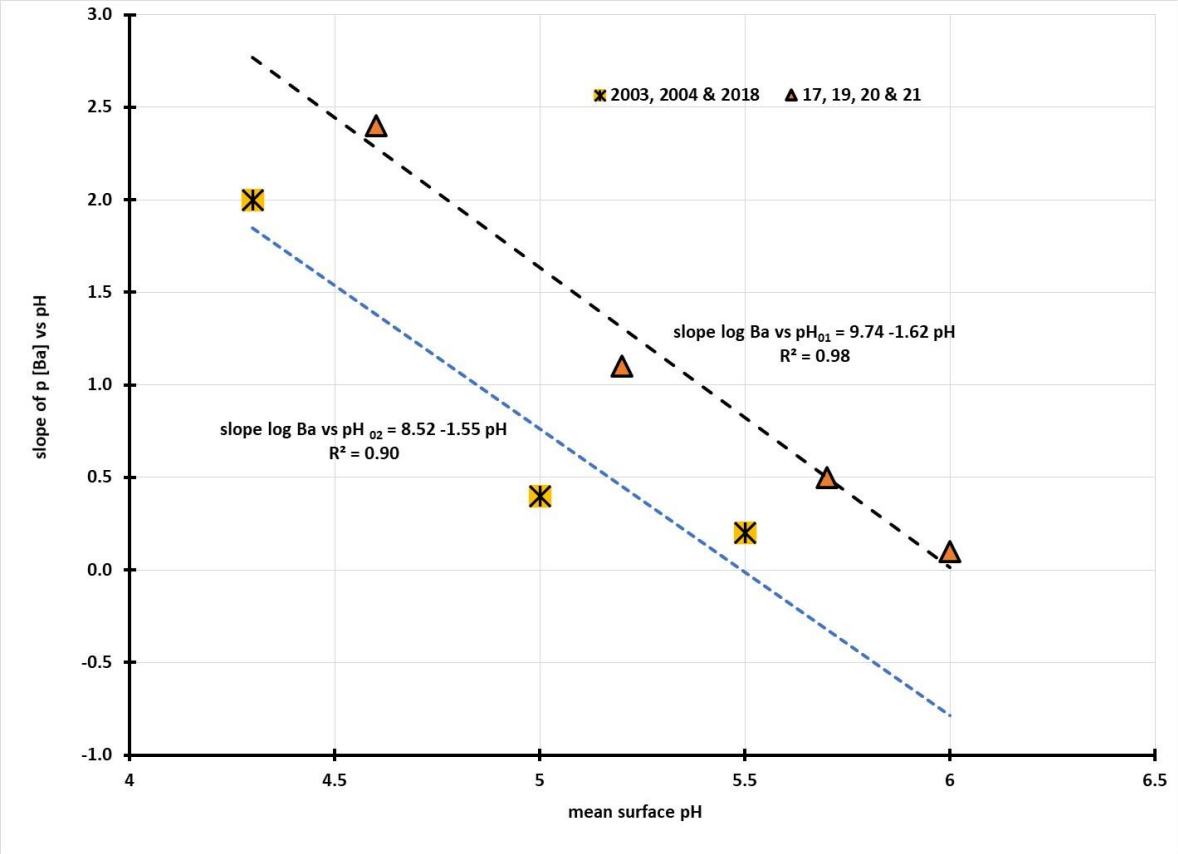

Figure 10: Plot of the seasonal variation in slope of p[Ba^{2+}] vs. pH 2003-2021

Inspection of the graph in Figure 10 shows two parallel lines, which indicates that the chemistry of the solubilisation of barium from the rock surfaces reflected the same mechanism. The slopes of the first regression line was -1.6 ± 0.2 which was experimentally the same as the second regression line, which had the slope of – 1.6 ± 0.5. The only difference between the two sets of data shown in Table 2 were the intercepts at zero slope i.e., where the solubility of the barium salts was independent of pH, and this means that there were no oxides or hydroxides of barium involved in the solubility parameters. The intercept values for the regression equations shown in Figure 10 were 9.7 ± 0.9 and 8.5 ± 2.6 which shows that they are not significantly different to each other i.e., the difference in the intercept values is not different when the errors in the regression lines are considered.

This means that despite a mean sulphate concentration of 7 ± 5 ppm there is still insufficient sulphate to cause any problems with precipitation of barium as barite on the rock surfaces. For the higher sulphate concentrations, the solubility of barium was given by equation 21,

$$[Ba]_{ppm} = 0.0033 - 0.0001\ [SO_4^{2-}]_{ppm} \quad \text{..... (21)}$$

There is nothing special about the chemistry of this equation, since it just relates to the way in which increased sulphate will decrease mobilisation on barium on the rock surfaces. There was a cluster of data points at the low sulphate region where there was no trend and for this zone the mean barium concentration was (1.9 ± 1.9)x 10^{-3} ppm and the mean sulphate was (1.1 ± 2.2) x 10^{-3} ppm. The zero slope for the p[Ba] vs. pH plots in 2021 simply indicates that the varying solubility of barium in the

wash solutions was not due to water reacting with any oxide or hydroxide species in the rock minerals. This also indicates that the presence of barium is tied up with complex surface mineralogy.

Mobilisation of metal cations from the rock surfaces

Boron

The sixteen rock washings provided an opportunity to see how mobile various transition and p-block metals responded to the post cyclonic rain and the average dry environments. The most soluble p-block metal was boron, with a mean pM of 6.23 ± 0.09. This equates to a molar concentration of 5.9 x 10^{-7}M , is below the 1 x 10^{-6}M concentration considered to be indicative of corrosion. The data from 2021 showed that the concentration of boron was pH independent. Since the mean pH of all the rock sites from direct surface measurements was 6.0 ± 0.3 it could be said that the cut off point for mobilisation of boron is close to the natural pH of weathered Burrup rock surfaces. Since the main boron containing mineral in the Burrup rocks is chlorite, which is a complex sheet silicate mineral $(Mg,Al,Fe,Li,Mn,Ni)_{4\text{-}6}(Si,Al,B,Fe)_4O_{10}(OH.O)_8$, the data on boron solubility has provided a de-facto measure of the way in which chlorite responds to the solution pH. The lack of major rainfall events in the preceding 12 months has resulted in the accumulation of measurable amounts of sea salts, which has led to the increased alkalinisation of the rock surfaces and so has diminished dissolution of chlorite and other mineral species.

In the 2020 season it was found from the p{ B} vs. pH plots that the mobilisation mechanism involved reaction given by equation no 22 and the corresponding connection shown in equation 23 viz.,

$$4\ H_3BO_3 \rightarrow HB_4O_7^- + H^+ + 5\ H_2O \quad \text{.....(22)}$$

For this equilibrium, the relationship between boron solubility and pH is

$$p[B] = -\ 2.28 + \tfrac{1}{3}\ pH \quad \text{.....(23)}$$

These two equations illustrate some of the complex solution chemistry associated with this metal, which has a remarkable ability to form multi-valent oxyanions. Plots of the pM vs. pH data from October 2020 had a slope of +⅓, which simply reflects the equilibrium between H_3BO_3 and $HB_4O_7^-$, which is governed by equation 22.

In determining the origin of the boron on the rocks it is instructive to look at the ratio of chloride to boron in the wash solutions, since the borate buffer system is the second most important to the carbonate system, which controls the pH of normal seawater. Chloride ions are dominant anion at 18,980 ppm in normal sea water and the boron level is only 4.6 ppm, giving a ratio of $\{^{Cl}/_{B}\}$ of 4,126 and for the 2021 Burrup rocks the mean ratio of $\{^{Cl}/_{B}\}$ was 227 ± 40, which is likely due to increased boron activities on the rock surface than in seawater. There was no statistically valid difference between the ratios observed on the granophyre compared with the gabbro rocks. The cause of the reduction in the $\{^{Cl}/_{B}\}$ ratio indicates that both the gabbro and the granophyre rocks are providing additional sources of boron through their own mineralogy. The response of boron solubility to pH showed a slight increase in solubility with increasing acidity which indicates a possible amphoteric response or very complex mineralogy that is to be determined. The detailed examination by CSIRO of the parent and weathered rock surfaces of the gabbro and granophyre rocks in the Burrup has provided an exhaustive list of the minerals that are present in the mineral crusts on the gabbro and granophyre rocks (Ramanaidou et.al. 2017. For more details regarding the complex solution chemistry of boron, the reader should peruse the Pourbaix Atlas (Pourbaix 158-167).

Mobilisation of metal cations

Iron

Analysis of the wash solutions collected in September 2021 showed that seven of the 16 assessment rocks gave soluble iron in the washing water. There was only one gabbro site, 23”b” that had any

iron being released and it was at the level of 6 ppb, which is only just above the limit of detection at 5 ppb. By way of contrast the mean iron concentration on granophyre rock testing locations was 8.8 ± 5.2 ppb or 1.6 x 10^{-7}M, which is below the normal 10^{-6}M concentration considered to represent corrosion of a metal or mineral species. The mean pH of all the sites in 2021 was 6.0 ± 0.3 and so very low mobility of iron was not unexpected.

Zinc

The concentration of zinc increased from a pM of 7.15 in 2019 to 6.84 in October 2020 and a mean value of 7.13 ± 0.13 for September 2021, which is the same as in 2019. There was a response to pH of the zinc concentration, with the slope in the pM {Zn} vs. pH plot being 0.75, which is consistent with mobilisation of the mineral $Zn_3(OH)_4Cl_2$. This stoichiometry is consistent with the increased chloride ion concentration on the rock surfaces which had developed to a higher level due to the lack of significant rain events.

Manganese

Although the data is limited, sites 7, 22 and the Climbing Man reference rocks gave equation 24, with a $p\{^{Mn}/_{pH}\}$ slope of 1.5 ± 0.1 which is consistent with mobilisation of the brown, black mineral Mn_2O_3, viz.,

$$p[Mn] = 0.13 + 1.5\ pH \quad \text{.....(24)}$$

This ratio is consistent with the following reaction scheme which results in soluble Mn^{3+}-hydroxy species, as shown in equation 25,

$$Mn_2O_3 + 3\ H^+ \rightarrow Mn(OH)_2^+ + Mn(OH)^{2+} \quad \text{.....(25)}$$

The formation of the dihydroxy and the monohydroxy complexes have their analogues with iron when there is acidic dissolution of Fe_2O_3.

Copper

The mean solubility of copper in the 2021 season was 3.0 x 10^{-8} M or a {p Cu} value of 7.51 ±0.22 and as such it cannot be a major contributor to the loss of surface entrained minerals in the granophyre and gabbro rocks. The mean slope of the {p Cu} vs. pH was 1.9 ± 0.4 which is consistent with previous experience in the more acidic monitoring season at various Burrup sites in 2003 and 2004, and the relevant dissolution reaction is given by equation 27 viz.,

$$CuO + 2\ H^+ \rightarrow Cu^{2+} + H_2O \quad \text{.....(26)}$$

The presence of tenorite (CuO) as part of the rock surface has been determined by the CSIRO applied mineralogy studies.

Arsenic, cadmium, chromium, cobalt, lead, nickel, and vanadium

For the second time since monitoring began for Yara in 2017 there was no arsenic, cadmium, chromium, or nickel detected in the 16 wash solutions. Additionally, only site 4"a" produced any vanadium and it was at 0.1 part per billion (ppb) and just above the limit of detection. This same rock also recorded 0.1 ppb cobalt so a more detailed examination in future monitoring programs will be done to ascertain if there are any specific micromorphological features that can explain the presence of ultra-trace amounts of vanadium and cobalt.

In terms of metal dissolution reactions, it is common to interpret an equilibrium metal ion concentration of 10^{-6} M or pM^{n+} of 6.0 as being as "no corrosion" and so all the metal ions shown in Table 3 fall into this category i.e., the rocks are giving off very little soluble material (Pourbaix 1974). While there is discernible mobilisation of the metal ions, given the high sensitivity of the analytical methods used at the Chemistry Centre of WA, it cannot be said that there is active mineral dissolution at the sites that were examined.

Table 3: Summary of solubility dependence of metals at Yara monitoring points

Element	Mean pM	Standard deviation	pM vs. pH slope
Boron	6.23	0.09	7.85 - 0.27 pH
Copper	7.51	0.40	3.29 + 1.87 pH
Lead	9.32	0.01	9.32 + 0.00 pH
Zinc	7.17	0.17	2.49 + 0.76 pH

For copper, the mean pM Cu of 7.5 ± 0.4 comes with a 1:2 pM to pH slope, which is consistent with the dissolution of tenorite (CuO) from the mineral surfaces. It is noted that the mean solubility of zinc is slightly higher than for copper. Lead is clearly the least soluble mineral, which is in line with the normal trends for metal ions in the natural environment.

Interpretation of the pH effects on iron and manganese mobilisation in the rock patina

Previously published work by MacLeod (2005) and MacLeod et. al. (2017, 2018) has shown that at the pH values recorded in 2003 and 2004 (Appendix IV) there was measurable mobilisation of iron and manganese containing minerals. Analysis of the wash solutions from the early data sets has shown up significant concentrations of aluminium, iron, manganese, nickel, copper and some zinc and lead from the parent rock crusts. Because the mineralogy of the highly weathered gabbro and granophyre is characterized by a series of mixed amorphous iron—manganese oxides, in the form of desert or rock varnish, iron(III) oxy-hydroxides and weathered minerals such as smectite, kaolinite, illite and mica (Clark 2004) it is not unexpected to find mobilization of metallic cations under the acidic conditions. It is helpful when undertaking a review of metal ion solubility to understand that the dissolution of the key elements in the rock patina is controlled by the pH or the acidity of the microenvironment.

The more acidic surfaces in the 2003 spring and the February 2004 summer measurements were amenable to this form of analysis and plots for iron showed that for both seasons the p[Fe] vs. pH plots have an average slope of +1.98 ± 0.06 pH which confirms the following mechanism:

$$FeOOH + 2H^+ \rightarrow Fe(OH)_2^+ + H_2O \quad \text{..... (27)}$$

The Pourbaix diagram for iron in the range of pH observed on the rock surfaces shows that the $Fe(OH)_2^+$ ion is the dominant form of soluble iron(III) under oxidizing conditions (Pourbaix 1974). The historic pH data for 2003-2004 is shown in Appendix IV. Similar plots indicate that copper is mobilized by dissolution reactions involving two protons per metal ion as is the case for nickel.

Using washing solution data for the mobilisation of aluminium allows similar plots for the solubility of aluminium with surface pH to be determined. For the Burrup rocks the aluminium mobilisation graphs had an average slope of 1.4±0.2 pH, which is consistent with the dissolution of kaolinite ($Al_2Si_2O_5(OH)_4$) to give the $Al(OH)_2^+$ ion and $AlSi_2O_5^+$, as shown in Equation 28,

$$Al_2Si_2O_5(OH)_4 + 3H^+ \rightarrow Al(OH)^{2+} + AlSi_2O_5^+ + 3\,H_2O \quad \text{..... (28)}$$

Kaolinite has been identified as one of the aluminium containing minerals on the Burrup rocks along with feldspar, chlorite, mica, smectite and some gibbsite (Clark 2004) and it was a major mineral identified in the CSIRO Accelerated Weathering experiments (CSIRO 2016). It is not unexpected for aluminium ions to have been mobilized under the very mild sample collection regime that was used. In September 2021 aluminium ions were found in the washings from sites 4, 5 and the Climbing Man, with a mean concentration of 0.012 ± 0.008 ppm or 4.5×10^{-7} M, which is twice the detection limit of 1.9×10^{-7} M. It is likely that the higher amount of chloride ions on the rock surfaces may have assisted in the mobilisation of aluminium through the formation of hydroxy chloride complexes, which are commonly used in deodorants. The impact of increased mobilisation of aluminium chloride complexes on the viability of the normal rock microflora is not yet established. However, the presence of aluminium in its' various hydroxy complexes, will increase the buffer

capacity of the salts on the rocks in the absence of major cyclonic rainfall events, which leads to higher pH values across those sites. Under the alkaline conditions found in 2021, the plots of p{Al} vs. pH do not provide any clear indication for dissolution from an individual mineral species but it is consistent with aluminium being solubilised from other mineral species including clays and other minerals associated with weathered metamorphosed volcanic rocks.

Table 4: Mean pH and solubility of iron and manganese minerals from rock irrigation

Time	Mean pH	Mean p Fe	mean p Mn	Slope p Fe/pH	slope p Mn/pH
Aug-03	4.97 ± 0.48	6.0 ± 2.0	7.2 ± 0.5	2.0 ± 0.1	0.9 ± 0.4
Feb-04	4.78 ± 0.27	6.3 ± 0.4	7.31 ± 0.35	2.0 ± 0.1	2.1 ± 0.1
November '17	5.69 ± 0.51	6.8 ± 0.2	5.03 ± 0.35	0.3	1.1 ± 0.1
September '18	5.52 ± 0.84	Nil soluble	6.79 ± 0.35	Not applicable	1.2 ± 0.9
August '19	4.62 ± 0.26	6.2 ± 0.4	6.91 ± 0.48	0.4	2.3 ± 0.4
October '20	5.21 ± 0.51	6.8 ± 3.2	7.02 ± 4.2	Not applicable	1.1 ± 0.1
September '21	6.02 ± 0.30	6.9 ± 0.2	7.45 ± 0.22	Not applicable	0.7 ± 0.1

The lower standard deviation of the Feb 2004 and the Nov 2017 data on iron solubility provides evidence that the solubility of the iron minerals decreases with increasing pH, despite the apparent change of mechanism. Plots of the mean p[Fe] versus annual mean pH over the whole period of measurements from 2003 to 2021 shows that, apart from the initial data in August 2003, the regression analysis (shown in equation 29) has a slope of 0.5 p{Fe} vs. pH.

$$p\{Fe\} = 3.96 + 0.50\ pH \quad \text{..... (29)}$$

The R^2 value was 0.84, with an associated error in the intercept of ± 0.67 and an error of ± 0.13 in the slope. The less than unity value for the slope of the p{Fe} vs. pH plot reflects the mobilisation of iron coming not from discrete minerals associated with iron-rich ore bodies, but most likely from amorphous iron degradation products. The take away feature of equation 29 is that the solubility of iron falls with increasing mean pH (Table 4).

As has been previously noted, manganese compounds are more soluble at neutral pH than their iron analogues are reflected in the 2017 data from the Burrup rock art washings when the mean solubility had increased to 9.3×10^{-6}M, and the corresponding level of iron was 1.6×10^{-7}M or sixty times less. The reasons for this lie in the underlying chemistry associated with the position of manganese and iron in the Periodic Table. This observation is supported by data from Krauskopf (1957) who found that Fe compounds are less soluble than corresponding Mn compounds under naturally occurring Eh-pH conditions. The mean p Mn values show an average of 50 times lower solubility in 2018 than in 2017, pMn 6.8 for 2018 compared with 5.0 in November 2017, as seen in Table 4. The mean solubility of manganese has continued to decrease between 2019 and in 2021 because of the mean pH increasing. With the decreasing manganese solubility, the iron levels are more dramatically affected by the changing pH.

The concentration of manganese in the rock irrigation measurements done in September 2021 had a maximum of 0.0057 ppm at site 4"a" or a pMn of 6.98 or 1.05×10^{-7} M. When all the manganese data was plotted as a function of surface pH, the regression analysis confirms that the likely dissolution reaction is shown in equation 30 for sites 7, 22 and Climbing Man as the p{Mn} vs pH plot had a ⅔ slope viz.,

$$Mn_2O_3 + 3\ H^+ \rightarrow Mn(OH)_2^+ + Mn(OH)^{2+} \quad \text{..... (30)}$$

There was a high degree of fit of the pM and pH data, with an R^2 of 0.99, and so the pM vs. pH slope was 0.68 ± 0.05. For this equation (30) the intercept pH was -0.09 ±0.32 which simply attests to the relative insolubility of Mn_2O_3 species as it would need a 1 M acid solution to get a I M solution of

manganese ions in solution. The sites that had this or a closely related slope included 6, 7, 22, 23 and the Climbing Man reference rocks.

Electrochemical characterisation of dissolution mechanism

Although in-situ measurement of pH and chloride ion activity has been part of the monitoring program since first measurements were done in June 2003, it was only after field experience on early bronze age sites in central Anatolia (Turkey) that the same methodology was applied to the rock surfaces as part of the Yara monitoring program in 2018 (MacLeod 2018). The measurement of the redox (reduction oxidation) potential is managed by placing a platinum wire electrode through a moistened sponge rubber to contact the rock surface and the reference electrode (an Ag/AgCl 1 M KCl reference) which is laid close to the point where the platinum electrode is placed, and this completes the electrical circuit.

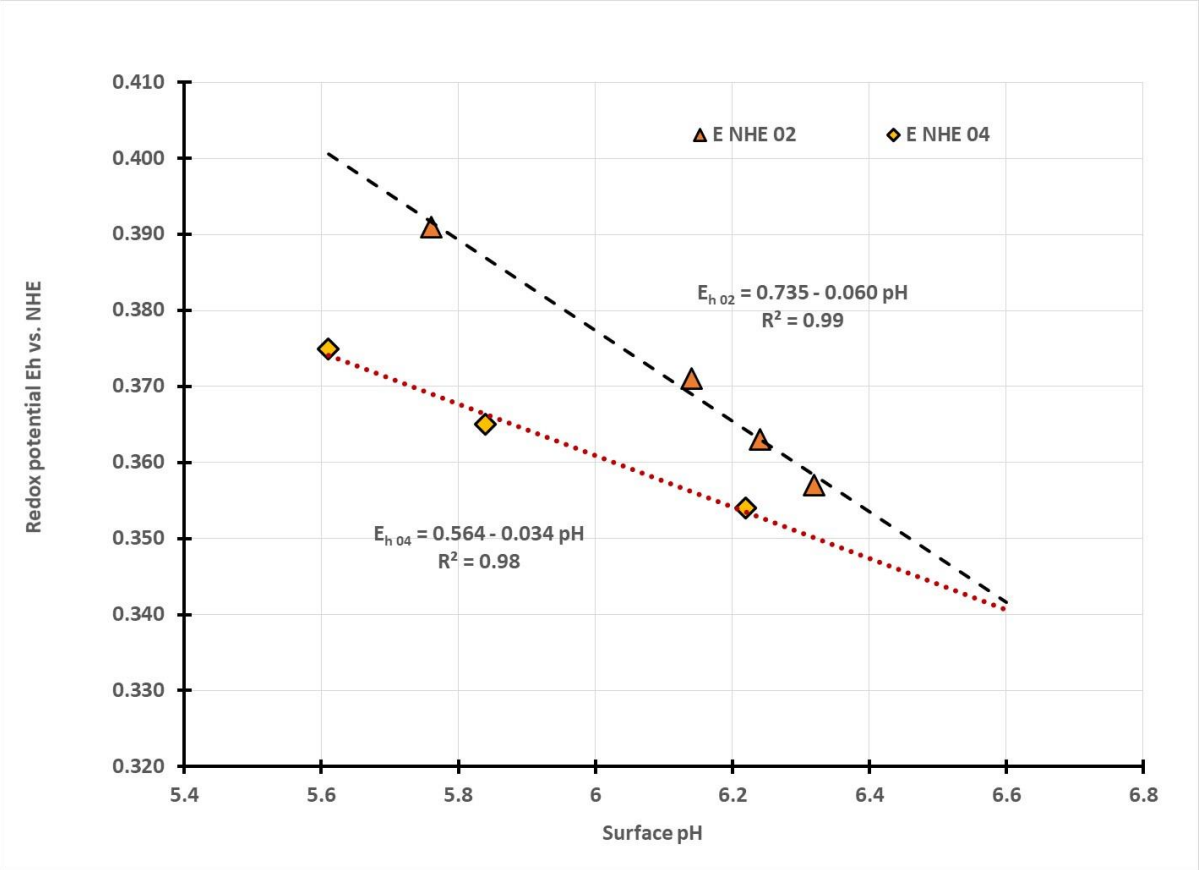

Figure 11: Pourbaix diagram for site 21, Sept. 2021 showing two manganese reactions

The redox data is collated and then the combination of the redox potential (corrected to the normal hydrogen electrode via the calibration of the silver chloride reference voltage which was + 0.210 volts vs. NHE) and surface pH is used to plot Pourbaix diagrams for each of the rock art monitoring sites. Inspection of the slopes in the Pourbaix diagram in Figure 11 shows that there are two mechanisms controlling the dissolution of soluble manganese species at site 21, the large flat sloping rock on top of the hill located immediately to the west of the main Yara plant. There are two reaction schemes shown in equation 31 and 32.

$$Mn(OH)^{+} + H_2O \rightarrow Mn(OH)_2^{2+} + H^{+} + 2e^{-} \quad \text{..... (31)}$$

$$Mn^{+2} + 2H_2O \rightarrow Mn(OH)_2^{2+} + 2\,H^{+} + 2\,e^{-} \quad \text{..... (32)}$$

For equation 31, the slope was 34 ± 3 mV/pH is consistent with the oxidation of the hydroxy Mn(II) via oxidative hydrolysis to produce the dihydroxy Mn(IV) complex ion. The standard redox voltage, obtained by the regression analysis, at zero pH is the intercept value in the equation shown in

Figure 11 is 0.720 ± 0.020 volts is consistent with the mechanism given in Equation 31. The reaction scheme shown in equation 32 produces one proton per electron and so the oxidized product is still the same $Mn(OH)_2^{2+}$ as in equation 31, but the starting material is the free manganous ion, Mn^{2+} itself, rather than the partially hydrolysed species shown in the same equation as the starting form of soluble manganese. Details of the regression analyses for this and all the other 2021 sites are given in Appendix II and are summarised below in Table 5.

Table 5: Redox equations deduced from the Sept. 2021 Pourbaix diagrams

$Mn^{2+} + 2\ H_2O \rightarrow MnO_2 + 4\ H^+ + 2\ e^-$, slope 120 mV/pH

Location	Pourbaix slope	Intercept	R^2
Site 5	-0.120 ± 0.008	1.142 ± 0.104	0.96
$Mn^{+2} + 2H_2O \rightarrow Mn(OH)_2^{2+} + 2\ H^+ + 2\ e^-$			**slope 60 mV/pH**
Site 4	-0.060 ± 0.002	0.774 ± 0.020	0.98
Site 21	-0.056 ± 0.003	0.719 ±0.021	0.98
Site 22	-0.055 ±0.006	0.706 ±0.035	0.96
Site 23	-0.058 ± 0.005	0.708 ± 0.029	0.99
Climbing Man	-0.057 ± 0.004	0.753 ± 0.047	0.94
$Mn(OH)^+ + H_2O \rightarrow Mn(OH)_2^{2+} + H^+ + 2\ e^-$			**slope 30 mV/pH**
Site 6	-0.026 ± 0.002	0.545 ± 0.012	0.96
Site 7	-0.035 ± 0.003	0.608 ± 0.009	0.98
Site 21	-0.034 ± 0.004	0.564 ± 0.023	0.98

Although the slope of the Pourbaix plots is helpful in determining the ratio of protons to electrons, there are alternative relationships that both give the same slope. For example, the same 30 mV/pH slope is found for any redox couple that has a ratio of two electrons per proton, as shown in equation 33 and 31 viz.,

$$2\ Fe(OH)^+ + H_2O \rightarrow Fe(OH)^{2+} + Fe(OH)_2^+ + H^+ + 2e^- \quad \text{..... (33)}$$

Inspection of the range of extrapolated voltages at zero pH (column 3 in Table 5) in combination with data collected from the rock washings, give the most likely candidates for the redox responses to pH. In other words, for sites where there was the same 30 mV/pH slope it can be readily discerned from the metal ion solubilities in the washing solutions which transition metal is the dominant one in determining the equilibria. The washing solution data also provides the $p\{M^{n+}\}$ vs. pH plots which can also signify the dominant equilibria controlling mineral mobilisation. The power of having the redox and pH measurements done on the rocks demonstrates that there are competing equilibria across the rock surface, which can vary from 2.4 m^2 for site 4, to 0.17 m^2 for site five.

The environment in 2021 was very different to that in 2020 when most of the rocks had a reasonable drenching, at least on some of the surfaces. On site 4 in 2020 the Pourbaix diagram included formation of Mn_3O_4 (see equation 34),

$$3\ Mn^{2+} + 4\ H_2O \rightarrow Mn_3O_4 + 8\ H^+ + 2\ e^- \quad \text{..... (34)}$$

but in 2021 the maximum Pourbaix slope for 2021 was 120 mV/pH associated with the formation of black manganese dioxide (Table 5). The Pourbaix data has provided unequivocal information about the competing reactions that are taking place on the surfaces of the rocks.

Increased surface chloride ions has resulted in increased mobilisation of aluminium into the washing solutions in 2021 and a similar impact was noted on iron solubility. In 2020 there was only

one site with a measurable amount of iron in the wash solutions but in 2021 there were sites 4, 5 21, 23 and the Climbing Man split rock site. The mean concentration of iron had a p{Fe} of 6.89 ±0.20 or approximately 1.3 x 10^{-7} molar. It is well established that iron(III) forms strong complexes with chloride ions and so the increased salinity appears to have been more than sufficient to overcome the elevated mean pH values and result in the increased reporting of iron into the wash solutions.

The only stable ionic species in the pH range of 4.0-5.5 is the Mn^{2+} ion. Redox processes that are commonly facilitated by fungi readily reduce Mn(IV) species to Mn^{2+} ions (Gadd 2004). There is a direct increase in the manganese ions in the wash solution with increasing acidity of the rock surfaces. The solution chemistry of manganese is extraordinarily complex, with solid phases of Mn^{2+} being MnO and $Mn(OH)_2$, for Mn^{3+} there is Mn_2O_3 and for the mixed valence of Mn_3O_4, which is a mixture, like its iron analogue magnetite, of one Mn^{2+} and two Mn^{3+} ions. In addition, there are equilibria involving the precipitation of manganese dioxide.

Part of the reason why there is a mixture of electrochemical reactions on the individual rocks can be gleaned from inspection of the pH data in the Appendixes or by looking at the annotated in Figure 12. In 2021 field assistant Erin Fish noted the values that were orally transmitted and so a complete record of the pH, chloride, and voltage data on all the sites was prepared. Statistical analysis of the pH data gives a mean value of 6.18 ± 0.29 with a maximum of 6.50 and a minimum of 5.58, indicating very low bacterial activity, since the minimum pH is associated with just the natural hydrolysis constants for iron and manganese ions on Burrup rocks. Inspection of the data in Table 5 for 2021 shows that rather than several sites showing dual behaviour of competing ionic and redox equilibria, like that shown on site 5, the heavier salt concentration at site 7 (mean 46 ± 34 ppm) has made for a more uniform microenvironment, as the salt levels the year before after the inundation from cyclone Damien was 4.8 ± 2.4 ppm.

As has been previously reported in reviews developed for Yara, the mean pH values at the top of the rock are more alkaline than at the bottom row at the foot of the rock. Thus, at site 7 the mean pH of the first six points in row 1 was 6.24 ± 0.39, while row 2 was the same but with less scatter at 6.25 ± 0.22 while the bottom row was 6.06 ± 0.24, which is 1.5 times more acidic than the top row. This is due to the angle of the rock which promotes gradual movement of water and micronutrients from the top to the bottom of the rock. Plots of the Pourbaix data for site 7 is 2021 shows only one oxidative process viz.,

$$\mathbf{Mn(OH)^{+} + H_2O \rightarrow Mn(OH)_2^{2+} + H^{+} + 2\,e^{-}}$$

This reaction (equation 21) describes the redox behaviour on this site, with an R^2 value of 0.98 with a $\{^{Eh}/_{pH}\}$ slope of 37 ± 2 mV and an intercept value of 0.614 ± 0.013 volts vs. the normal hydrogen electrode.

An additional complication to the electrochemistry of site 7 at times of higher chloride concentration is that there is a distinct correlation between increased chloride ion and increased acidity i.e., there appear to be chloride obligate bacteria which become more biologically active in an increased salty microenvironment. The regression analysis for this data gave an R^2 of 0.98 for six data spots and the regression analysis was given by equation 35,

$$pH_{\text{Cl dependent bacteria}} = 6.62 - 0.019\,[Cl] \quad \text{..... (35)}$$

The slope or pH dependence on chloride concentration was -0.019 ± 0.001 $\{^{pH}/_{Cl\ ppm}\}$ and the pH intercept at zero chloride concentration was 6.62 ± 0.05. Five of the eighteen pH measurements showed no response to changes in the chloride ion activity across the rock surface. This is an excellent example of how the rock microenvironment will dictate the localised responses to environmental stimuli.

When the redox potential was plotted as a function of chloride ion activity there was a strong correlation across the scattered data, with an R^2 of 0.83 and a relationship given by equation 36 viz.,

$$^{Cl}E_h = 0.358 + 0.0007\,[Cl]_{ppm} \quad \text{..... (36)}$$

The intercept value for E_h was 0.358 ± 0.005 volts and the slope was 0.70 ± 0.13 µV per ppm chloride.

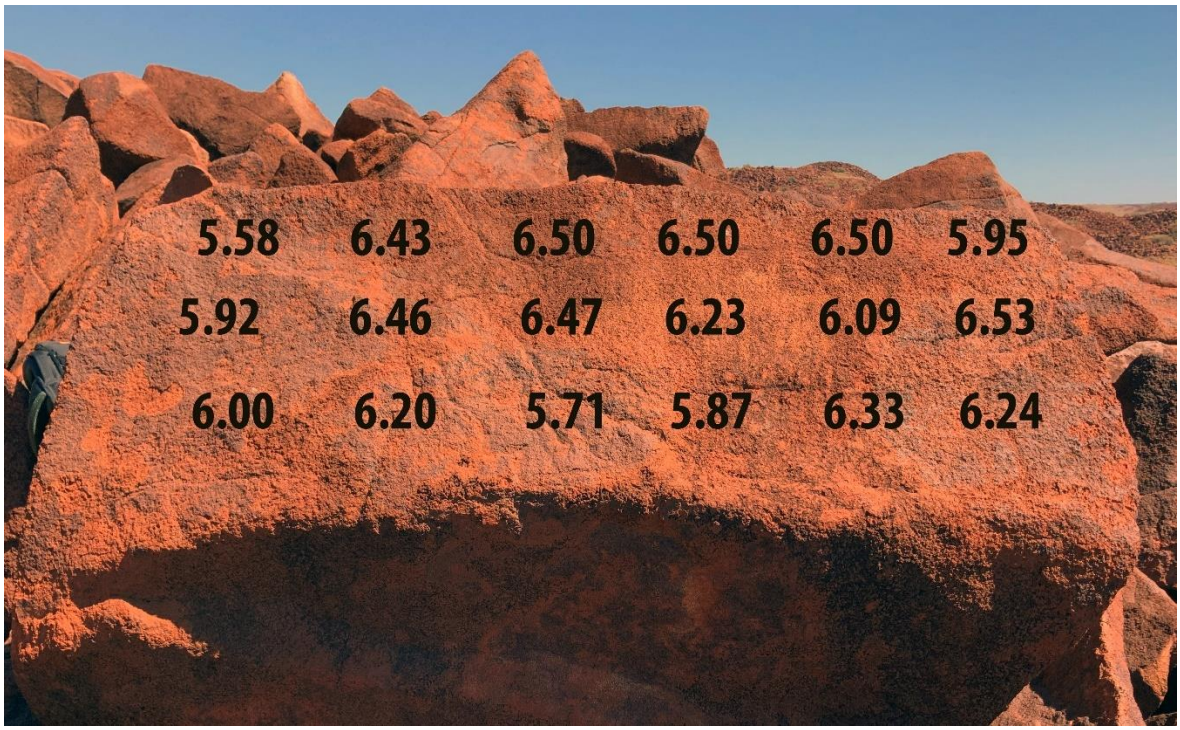

Figure 12: Deep Gorge site 7 with pH data recorded onto the image, Sept. 2021

Examination of the chloride distribution data across rock 7 showed a high degree of correlation, with an R^2 of 0.94 for the top row of measurements, that showed a linear increase in chloride activity of 0.75 ppm/cm in moving from left to the windward direction (right-hand side) which is the position closest to the source of chlorides blowing across the flat land near the Hearson's Cove Road, with clear ocean views beyond the hills to the east of the NW Shelf gas plant. The maximum was 130 ppm, compared with only 11 ppm in 2020. This relationship is given by equation 37,

$$^{2021}[Cl]_{first\ row} = 76 + 0.75\,d \quad \text{.....(37)}$$

For the regression equation no 36, the value of *d* is the distance in cm from the left side of the rock. The second and third row of chloride measurements showed no systematic trends with distance across the rock.

It is instructive to review the full range of pH data on this site, which dates to the first measurements in August 2003 and this information is shown graphically in Figure 13. A cyclonic rain event between August 2003 and February 2004 saw the pH increase from 4.6 to 5.0, thus a reduction in acidity by being washed with fresh water. The series of cyclonic rain events see Table 6, in between the years leading to 2017 saw the pH increase to 5.6, which is the natural pH of iron and manganese minerals hydrolysing in distilled water to produce a mildly acidic microenvironment. Solubilisation of Mn and Fe compounds in rock varnish can lead to removal of important compounds required to bind clay minerals to form the hard, outer layer of the varnish and to bind it to rock inner surfaces. A predominant Mn compound in rock varnish is birnessite, which has hexagonal structured sheets with binding clay minerals $\{(Na_{0.3}Ca_{0.1}K_{0.1})(Mn^{4+},Mn^{3+})_2O_4{\cdot}1.5H_2O\}$. Lefkowitz et al. (2013) demonstrated that birnessite sheets were disrupted when pH was < 7.0. Under the mildly acidic conditions observed in the Burrup, the varnish would become thinner and softer with removal of these manganese compounds. The alkaline excursion to a mean pH of 6.88, which then fell to a mean pH of 4.42 in 2019 is most likely due to a combination of NO_x adsorption processes plus the reaction of

bacterial nitrification converting the adsorbed ammonia into nitrate ions, hence the increased acidity. Alternatively, the changes with other industrial emissions in the airshed may have been the underlying cause of the changes.

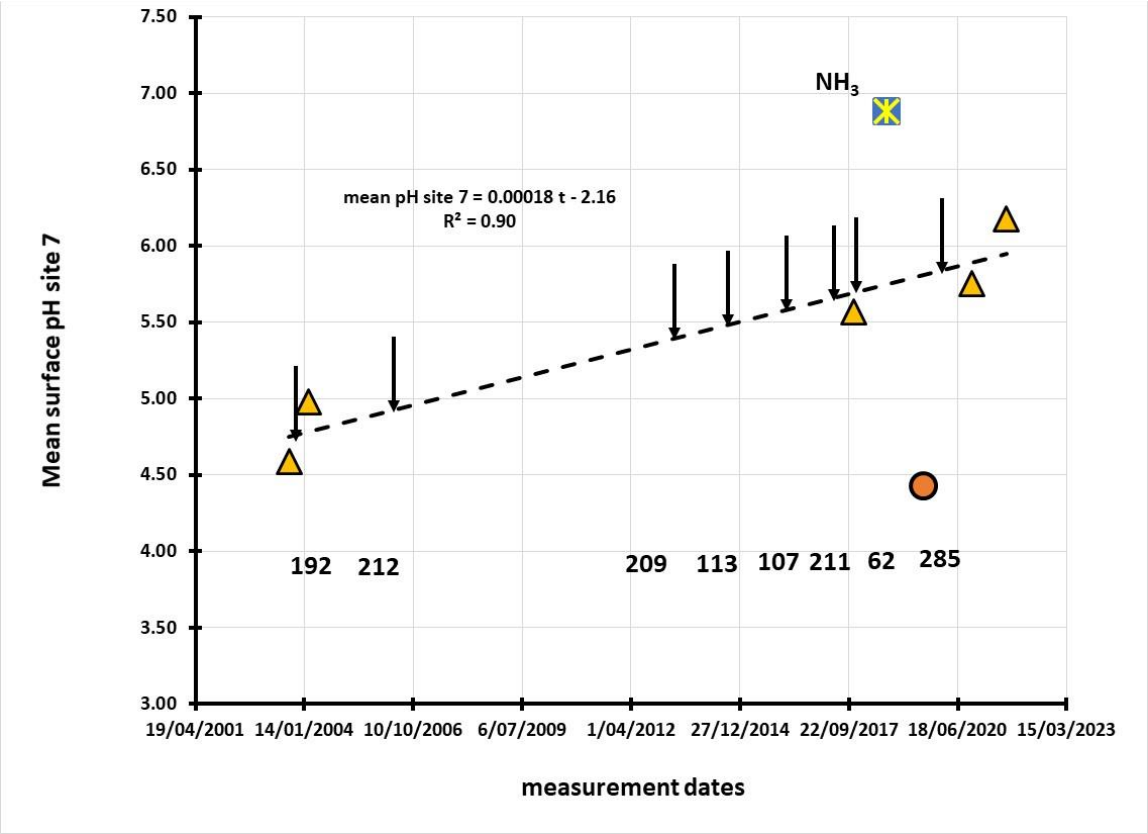

Figure 13: Mean pH at Deep Gorge between 2003 and 2021

When the "anomalous" data potentially associated with the accidental loss of ammonia in 2018 and the apparent activity of nitrifying bacteria are removed from consideration, it is apparent from the regression line in Figure 13 that there is a systematic trend towards increasing alkalinisation of the Yara monitoring rock art site no 7 at the rate of 0.000182 ± 0.00003 pH/day or 0.067 pH per year, as shown in equation 38 viz.,

$$^{mean}\text{pH site 7} = 0.000182\ t - 2.16 \quad \text{.....(38)}$$

In equation 38 the *t* interval is one day. The R^2 was moderately high at 0.90 with an associated error in the slope of equation 37 being ± 3.44 x 10^{-5} and the intercept value was -2.16. The listing of major rainfall events on the Burrup, as reported at the weather station for "nearby" Karratha airport, is shown in Table 6. It is noted that when there are major rainfall events directly impacting on the engraved rock surfaces

The Yara ammonia plant had an accidental loss of ammonia before the 2018 pH measurements were done and this may have contributed to a pH alkaline spike when the mean value at this site increased to 6.9. There was no significant alkaline response at any of the other nearby monitoring locations. However, a local increase in nitrate concentration on the rock surface saw the pH fall to 4.4 in 2019 and it is likely that the local increase in nitrate was due to bacterial activity oxidizing the ammonia to nitrate. When the mean pH is plotted against the mean nitrate concentration (Table 7) from the periods 2003-2004 followed by the interregnum of data collection to the continuing assessment from 2017-2021, it was possible to discern some systematic behaviour, which is found in equation no 39 viz.,

$$^{mean}\text{pH site 7} = 5.92 - 0.28\,[NO_3]_{ppm} \quad \text{.....(39)}$$

For this relationship the R^2 is 0.86 and the intercept error at a theoretical zero nitrate was ± 0.17 or ± 2.8% and the error in the slope of $\{^{pH}/_{NO3}\}$ was ± 0.065, which amounts to 23%.

Table 6: Major rainfall (mm) events in the Burrup 2003-2021

Date of rain event	Rainfall mm
2-Mar-04	190.8
10-Jan-06	212.4
25-Jun-13	209.4
31-Dec-13	112.8
6-May-14	107.4
9-Feb-17	210.6
6-Jun-18	62.4
8 & 9-Feb-20	235.2
11-Dec-20	63.8
5-May-21	62.8

Table 7: Mean nitrate and mean pH at site 7, 2003 – 2021

Date	mean NO_3^- ppm	mean pH
28/08/2003	5.0	4.59
23/02/2004	3.0	4.98
8/11/2017	0.4	5.57
4/09/2018	0.8	6.88
19/08/2019	2.1	4.42
23/10/2020	0.3	5.75
8/09/2021	0.4	6.18

Inspection of the pH versus nitrate concentration shown in Figure 14 it is not surprising to find some significant scatter around the low nitrate concentrations owing to the sensitivity of the sites to small nitrate concentration increases from a very low level will provide the microflora with stimulants for growth. There are two significant excursions from the regression equation, which were parked for the analyses, but they possibly relate to an accidental loss of ammonia in 2018 when the pH on rock 7 had a mean value of 6.88, the most alkaline of any of the 1,300 pH measurements done on the Burrup since 2003. During the interpretation of the reported data on rock nitrate concentration found in 2019, there was no apparent explanation for the high concentration. It has now become apparent that there is a strong likelihood that the local microflora were able to convert the absorbed ammonia into absorbed nitrate ions during the 11 months between the 2018 and the 2019 measurements. Alternatively, increased levels of NO_x from airshed emissions may have been a contributory source of the changes, for at this time there were no major cyclonic rain events to wash the micronutrients from the rock surfaces. When cyclone Damien arrived in February 2020 and dumped 235 mm of rain in the region within a 24-hour period, this would have drenched the exposed rock at site 7 and so removed any significant excess amounts of nitrate. This was reflected in the fall of the nitrate concentration from 2.1 to 0.3 ppm recorded in October 2020. The weaker rainfall events in December 2020 of 64 mm and 63 mm in May of

2021 appear to have had minor impact by the time the measurements were done in September 2021. At this point the site had received a significant deposition of sea salt and so the surfaces were provided with an increased alkaline buffer reserve, which assisted in reducing the impact of microflora metabolites on the local rock surface pH values.

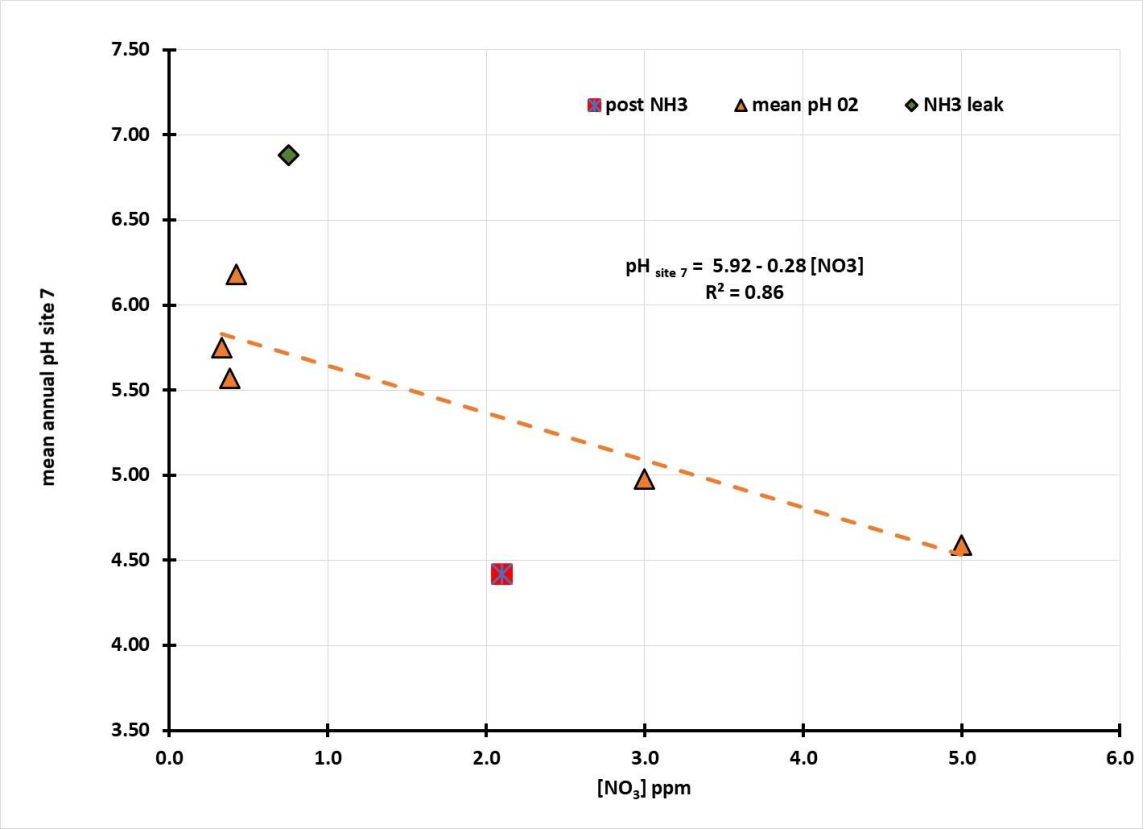

Figure 14: Plot of mean pH at site 7 versus mean nitrate concentration 2003-2021

During the statistical analysis of the historic data on surface pH across the Burrup undertaken by Fox (Fox 2020) it was noted that there seems to be a trend toward increasing acidity when moving down the rock face and that the values tend to be isobaric moving laterally. The 2021 measurements at site 7 are illustrated in Figure 12 and show these common trends. Plots of the acid profiles down the rock faces across all the sites varied, without systematic differences between granophyre and gabbro rocks, in terms of the intercept or pH values at the upper most parts of the rock surfaces. This is only natural since the mean pH of each site is dependent on the amount of chloride and the amount of both nitrate and to a lesser extent, the amount of sulphate, present in the local environment. However, the graphs of the pH/cm slope as a function of the pH at the top of the rocks all have the same slope of-34.5± 0.5 pH/cm distance down from the top of the rock.

Anions in wash solutions

Oxalates:

Analyses from the five field trips showed that only two reference rocks in the collection of the Western Australian Museum had measurable amounts of oxalate ions, $C_2O_4^{2-}$, which were 1.8 mg/l from Enderby Island (B7477) and 0.7 mg/l from Happy Valley (B2494) in the Burrup. These rocks were collected at a time before there was any industrial activity on the Burrup. The washing samples analysed for oxalate were from June and August 2003, February 2004, November 2017, September 2018, August 2019, October 2020, and September 2021. Other than in 2020, there were no oxalates found in the wash solutions. The only sites to return oxalates in the wash solutions in 2020 were site 23, which had a mean pH of 4.6 ± 0.4 and this indicates that there were active microflora or lichens

etc. that were biologically active. The other location was one of the rocks by the Climbing Man, but which was located close to the gully floor. Oxalates are major biodeterioration of pigments in the Kimberley region where the monsoonal climate has characteristic wet and dry periods. By comparison, the arid climate of the Burrup is less amenable to a wide range of bacteria and plants which produce oxalates as their metabolites. The mean level of oxalate at the two locations in 2020 was 0.13 ± 0.03 ppm which indicates that oxalate does not appear to have a significant present role in biodeterioration of the rock art in the current Burrup microenvironment.

Chlorides:

The amounts of surface chloride detected on the rock surfaces provide direct evidence of the impact of the marine environment and indicates that salt weathering of rocks, with extensive dehydration and rehydration cycles, play a significant role in the local environment. The wash solutions from the rock surfaces showed up a range of ions commonly associated with sea water, namely Na^+, K^+, Mg^{2+}, Ca^{2+}, Ba^{2+}, B^{3+}, SO_4^{2-} and Cl^-. Analysis of the way in which the concentrations varied across the Burrup was possible as the February 2004 data included several remote sites such as Gidley and Dolphin Islands in the Dampier Archipelago (MacLeod 2005). The deposition of sea salt on the rock surfaces means that the carbonate and bicarbonate ions will tend to act as buffers and minimize any changes in the surface acidity resulting from a combination of microbiological and chemical reactions on the surfaces.

The initial monitoring conducted in 2003 and 2004 involved direct measurement of the surface pH and the surface chloride ion concentrations. In addition, the washing of the rock surfaces in August 2003 and February 2004 provided data on the solution concentrations of chloride ions. All the data was then assessed through linear regression analyses and the results are summarised in Table 7, which showed that the pH increased with increasing chloride ion activity. This buffering reaction is demonstrated by the relation between the pH and chloride concentration on the rocks as shown in Equation 40,

$$pH_{mean} = a + b\,[Cl^-] \quad \text{..... (40)}$$

The 2003-2004 linear regression analyses showed that there was a common slope of the pH vs [Cl] plots but they had different intercepts, as shown in Table 7. The intercept values relate to their primary geology of the underlying rocks and the impact of factors such as the amount of nitrate on the rock surfaces, which is discussed in the following section of this report.

When the mean surface pH from 2021 is plotted against the mean surface chloride values it was found that there appeared to be no different behaviour or response based on the geological rock type. for the granophyre rocks, the post cyclone Damien response was given by Equation 41, and in Figure 14.

$$^{2021}pH_{mean} = 6.31 - 0.003\,[Cl]_{surface} \quad \text{..... (41)}$$

Because of the scattered data at the lower levels of chloride, where there was significant standard deviation in the mean values, the R^2 was only 0.86 and equation 39 had an intercept error of ± 0.08 and a slope $\{^{pH}/_{Cl}\}$ error of ± 0.0006 or 20% of the stated value. The pH decreases with increasing chloride, as expected if the dominant microflora are chloride obligates. In 2020 when the mean salt levels were significantly less, due to the washing impact of cyclone Damien rains, the pH was more sensitive by more than a six-fold difference, and this is due to the higher buffer capacity of the saltier surfaces to resist pH changes due to metabolic activities of the endemic rock microflora.

The two outlying points in Figure 14 are the sites at 21, where there were some very salty areas since the mean value was 179 ±92 ppm chloride, so the pH is being dominated by the sea salts on the rock surface. For site 23 the lower pH is probably due to the relatively high concentration of nitrate ions, at 0.65 ppm, compared with 0.25 ppm at site 21. Elucidation of the acidification and alkalinisation mechanism would be assisted if metagenomic analysis of the rock surfaces in the field

conditions be conducted to establish the nature of the distinct groups of organisms that are controlling the pH and to see if there are measurable biological differences in the colonisation of the two rock types.

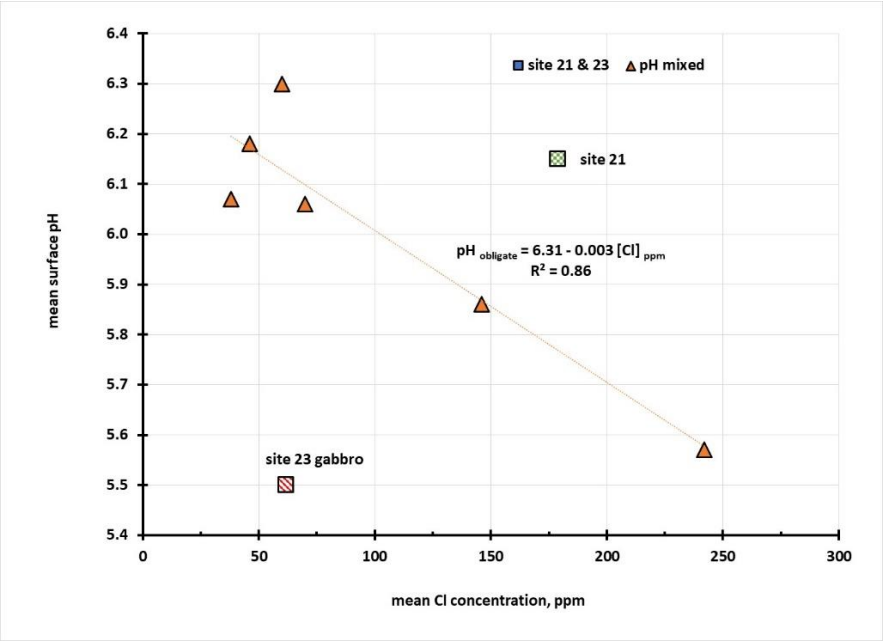

Figure 15: Plot of mean surface pH vs. mean rock surface chloride (ppm) for 2021

The data in Table 8 covers all the sets of measurements of rocks in the Burrup and in the Dampier, Archipelago shows that the build-up of sea salt deposits on the rocks does have a measurable impact on the way in which the rocks respond to changes in the chemical environment. One way of eliminating the impact of chlorinity on the pH of the rocks is to plot data from the individual rock locations, where the pH dependence on the chloride concentration has been extrapolated to zero ppm chloride i.e., to pH_{zero}. Analysis of the data presented in Table 8 shows that there is a systematic decrease in the slopes of the pH vs. [Cl] graphs between 2002 and 2021, as shown in Figure 16 and equation 42 viz.,

$$\text{slope } \{^{pH}/_{Cl}\} = 0.072 - 0.012\ pH_{zero} \quad \text{..... (42)}$$

Equation 42 had an R^2 of 0.95 with an error of ± 0.0052 in the intercept value and an error of ± 0.0011 or 9% in the slope. This relationship confirms that all the pH_{zero}, obtained from extrapolation of the pH vs. Cl plots to the zero-chloride concentration (intercept pH value), and chloride data are intimately linked. In the absence of other factors, the ability of the rocks to minimise the response to the development of an acidic microenvironment is largely controlled by the amount of salt deposition.

Inspection of the data in Table 8 shows that the solution washing concentration of chloride generally reflects the surface data, except for situations like on site 6, 21 and 23 where local wind eddies tends to focus chlorides on specific parts of the CSIRO monitoring rocks. On some sites the washing concentration was lower than the surface values, so it is these anomalous data sets that were removed from the mean calculations of the $pH/Cl_{surface}$ slopes and the mean pH. It should be noted that the solution washings were taken on rocks adjacent to the chloride and pH testing sites Improving the methodology began in 2020 by taking washings from two adjacent rocks, within 2 metres of the test rocks, an improvement in the degree of confidence of the results was made. Many of the Yara /CSIRO reference rocks have near vertical surfaces and this makes it impractical to recover samples of enough volume to allow for reliable chemical analysis of the surface wash solutions.

Table 8: Analysis of the relationship between chloride and mean pH

Date	mean Cl ppm	Intercept (*a*)	Slope(*b*) or$\{^{\delta pH}/_{[Cl]}\}$	R^2
June 2003	38 ± 40	3.4	0.030	0.98
August 2003	34 ± 31	3.4	0.033	0.98
February 2004	21 ± 15	4.1	0.023	0.98
November 2017				
Site 5: Burrup Road West	32 ± 28	5.0	0.008	0.95
Site 6: Water tanks	191 ± 97	5.4	0.001	0.96
Site 7: Deep Gorge	22 ± 12	5.0	0.026	0.77
Site 21 Yara west	125 ± 44	5.8	0.006	0.64
Site 22: Yara north east	373 ± 24	5.3	0.009	0.70
Site 23: Yara east	13 ± 17	5.5	0.021	0.77
September 2018				
Site 4 Withnell Bay Road	2.2 ± 2.1	3.0*	2.7	0.93
Site 5: Burrup Road West	4.1 ± 3.4	4.5	0.22	0.45
Site 6: Water tanks	2.3 ± 3.2	6.1*	0.13	0.01
Site 7: Deep Gorge	19 ± 8	6.0*	0.03	0.99
Site 21 Yara west	20 ± 13	5.0	0.12	0.94
Site 22: Yara north east	10 ± 11	5.5	0.03	0.34
Site 23: Yara east	30 ± 17	3.9	0.02	0.96
August 2019				
Site 4a Withnell Bay Road	4.9 ± 2.0	4.75	0.092	0.96
Climbing Man site, split	14.4 ± 0.2	4.27	0.020	0.93
Site 5: Burrup Road West	6.3 ± 2.5	4.51	0.026	0.98
Site 6: Water tanks	9.7 ± 6.3	4.41	0.029	0.94
Site 7: Deep Gorge	8.6 ± 3.8	2.57	0.110	0.99
Site 21 Yara west	95 ± 70	4.87	0.004	0.91
Site 22: Yara north east	30 ± 5	4.18	0.015	0.98
Site 23: Yara east	30 ± 10	2.46	0.015	0.97
October 2020				
Site 4a Withnell Bay Road	11.0 ± 5.6	3.88	0.073	0.94
Climbing Man site, split	10.5 ± 8.8	5.86	0.018	0.95
Site 5: Burrup Road West	5.5 ± 4.2	3.76	0.065	0.99
Site 6: Water tanks	29 ± 17	4.39	0.015	0.98
Site 7: Deep Gorge	4.8 ± 2.4	4.75	0.112	0.88
Site 21 Yara west	43 ± 31	4.67	0.013	0.98
Site 22: Yara north east	54 ± 73	4.60	0.010	0.93
Site 23: Yara east	65 ± 20	3.44	0.018	0.94
September 2021				
Site 4 Withnell Bay Road	38 ± 12	6.83	-0.015	0.96
Climbing Man site, split	70 ± 19	6.42	-0.007	0.91
Site 5: Burrup Road West	60 ± 16	6.92	-0.008	0.99
Site 6: Water tanks	242 ± 84	7.87	-0.012	0.94
Site 7: Deep Gorge	46 ± 24	6.62	-0.019	0.98
Site 21 Yara west	179 ± 92	6.98	-0.002	0.98
Site 22: Yara north east	146 ± 26	7.36	-0.014	0.85
Site 23: Yara east	62 ± 37	6.85	-0.029	0.99

- Stared sites excluded owing to systematic errors in the intercept values

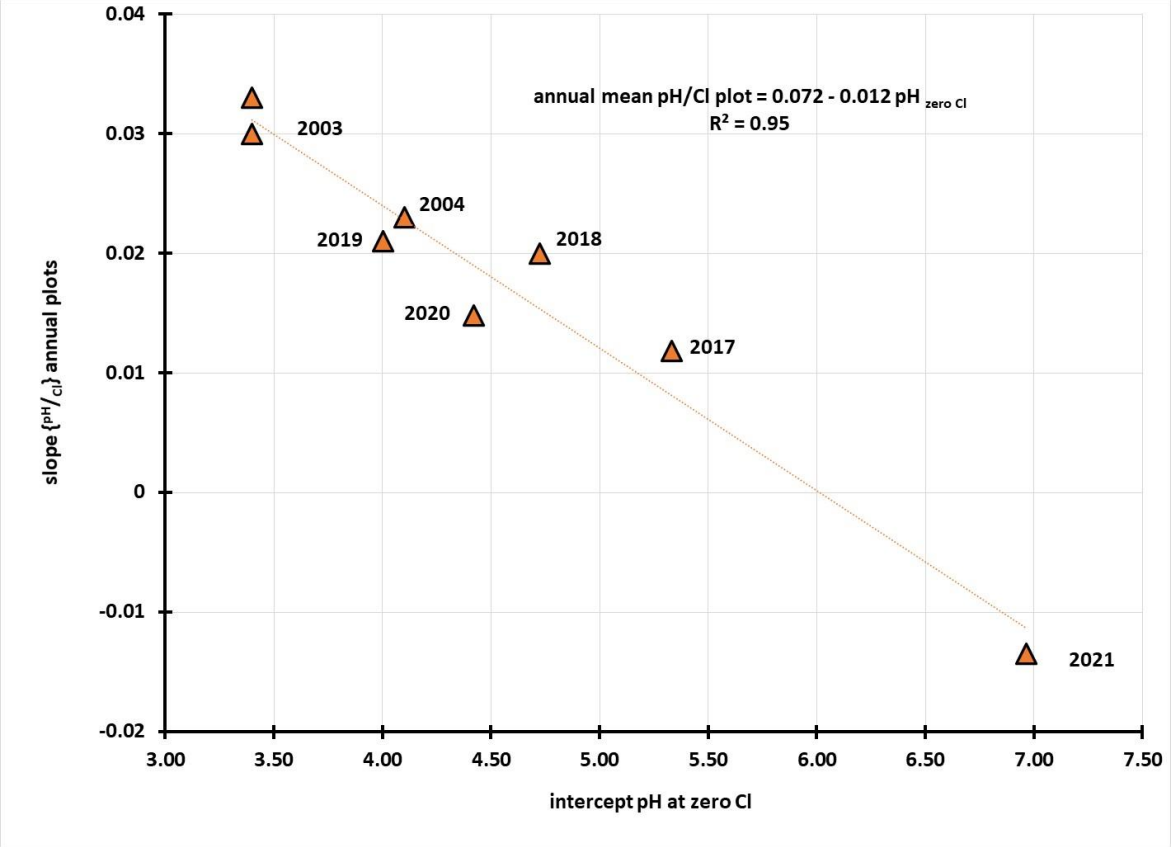

Figure 16: Plot of the slope of the pH/Cl graphs vs pH intercept at zero ppm chloride

It is interesting that the slope of the graph has not been materially affected by cyclone Damien, for the 2020 data points for the mean slope and pH_{zero} plots lie in between the values observed in 2019 and 2018. The lack of significant rainfall in the time preceding the measurements in 2021 resulted in moving the slope of $\{^{pH}/_{[Cl]}\}$ from positive to negative values because of the accumulated salts which moved the intercept pH values to the most alkaline of those ever observed on the Burrup sites.

Nitrates:

Previous studies in 2003 and 2004 had focused on the acidity and the concentration of nitrate ions, since there was strong data supporting the inference that nitrate ions were stimulating the overall microbiological activity on the rocks. Since bacterial and fungal metabolites are often acidic it was decided to check to see if there was a correlation with the number of bacteria and the nitrate levels. Data published in 2005 by MacLeod demonstrated that the logarithm of the number of bacteria was causally related to the decreasing pH, thus the amount of nitrate ions, from both natural and human sources, was likely to be a key determinant in the overall rates of weathering of the rock surfaces in the Burrup. Owing to the contrasting nature of the engraved and background areas there was concern about the long-term impact of such accelerated ageing on the rock surfaces. Surface pH values as low as 3.5 were recorded on rocks at site 4, which was 250 metres closer to the road in the same gully as the Climbing Man panels. When the initial surface pH readings were done on the engraved goanna site 4, it was assumed that by being adjacent to the Woodside operational flare tower servicing trains 1-4, that it would be due to a high nitrate concentration. As part of the February 2004 data collection, samples of rock pH, chloride and nitrate ions were collected on rock engraving sites at Gidley and Dolphin Islands in the Dampier Archipelago, in the belief that these remote sites would be low in nitrates, owing to their distance from apparent point sources on the coastal lands associated with industrial developments.

A summary of the relevant data is shown below in Table 9, which lists the mean nitrate for 2003, 2004, 2017 through to 2021 as well as the range of the maximum to the minimum values that were recorded in the analyses of the washing solutions. The major cyclonic rainfall in February 2020, when 235 mm were recorded over two-days, appears to have had a major impact on washing the accumulated nitrate ions from the rock surfaces. Inspection of the data in Table 8 shows a four-fold reduction in the amount of nitrate, as measured on sites in a total of sixteen (16) rock locations at the eight monitoring areas. During the dry period of 2021 there were a couple of major rainfalls when 60 odd mm of rain fell on two occasions during the interval between assessment measurements. It is likely that this moisture provided enough of a wetting of the rock surfaces to assist in the adsorption of NO_x from the atmosphere. It is noted from Table 9 that site 7 at Deep Gorge is very sensitive to absorption of emissions since it had the maximum values for three years in a row.

Table 9: Nitrate concentration ranges across Burrup

Date	Maximum $[NO_3^-]$ ppm	Minimum $[NO_3^-]$ ppm	Mean ppm
Aug-03	Withnell Bay, 19	Burrup SW 1–2 1.5	6.3 ± 5.1
Feb-04	Rock 938, 9.2	Deep Gorge 1.3	4.5 ± 3.7
Nov-17	Site 21 1.8	Site 5 0.10	0.6 ± 0.7
Sep-18	Site 7 1.4	Site 22 0.19	0.7 ± 0.4
Aug-19	Site 7 2.1	Climbing Man split 0.15	0.7 ± 0.7
Oct-20	Site 7b 0.46	Site 22 b 0.06	0.17 ± 0.10
Sep-21	Site 6a 1.1	Climbing Man b 0.08	0.31 ± 0.27

Although the mean nitrate concentration was the same in August 2003 and February 2004 (within experimental ranges) the amount of $[NO_3]_{ppm}$, as seen in Table 9, diminished by over 40%. This is in line with the 30% reduction in the mean nitrate concentration between the two sets of measurements. The data in Table 10 shows that common intercept pH values, at zero nitrate, at 5.69 for the 2003 and 2004 analyses. The common intercept value shows that the same chemical mechanism is controlling the response of the rocks in those two seasons of measurements. It should be noted that with the R^2 value of 0.97 the 2003 intercept value of 5.33 value is within experimental line fitting error the same as the 5.44 from rocks in the museum compound that was noted in February 2004. Of concern were the lower $pH_{intercept}$ values of 4.95 and 4.66 for sites that included rocks in the museum compound as well as those at the Climbing Man, Deep Gorges and Withnell Bay sites.

In the 18-years since the February 2003 data was collected, there were eight cyclonic rain events, as listed in Table 6, which deposited between 63-212 mm of rain in the region in a 48-hour period. These periods of inundation of the rock surfaces are likely to be the underlying reason for the big drop in the nitrate ion concentration found in the rock washings in November 2017 and again in October 2020. There was a 62.4 mm rainfall event on 6th June 2018 which would have caused significant washing of the rocks in the test areas. The five-fold fall in nitrate concentration would have been expected to reduce the impact of the biological activity due to the nitrate concentration, but other factors appear to have weighed heavily in bringing about a change in acidification. It has been noted that the mean chloride ion concentration on the Yara sites is approximately 30 times saltier in November 2017 than the rocks that were sampled in February 2003. For the most recent season of measurements there was a better correlation of the minimum pH with the solution concentration of nitrate ions. For most of the sites the R^2 value of 0.95 have a slope of $\{^{pH}/_{[NO3]\ ppm}\}$ of -1.59 ± 0.18 and an intercept pH of 5.97 ± 0.06. The three other sites with a lower R^2 value of 0.90 had larger errors and so the slope for sites 6 and 22, was -1.68 ±0.40 which makes it the same nitrate

dependence as all the other sites. The intercept value was at a pH of 5.58 ± 0.13 and so the extrapolated pH values are not sensitive to specific rock types, as both relationships contained both representatives of gabbro and granophyre rocks.

Table 10: Dependence of pH on the nitrate concentration found in wash solutions

Date	$pH_{zero\ NO3}$	Slope pH/[NO3]	R^2
Aug-03	5.69, Climbing man, Deep Gorge & Compound	-0.14	0.92
	5.33, Burrup SW, King Bay & Compound	-0.14	0.97
Feb-04	5.69, Withnell & Compound	-0.08	0.91
	5.44, Compound	-0.08	0.99
	4.95, Withnell & Compound	-0.07	0.66
	4.66, Deep Gorge & Climbing Man	-0.08	0.78
Nov-17	6.18, Sites 5,6,7, 21, 22 & 23	+0.94 log [NO_3]	0.99
Sep-18	3.14 all sites other than 22	non-linear	0.86
Aug-19	4.41_{min}, sites 5, 21 & 22	0.39	0.97
	3.76_{min}, sites Climbing Man, 7 & 23	-0.22	0.87
	4.60 $_{median}$, sites CM, 6, 7, 22 & 23	-0.04	0.43
	5.56 $_{median,}$ sites 4a, 5 & 21	-1.13	0.79
Oct-20	6.68_{mean}, sites 4, 5, 6, 21 and CM split	-8.7	0.93
	5.82_{mean}, sites 4, 21 & 23	-7.2	0.81
	$5.67_{minimum}$, granophyre & 23	-5.7	0.96
	$4.96_{minimum}$, sites 5 & 22	-4.7	n.a.
Sep-21	$5.97_{minimum,}$ sites 5, 7, 21, 23 & Climbing Man $5.58_{minimum,}$ sites 6 a & b, 22	-1.6 -1.7	0.95 0.90

The rougher and more complex surface of the gabbro rocks hold onto moisture for longer periods and, able to retain nitrate nutrients, and so provide a better microenvironment for the microflora. However, it is noted that the data scatter for the nitrate concentration values across these groups is not statistically significant. The nitrate dependence (slope) of the rocks in 2021 were much smaller than in 2020 because of the higher sea salt surface concentrations. Sea salt evaporites deposit calcareous minerals and so some of the acidity produced by the microflora is adsorbed by the carbonates and is converted to less alkaline bicarbonate ions and this tends to be quite soluble and is readily lost to the external environment. When the $\{pH/_{[NO3]}\}$ slopes are the same it is a strong indication that the degradation mechanisms are the same. In the case of the Burrup granophyre and gabbro rocks the principal form of degradation relates to acid assisted dissolution of microscopic amounts of the rock patina.

Examples of the impact of NO Major Rainfall events is seen in a comparison of the 2020 and 2021 sensitivity of the $\{^{pH}/_{NO3}\}$ slope for in 2020 there was little salt to buffer the impact of the microflora responding to increases in the nitrate concentration and so the slope had an average value of -8 ±1 for nitrate being ≤ 0.25 ppm. In 2021 when there had been much less rain and therefore an accumulation of sea salts, the $\{^{pH}/_{NO3}\}$ slope was -1.87 ± 0.07 pH/ppm, for nitrate concentration being ≤ 0.70 ppm. This comparative data shows the real value of doing repeated measurements at the same points and at roughly the same time of the year so that subtle or gross changes, such as cyclonic rainfall, can be assessed for their overall impact on the corrosion chemistry of the rock surfaces.

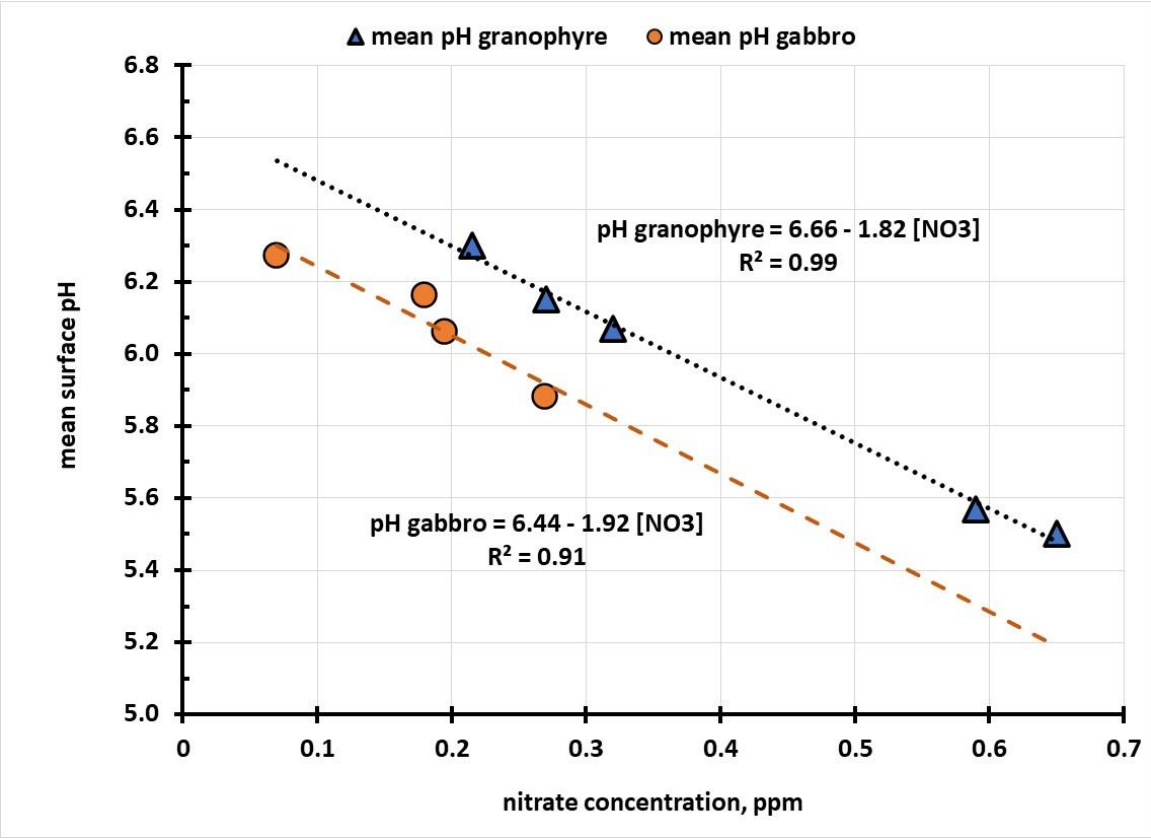

Figure 17: Plot of mean pH in 2021 against the nitrate surface concentration

Analysis of the regression statistics for the data plotted in Figure 17 shows that the granophyre slope of -1.82 ± 0.19 is statistically the same as the gabbro slope of -1.92 ± 0.28, as could be anticipated since the deposition of buffering sea salts is not going to differentiate between the two main rock types. Inspection of the graph shown in Figure 17 does indicate that the more complex surface of gabbro rocks gives a lower intercept pH value of 6.44 ± 0.04 while the smoother surface of the granophyre rocks had an intercept value of 6.66 ± 0.12, which is statistically significantly different to the gabbro intercept. This reflects the differences in the two rock types of being able to provide a higher moisture content from the gabbro's deeply tortuous surface for hosting viable microflora populations.

In a similar vein, there are similar differences in the way in which the minimum pH responded to increases in the nitrate concentration between data collected in 2020 and 2021. Typically, the mean pH response, as indicated by the value of $\{^{pH}/_{[NO3]}\}$ was one third the sensitivity in 2021, due to the higher surface salt concentration giving good buffering of the acidic metabolites. The plots of the minimum surface pH vs. nitrate are going to be subject to more errors than the mean, which is a weighted average of all the pH readings across the rock surfaces. The natural grouping of the data from the minimum pH values does not discriminate between granophyre and gabbro rocks. The lack of differentiation is because the minimum pH is a site-specific value that reflects areas of greatest microbial activity.

The data in Figure 18 included additional monitoring sites towards Burrup Road, to the west of the monitoring points at sites 21 and seven, where the Perdaman Urea plant might be constructed. The data points associated with these readings are designated P1-P3 and the pH and nitrate concentration fell into the same groupings as the minimum pH values recorded on the normal Yara monitoring sites.

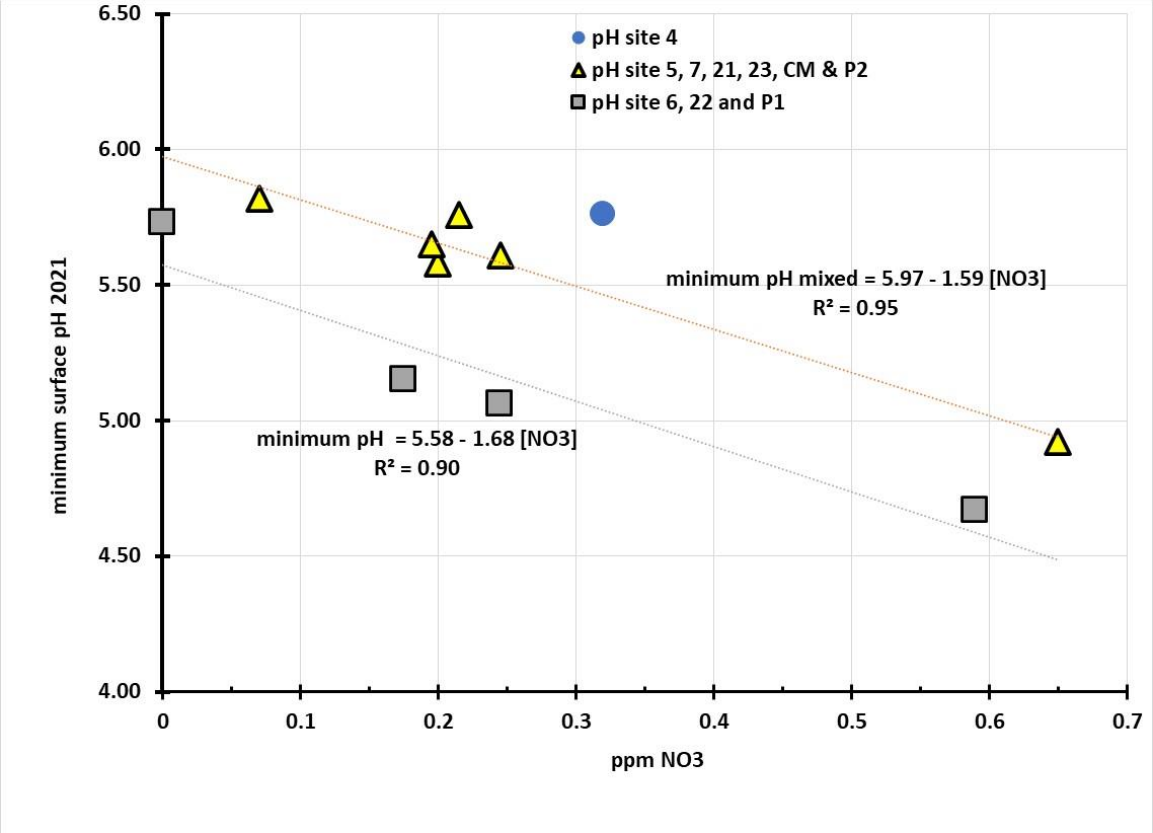

Figure 18: Plot of minimum pH versus nitrate concentration on rock surface

Sulphate

The amount of sulphate in the washings also varied from one year to the next, as shown in Table 11, which reports the data from the August 2003 and February 2004 rinses, along with the data on the Yara sites from November 2017 through to September 2021.

Table 11: Range of sulphate ions in the wash solutions on Burrup and Yara sites

Date	Maximum		Minimum		Mean [SO_4^{2-}] ppm
Aug-03	Rock 938,	66.7	Burrup SW2,	1.2	9.8 ± 14.2
Feb-04	Rock 938,	26.1	Deep Gorge,	0.8	4.9 ± 5.5
Nov-17	Site 23,	9.8	Site 22,	1.5	5.2 ± 3.0
Sep-18	Site 6,	2.2	Site 22,	0.3	1.2 ± 0.7
Aug-19	Site 21,	19.1	Site 4a,	0.4	4.5 ± 6.4
Oct-20	Site 23b,	9.3	Site 4a,	0.2	1.5 ± 2.2
Sep-21	Site 6,	20.2	Site 22,	0.2	3.5 ± 6.1

The apparent drop in sulphates reporting to the surface washings in 2020 appears to be part of the cycling of values, for the mean sulphate levels in 2018 were the same as in 2020. Since the cessation of burning inferior quality fuel in the iron ore ships it had been supposed that there would be a measurable decrease in the sulphate concentration, but the data does not discriminate from higher sea salt deposition leading to higher sulphate ion concentrations. It is however of significance that for three out of the last five years, site 22 (Yara NW) had the lowest sulphate concentration. The high sulphate concentration at site 6 is also associated with a high chloride ion activity, you can see

the halite crystals glistening in the afternoon raking light. Nevertheless, as commented upon in the section on the ratios of seawater anions to each other, site 6 may be receiving extra sulphate from SO_x adsorption onto the concentrating rock surface, before the moisture from the salt spray evaporates. If this is the mechanism, it can be noted that the extra sulphate is coming from emissions coming from the NW Gas Shelf processing plant on the windward side of the hills lying between site 6 and the ocean.

It is apparent that there is a two-fold drop in the mean sulphate concentration in the wash solutions between August 2003 and February 2004. The data shows that there has been essentially no change in the amount of sulphate present in the 2017 compared with the 2004 readings. The highest values reported were found on rock 938 in the "museum compound" which lay inland from the Climbing Man gully and was located behind the hills from the Woodside gas production facility. Unfortunately, there is no corresponding wash solution data from the relocated rock 938 in the June 2017 report. In August 2003, the pH was 4.8 ± 0.4 and in February 2004 it was 4.9 ± 0.6 which makes them statistically the same i.e., there was no correlation between the wash solution sulphate concentration and the underlying acidity. It is not possible to state if the mean sulphate levels recorded in 2019 are fully reflective of the current environment for the data measurements in 2018 and 2020 followed cyclonic rainfall events. However, in the absence of major rainfall events such as cyclone Damien, the 2021 mean sulphate levels are back to those found in 2019.

Although recent statistical analyses (Fox 2020) had indicated that there might be some association of pH with sulphate in the wash solution, there was insufficient data to obtain a valued opinion, for his analysis was done prior to measurements in the past two years. The decision to conduct duplicate rock sampling at each site has proved to be a wise investment in time and money and the results are shown in Figure 18 and in equations 43 and forty-four. There is a strong correlation between decreasing pH and increasing sulphate, as shown in Equation 43 below.

$$^{minimum}\,pH_{SO4} = 6.38 - 0.088\,[SO_4^{2-}]_{ppm} \quad \text{..... (43)}$$

Although limited to three data points from the higher chloride and thus higher sulphate activity, the R^2 value was high at 0.97. It has been previously noted that in the presence of halophytic microflora, the pH will fall with increasing chloride ion activity. In the previous discussion on the impact of chloride on the mean pH it was noted that the $\{^{pH}/_{[Cl]}\}$ slope was -0.003 for the 2021, so if this fall in pH is corrected for the impact of increased chlorinity then the sensitivity due to sulphate by itself is reduced by only 3%. In this case the lower sensitivity of the pH to sulphate concentration is roughly one-tenth that found after cyclone Damien, and this indicates that the carbonate sea salts are buffering the surface acidity. Inspection of the data plotted in Figure 18 shows two distinct areas for the lower sulphate levels, with values of ≤ 2.2 ppm sulphate. For three data points there was a significant decrease in pH with increasing sulphate, as shown in equation 44.

$$^{minimum}\,pH_{SO4} = 5.18 - 0.46\,[SO_4^{2-}]_{ppm} \quad \text{..... (44)}$$

The sensitivity of the $\{^{pH}/_{[Cl]}\}$ slope at low sulphate in 2021 is roughly half that of the response post cyclone Damien and this is again a reflection of the increased buffer capacity associated with increased chlorinity on the rock surfaces. There is a group of nine readings with a mean pH of 5.68 ± 0.08 at a mean $[SO_4^{2-}]$ concentration of 1.0 ± 0.6 ppm where the pH is independent of the sulphate ion concentration. This form of behaviour may be an indication that the sites 4, 5, 7, 21a, and the Climbing Man reference rocks may not be colonised by organisms that can metabolise sulphate ions. The higher intercept on high chloride and sulphate pH response at 6.38 is significantly higher than the zero response mean pH of 5.68 ± 0.08, so the difference of 0.7 pH (an increase in alkalinity of five) is a measure of the impact of accumulated salt spray on the rock surfaces.

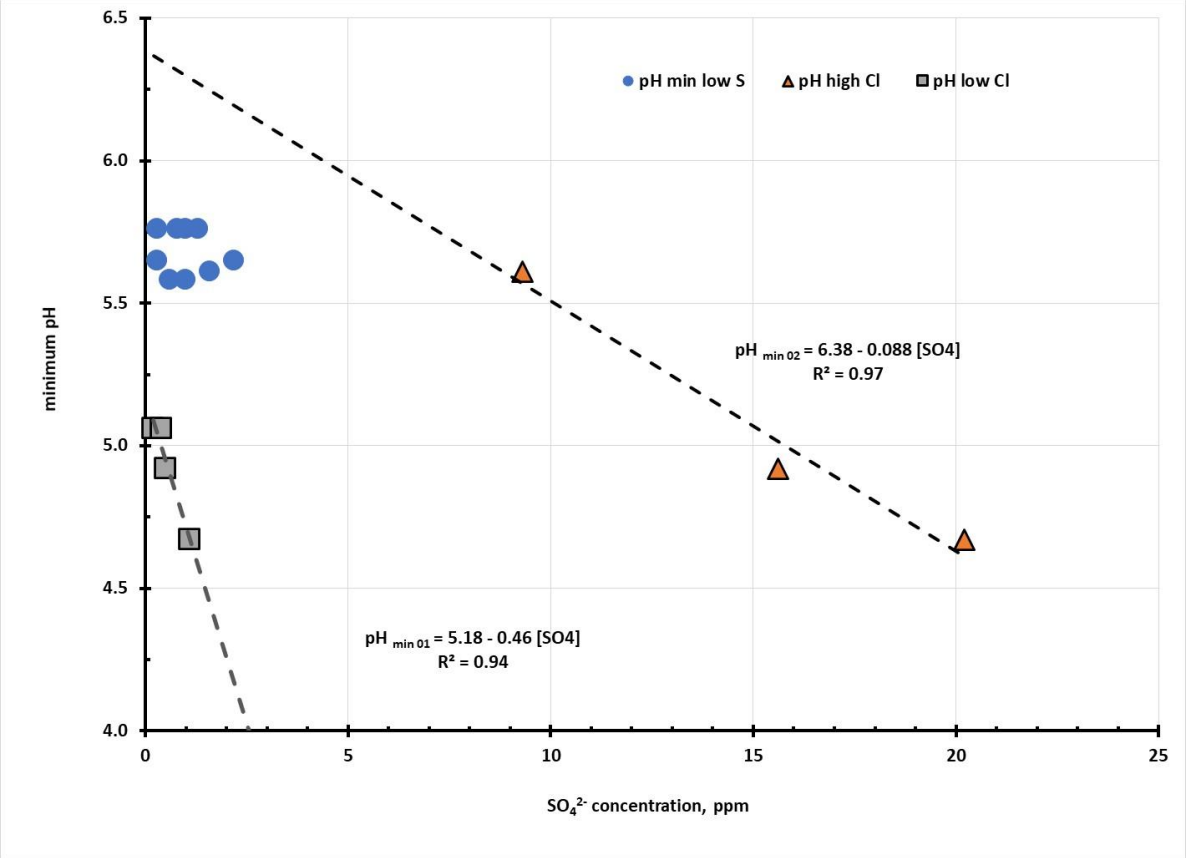

Figure 19: Plot of minimum pH versus sulphate concentration September 2021

The corresponding slope for the way in which the minimum pH responds to nitrate ions is 1.6 per ppm [NO_3^-] and the associated intercept pH values were 6.0 and 5.6, which is the same the mean zero response to sulphate pH value of 5.7, for the lower chloride environment that is consistent with the impact of rain on the rocks. The nitrate-pH correlation is significantly more sensitive than the corresponding response to sulphate ion values. It has been previously noted that the pH of the rock surfaces is significantly affected by the chloride levels, coming from the sea salts, so it is instructive to see how the $^{Cl}/_{SO4}$ ratios vary across the Burrup in the different periods of measurement. The normal ratio of chloride to sulphate ions in seawater is 7.1 so values that are lower than this indicate that this is due to either additional sources of chloride ions or that sulphate ions have been in some way sequestered on the rock surfaces.

Even a cursory inspection of the data in Table 12 shows that cyclone Damien has had a major impact on the amount of sulphate on the rock surfaces. Data from 2020 for sites 4, 5, 21 and the Climbing Man split rock the amount of sulphate was ≤0.5 ppm but in 2021 the mean amount of sulphate was 3.5 ± 6.1, which is associated with increased deposition and accumulation of sea salts on the rock surfaces. Since the detection limit for ion chromatography for the sulphate ion is 0.1 ppm the errors in the ratio are significantly amplified at low sulphate levels. The two sites with high $\{^{Cl}/_{SO4}\}$ ratios were the rocks at site 4b and 22a, both of which have microfossils on the rock surface, and this can lead to lowered sulphate activity due to the formation of gypsum ($CaSO_4.2H_2O$).

During the inspections of the Climbing Man site in 2019 - 2021 it was noted that there were “streams” of iron containing minerals flowing down from the rocks above the panels, which coursed down behind the main rock. These light-coloured iron minerals may be due to upward facing rocks lying at higher elevations than the Climbing Man becoming increasingly weathered, as the condition

of the engraved panels on the near vertical rock surface do not appear to have changed in the past 18 years.

Table 12: Ratios of chloride to sulphate ions in the wash solutions from Burrup rocks.

Date	mean Cl/SO4	high Cl/SO4	low Cl/SO4
Aug-03	5.7 ± 5.4	11.8 ± 6.6, rock 162 & CM†	3.1 ± 1.2, covering 14 sites
Feb-04	21 ± 15	9.9 ± 5.1, 14 sites including CM, Rock 3	4.3 ± 1.2, covering 27 sites with Gidley & Dolphin Islands
Nov-17	1.1 ± 0.3	2.2, site 22	0.7, site 7,
Sep-18	2.8 ± 1.8	6.0, site 22 Yara NE	0.7, site 4
Aug-19	3.0 ± 1.3	4.7 ± 0.5, sites 21, 22 & CM	2.1 ± 0.5; 4, 4a, 5, 6, 7, 23
Oct-20	52 ± 49	**64 ± 48**; sites 4, 5, 6,7a, 21,23a & CM	**5.0 ± 3.4**; 7b, 22a & 23b
Sept -21	3.6 ± 1.9	**8.0 ± 2.0 sites 4b & 22a**	**3.0 ± 0.8, all other sites**

† CM relates to the split rock to the left of the main panel at Climbing Man

It would be prudent to have experienced rangers and supervised personnel inspect the upper rocks in the gully which lie above the main engraving to see if there are any specific forms of deterioration, and to take representative pH readings.

Comparison of pH between 2017 - 2021

Granophyre sites

A summary of the differences between the two seasons of measurements is found in Table 12 and in Figures 19 – 21 below. The granophyre sites nominated by the CSIRO are those listed as sites 4, 5, 6 and number 21 and the seasonal mean pH values for the five years of monitoring for Yara are shown in Figure 19. For site 4 at the head of the Woodside Gully there is a progressive decrease in acidity from the very low value of 3.8 in 2017 to 4.3 in 2018 and then a smaller increase in alkalinity to a pH value of 4.4 in 2019, which is within experimental error of there being no change in acidity. This site was clearly impacted by heavy rainfall events associated with cyclone Damien which increased the pH to 4.8. Finally, the 2021 mean pH was 6.1 due to the accumulation of sea salts from the wind borne salinisation reactions.

By way of contrast the small rock numbered 5 by CSIRO, the engraved cormorant near the Burrup Road adjacent to the Yara monitoring station and close to the Woodside Pluto flare tower, showed a progressive decrease in pH between 2017 and 2020, where the mean pH was the same as site 4. Clearly this site was not positively impacted by cyclone Damien as there was no decrease in acidity and so it appears that the rock was in a rain shadow area during the heavy inundation period. When the site was inspected in 2021, it was noted that there were sparkling crystals of halite (NaCl) on the rock and this has impacted on the mean pH by shifting the values from 4.7 to 6.3, or a 40-fold decrease in acidity.

The Water Tanks, site 6, was the third most acidic site at an initial pH of 5.7, which increased (like site 4) to a value of 5.8, which is well within the standard deviation of the mean values. The pH then fell to 4.7 in 2019, a ten-fold increase in acidity before the impact of cyclone Damien, which increased the pH to 5.3 or a five-fold decrease in acidity, which made it the same pH as the nearby site 21, on top of the hill to the west of the Yara ammonia storage tanks. The increased chlorinity

associated with the accumulation of sea salts on the large rock at site 6 saw the pH increase to 5.6, which is only a small decrease in acidity by a factor of two times, but a nevertheless a welcome change.

The Yara West site (CSIRO no 21) sits as an inclined flat top rock abreast the top of a steep hill within easy striking distance of the main Yara ammonia tanks. The overall trend in the pH of this site is like the other nearest site, no 5, at Burrup Road with a linear distance of 1.8 km between the sites, in that there was increased acidity in 2018 and 2019, followed by a plateau after cyclone Damien, which appears not to have directly impacted on the monitoring site. The final 2021 measurement was done at a time of increased chlorinity, and so the pH increased from the 2020 value of 5.3 to 6.2 or an eight-fold decrease in acidity.

At the conclusion of the 2021 monitoring program three of the four granophyre sites had the same pH, with an average value of 6.02 ± 0.32 and the extended period of dry weather has provided a new measurement baseline. The complexities of site 6 have already been alluded in previous discussions of the impact of rain shadows on the site, which explains why it had the widest range of pH values of 1.89, from the minimum of 4.67 to a maximum of 5.57.

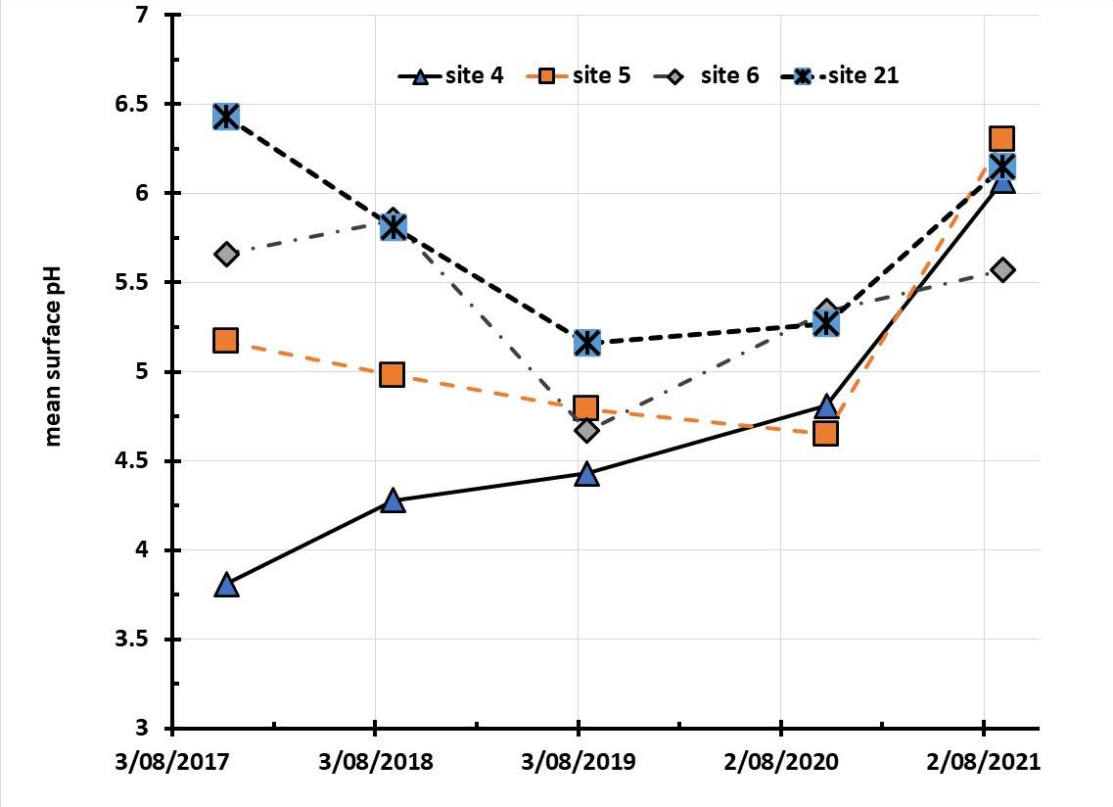

Figure 20: Plot of mean pH between 2017-2021 for the granophyre CSIRO sites

Gabbro sites between 2017-2021

Inspection of Figure 20, the plot of mean pH for the gabbro sites at 7, 22 and 23 (CSIRO labels) shows some significant swings in the pH for site 7. The jump from a mean pH of 5.6 to 6.7 was due to the site being downwind of the Yara ammonia tank farm and the local environment monitoring station, before it was relocated closer to Hearson's Cove, provided pivotal information about why the jump occurred as rainfall near the time of the event confirmed the significant alkalinisation of the rain water by ammonia and ammonium mixtures. During the year between the alkaline excursion, it is

possible that nitrifying bacteria converted the adsorbed ammonia into nitrate since the drop to a pH of 4.4 was also associated with the highest NO_3^- concentration for 2019. The Deep Gorge site was severely impacted by cyclone Damien as the rock surface was stripped of chloride and nitrate in heavy rain, which brought the pH up to 5.75. With no large rainfall event in the year before the 2021 measurements were taken the increased surface chloride readings and low nitrate brought the pH up to 6.18, which is the same mean pH as observed for three of the granophyre sites, as described above.

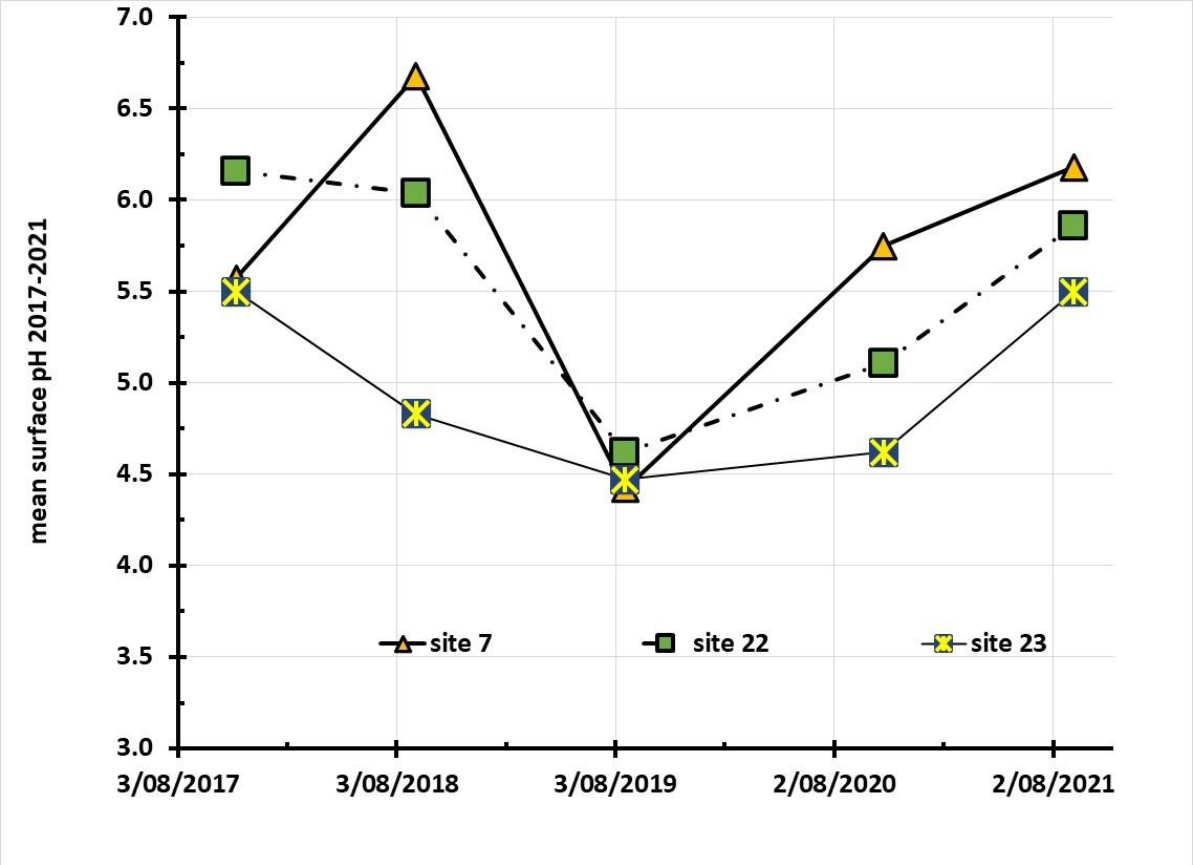

Figure 21: Plot of the mean surface pH on the gabbro sites in 2021

In reviewing the pH-time profiles for sites 22 and 23 it should be noted that site 22 sits high on a ridge above a gully and at times the winds can be so strong as to topple a standing adult, with gusts of up to 55 km/hour being recorded in 2018. These two sites have a similar easting bearing and are only 645 metres from each other, with site 23 being down on the flat area that characterises the upper section of the ancient flood plain. For site 22 there was a high local concentration of nitrate found in 2019 which may have been associated with wind borne debris from the Technical Ammonium Nitrate plant which is on a NE bearing from the TAN plant. Rainfall from cyclone Damien resulted in an alkaline pH shift of 0.5 and then the increased sea salt deposition further increased the pH to 5.9, which is within the standard deviation of site 7 mean value.

The monitoring rock no 23 is a near vertical site with a large expanse of engravings that are sheltered from the sun in the morning and are exposed in the afternoon light. The low pH value in 2019 was also associated with a high nitrate concentration and it was thought that this might be due to dust being carried from the TAN plant across the plain in an easterly direction. The mean pH value in 2020 is essentially the same as it was in 2019 and this is most likely due to protection of the surface from the prevailing winds that would have brought in the cyclonic rain. The increased

chlorinity on the rock resulted in the same jump in pH as had been observed on site 22, as can be seen in Figure 20.

Climbing Man sites (non-CSIRO)

Apart from a hiatus in 2018, when field operations prevented the recording of the pH on the split rock to the left of the Climbing Man panel, the Yara monitoring was done on a complimentary basis to provide essential information to the Murujuga Aboriginal Corporation and to Yara about the conditions prevailing on this most iconic of rock art sites in the Burrup. Owing to the deep social significance of the main Climbing Man panel, which is almost vertical in orientation, and to the very exposed conditions for footholds, it was not possible to record the chloride ion and the redox potentials directly on this site. Therefore, the conjugate rock, which split across on a diagonal line in 2018, was monitored in full detail like the seven Yara sites, which included the additional site 4 at the head of the Climbing Man gully, adjacent to the Withnell Bay Road, but some 25 metres down in a gully.

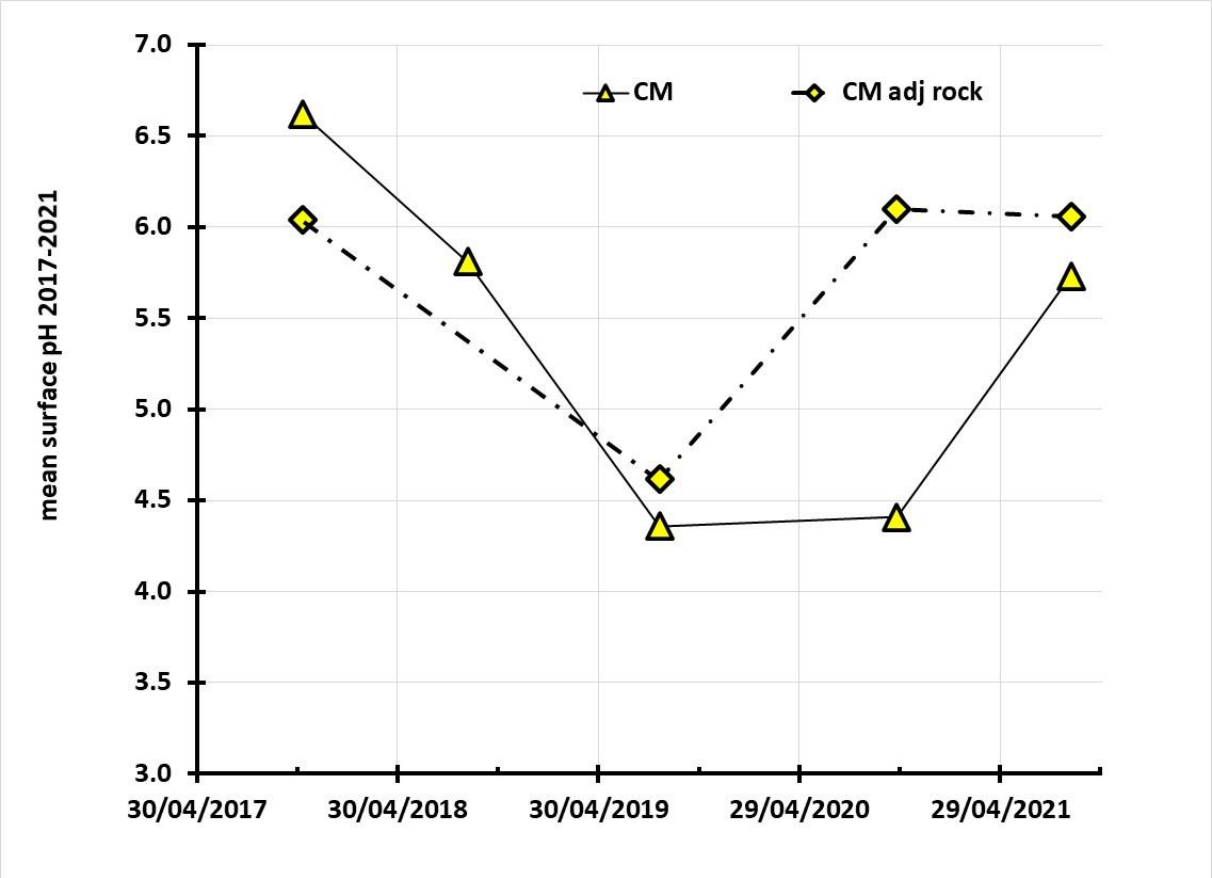

Figure 22: Comparative plots of mean surface pH at the Climbing Man sites

The data on the Climbing Man site was initially alarming as the pH fell by 0.41 (2½ increase in acidity) between the first season of measurements in 2017 and the following year. This was followed by a continued drop in pH of an additional 1.45 units, giving a total fall of 1.86 or an increase in acidity by 72 times. When the site was inspected again in 2020 the pH was experimentally the same but when the 2021 measurements were done the mean pH had increased to 5.73, at which very little iron and manganese minerals will be mobilised (see above discussions on mobilisation of these indicator transition metals). Clearly, the cyclonic rain from the direction of the ocean had not come to the Climbing Man since the 2020 pH was the same as in 2019. During the long dry period it is apparent

that the site adsorbed sea salt spray and this neutralized the acidity from the microbial activity and brought the pH back to a much safer condition.

The value of collecting data on the adjacent (now split) rock, which is approximately two metres further up the gully than the main panel, is that it is on a 35-degree slope from the horizontal and so it is possible to collect reliable in-situ data and to collect washings. Because this site is in the open it was directly affected by the cyclonic rainfall and so the pH went from 4.6 to 6.1 with the rain i.e., the acidity clock was reset. The accumulation of salts on this site was not as severe as on other areas, such as at sites 5, 6, 7, 21, 22 and 23 and so the pH remained constant between the measurements in 2020 and 2021.

The overall impact of the period of low rainfall and plenty of wind-borne sea salt deposition is illustrated by the data in the right-hand column in Table 13. The greatest increase in alkalinity was noted on the Climbing Man and the Burrup Road (no 5) sites with a shift of 1.65 in pH and the least affected was site 6, which was already partly stabilised at a pH of 5.34. The deposition of sea salts and the localised rainfall events, which are a characteristic of the arid hot environment of the Burrup, had moved the most acidic site 4 (Woodside) monitoring rock from an initially very low value of 3.8 in 2017 to 6.1 five years later.

Table 13: Mean surface pH between 2017 and 2021 and delta $pH_{2021-2020}$

Location	2021	2020	2019	2018	2017	pH change '21-'20
site 23	5.50	4.62	4.47	4.83	5.50	0.88
site 22	5.86	5.11	4.62	6.04	6.16	0.75
site 21	6.15	5.27	5.16	5.81	6.43	0.88
site 7	6.18	5.75	4.42	6.68	5.57	0.43
site 6	5.57	5.34	4.67	6.03	5.66	0.23
site 5	6.30	4.65	4.79	4.98	5.17	1.65
site 4	6.07	4.81	5.52	4.28	3.81	1.26
Climbing Man	6.06	4.41	4.36	5.81	6.04	1.65

In summary, the natural environment of the Burrup dominates the surface acidity of the rock surfaces when periods of prolonged low rainfall events allow the accumulation of alkaline sea salts. The salts have a neutralizing effect on the acidity produced by the microflora. It is readily apparent that the pH falls in response to increased nitrate availability on the surface. It would be unreasonable to assume that just because of its iconic nature that the granophyre vertical engraved surfaces on the main Climbing Man panel is not subject to the same environmental parameters as the other granophyre rocks. Thus, it can be inferred that the cause of the increasing acidity at this site during the 2018 and 2019 seasons is due to there being enough moisture around to facilitate the adsorption of NO_x from the atmosphere. Owing to the local microtopography, the main panels are not readily exposed to rainfall events and so therefore the acidic environment was not changed by the heavy rains associated with cyclone Damien in February of 2020.

Summary of the surface pH, chloride & redox at Yara sites

It should be noted that in the 2017 measurements on the Yara test sites only the surface pH and chloride ion activities were recorded. The utilisation of redox data on the Burrup rocks was not developed until July 2017 and was not adopted until after peer review had confirmed it was a viable indicator of chemical activity on the rock surfaces (MacLeod 2019). For this section of the report, the statistical analysis of the distribution of pH, chloride, and redox potentials for each of the sites is discussed in turn.

Summary observations on site 23

There was concern noted that there was an acidification trend for this reference rock, with a steady decrease in the pH value from 2017 through 2018 and down to 2019. There appears to be a moderate amount of nitrate in the surface washing of the rock which could supply extra micronutrients for the microflora living on the rock.

Table 14a: Statistical analysis of pH values on site 23 from 2017-2021

	2021	2020	2019	2018	2017
Mean	5.50	4.62	4.47	4.83	5.5
Standard Error	0.10	0.13	0.08	0.18	0.2
Median	5.53	4.68	4.6	4.63	5.65
Mode	5.46	4.76	4.62	4.63	#N/A
Standard Deviation	0.33	0.44	0.28	0.64	0.62
Range	1.03	1.52	0.9	2.15	1.97
Minimum	4.92	3.82	3.8	4.16	4.42
Maximum	5.95	5.34	4.7	6.31	6.39
Count	12	12	12	13	10

Although the standard deviation of the pH values in 2019 and 2020 show that the slight increase in pH between the mean values, due to the cyclonic rains in February 2020, it is more telling to see that the rains kept the minimum pH at the same level and that the rain impact was more noticeable in the five-fold decrease in acidity after the big rain. The reassuring shift in the mean pH took place in the period before the 2021 measurements, when the accumulation of sea salts restored the buffering capacity of the rock.

Table 14b: Statistical analysis of redox potentials on 23: 2018-2021 volts vs. NHE

	2021	2020	2019	2018
Mean	0.357	0.323	0.397	0.484
Standard Error	0.004	0.005	0.006	0.004
Median	0.354	0.322	0.395	0.482
Mode	#N/A	0.311	0.395	0.287
Standard Deviation	0.015	0.018	0.019	0.016
Range	0.053	0.07	0.064	0.068
Minimum	0.339	0.294	0.361	0.238
Maximum	0.392	0.364	0.425	0.306
Count	12	12	13	14

There was a steady decrease in the E_h values during 2018-2020 which is consistent with lower solubilities of electrochemically active iron species, which may also be expressed in terms of a changed energy source for bacteria which can utilise the latent power in changing oxidation states with iron and manganese minerals. The increased E_h value in 2021 is due to some more soluble iron minerals, since the reference rock 23b had 5 ppb iron, but rock 23a was below the detection limit. It is noted however, that this reference site had the only measurable amount of iron present in the wash solutions on the adjacent rock, some 1.5 metres away but which were essentially horizontal in aspect rather than being vertical.

The full list of chloride-based sea salts, as indicated by the free chloride reporting to the wash solutions and by the direct measurements of chloride activity on the rocks with the ion-specific electrode, is listed in Table 14c. The winds coming up from Hearson's Cove explain the relatively rapid build of chloride concentration after the cyclone and the local wind patterns must have remained constant in the area since the mean chloride activity in 2021 is experimentally the same as in 2020 and are roughly three times the initial data reported from 2017. Clearly, there are salty patches on the rock surface owing to the complex topography of the near vertical surface of the engraved panel, as shown by the highest chloride level in 2021 being 161 ppm, which indicates that rainfall events have not been common on this site for over a year.

Table 14 c: Chloride readings on site 23 between 2017-2021, values in ppm

	2021	2020	2019	2018	2017
Mean	61. 7	65.3	30.4	29.6	18.5
Standard Error	10.6	6	2.8	4.6	5.5
Median	48.5	70.5	30	25	11.5
Mode	#N/A	70	32	#N/A	6
Standard Deviation	37	20.7	9.7	17.2	17.4
Range	133	71	40	53.7	50.5
Minimum	28	15	16	11.5	4.5
Maximum	161	86	56	65.2	55
Count	12	12	14	14	10

Summary observations on site 22

This site lies high on top of a hill on a ridge running towards the coast and the small, engraved rock looks to the east and lies at about 75° to the vertical, so it is well drained. The cyclone Damien shifted the mean pH by 0.49 or decreased the acidity by a factor of three times (see Table 15a). A year without significant rainfall saw the mean pH increase from 5.11 to 5.86 and this is due to increased salinity due to the accumulation of sea salts, which ranged from 39 to 245 ppm, which is a three-fold reduction in acidity. The increased salinity on the rock has increased the surface buffering, which resisted the impact of microflora capitalising on a relatively high amount of nitrate at a mean value of 0.25 ± 0.03 ppm. The maximum pH of 6.5 is associated with the areas of highest surface salt concentration. During the 2019 on site measurements the wind was gusting strongly, with estimates of speeds up to 70 km per hour, which tended to knock the assessment team off their feet. The location is to the North East of the Pilbara nitrates plant and the mean pH for 2019 was significantly lower than it was in the two previous years, and this is due to the relatively low chloride surface readings not being able to buffer the acidity from the bacterial response to the increased nitrate levels, which are likely to be transported by strong winds and may be sourced to operational emissions of ammonia from the Yara Pilbara plants.

The data listed in Table 15 b summarises the way in which the electrochemically active minerals are reporting to the platinum electrode. Between 2018 and 2019 there was a drop of more than 100 mV in the E_h of the surfaces and this is a meaningful change, which is likely associated with changes in the solubility of both iron and manganese minerals. Inspection of the iron solubility reports for 2018 show that there is low solution activity on the surface and so the more positive E_h value is likely due to increased surface concentrations of oxidized forms of manganese minerals. Plots of the 2021 E_h data as a function of chloride ion activity shows only a small dependence of E_h on chloride at about 3 mV per ppm chloride. After the initial fall in the redox potential at site 22 it has remained remarkably

constant, which indicates that the chemical environment is not changing, despite the very large changes in chloride ion activity shown in Table 15c below.

Table 15a: Statistical analysis of pH values on site 22 from 2017-2021

	2021	2020	2019	2018	2017
Mean	5.86	5.11	4.62	6.04	6.16
Standard Error	0.12	0.1	0.03	0.17	0.15
Median	5.87	5.15	4.61	5.82	6.42
Mode	6.26	n.a.	4.55	n.a.	6.42
Standard Deviation	0.42	0.41	0.1	0.57	0.48
Range	1.42	1.35	0.37	2.01	1.3
Minimum	5.06	4.58	4.48	5.3	5.3
Maximum	6.48	5.93	4.85	7.3	6.6
Count	12	16	14	12	12

Plots of the chloride distribution across the rock were made, consisting of four measurements at a common height then 13 cm down and a total of 26 cm down from the top row. This analysis showed up atypical phenomena. Instead of the normal isotropic chloride values across the rock, the chloride ions were highly anisotropic. Plots of chloride concentration against the distance from the LHS of the rock showed sequential falls in chloride: the uppermost row had a calculated edge value of 332 ppm the second row gave 279 ppm and slightly lower at 257 ppm for row 3. Instead of gravity fed solutions resulting in increased chloride at lower levels, the winds had driven the salts upwards and backwards across the rock at the rate of +5.5 ± 1.6 ppm/cm distance. On the left side of the rock, the chlorides fell from 250 ppm to a steady value of 200 ppm for the second and third rows. Just 13 cm across the rock from the first column, the second column had a value of 125 ppm which increased to a steady value of 200 ppm in the lower levels. The third column showed similar trends to the first, with a 70-ppm fall from 170 ppm to a steady value of 100 ppm. Data from the right side of the rock was the mirror image of data from the left since it had a common level of 50 ppm for the first and second row before climbing to 100 ppm on the bottom row. This complex chloride distribution is consistent with a swirling wind pattern creating a series of microenvironments on the surface of the quite small 48 x 40 cm sized rock.

Table 15b: Statistical analysis of redox potentials vs. NHE at site 22: 2017-2021

	2021	2020	2019	2018
Mean	0.386	0.392	0.382	0.492
Standard Error	0.008	0.004	0.005	0.004
Median	0.385	0.39	0.387	0.495
Mode	0.345	0.408	0.388	0.491
Standard Deviation	0.029	0.014	0.018	0.012
Range	0.082	0.048	0.059	0.044
Minimum	0.345	0.365	0.348	0.458
Maximum	0.427	0.413	0.407	0.502
Count	12	16	14	12

Since there is the likelihood that some of the increased acidity is due to chloride obligate bacteria, the pH measurements made in 2021 were plotted against the chloride ion concentration and the

data shows support for this supposition. Where there are no obligate bacteria the mean surface pH increases with chlorinity, due to the increased presence of alkaline sea salts on the rock surface. A typical plot of pH vs. chloride gave a regression line given by equation 45 viz.,

$$pH_{\text{site 22}} = 7.05 - 0.015\,[Cl] \quad \text{..... (45)}$$

The R^2 for the regression line was 0.99 and the intercept at zero chloride had an error of ± 0.15 or 2%, while the error in the slope $\{^{pH}/_{[Cl]}\}$ was ±0.002 or 10%.

Table 15c: Statistical analysis of chloride ion activity (ppm) at site 22: 2017-2021

	2021	2020	2019	2018	2017
Mean	146	54.2	30.3	10.2	33.3
Standard Error	19	18.3	1.4	3.4	7.7
Median	158	16.8	30	8.5	26.3
Mode	#N/A	16	33	n.a.	n.a.
Standard Deviation	66	73.1	4.9	11.2	24.3
Range	206	236	18	40	82.5
Minimum	39	4.2	21	1.4	14.5
Maximum	245	240	39	41	97
Count	12	16	14	12	16

The increased salinity on the surface in 2021 has changed the corrosion equations used to describe the Pourbaix diagram for site 22. After cyclone Damien all the E_h / pH profiles had the same slope of -29 mV/pH, but for the new environment the slope was -55 ± 4 mV/pH. Inspection of Table 5 shows that the 2020 slope was due to $\mathbf{Mn(OH)^+ + H_2O \rightarrow Mn(OH)_2^{2+} + H^+ + 2\,e^-}$ and the dominant reaction for the 2021 season was $\mathbf{Mn^{+2} + 2H_2O \rightarrow Mn(OH)_2^{2+} + 2\,H^+ + 2\,e^-}$ with the most likely reason being due to the higher chloride background will stabilise the Mn^{2+} ion through the formation of chloride complexes and so avoid the formation of mono-hydroxy manganous ion.

Summary observations on site 21

This granophyre site is uniquely positioned on top of what is a steep sided hill which rises 25 metres above the flat land surrounding the Yara ammonia plant and it is subject to winds from the seaward, either from the open ocean waters of the Dampier Archipelago or from winds coming up across Hearson's Cove. Since the rock is almost one metre square it can be expected to exhibit some complexity in the physical chemical and electrochemical microenvironment. Inspection of the Pourbaix diagram in Figure 22 shows that there are two electrochemical processes controlling the interplay between the redox potential and the surface pH. Inspection of table 16c shows that there are areas where the $[Cl]_{max}$ was a very high 360 ppm and the minimum value was 59 ppm. At these levels of chlorinity it is not unexpected to find that there has been stabilisation of the bare Mn^{2+} ion through formation of chloro-complexes which minimise the amount of hydrolysis taking place.

For the high chloride areas of the rock the dominant redox reaction is oxidation of Mn(II) to Mn(IV) in its partially hydrolysed state of $Mn(OH)_2^{2+}$ viz., $\mathbf{Mn^{+2} + 2H_2O \rightarrow Mn(OH)_2^{2+} + 2\,H^+ + 2\,e^-}$ and these zones have a Pourbaix slope of -59 mV/pH. The redox potential and pH in the lesser saline areas on the large rock give a different Pourbaix slope of -29 mV/pH viz.,

$$\mathbf{Mn(OH)^+ + H_2O \rightarrow Mn(OH)_2^{2+} + H^+ + 2\,e^-}$$

Inspection of the pH data in Tables 16 a, 16b & 16c, shows that the accumulation of the extra saltiness, in the absence of the cleansing rain, was responsible for a much larger shift in pH of one unit or a ten-fold reduction in acidity, than cyclone Damien and its associated rain which achieved only a 0.11 pH shift to more alkaline values or a 30% reduction in acidity. For Site 21 (Yara West)

there is an apparent systematic fall in the mean pH from 2017 through 2018 to 2019, however the large standard deviation of the 2018 data means that there is no statistically significant difference between the successive years. However, there is a continuing fall (increase in acidity) in the pH for the minimum value from 5.8 in 2017, to 4.9 in 2018 to 4.6 in 2019, which follows the trend in the mean values. Following the 2019 pH data in Table 16a, the minimum pH has increased significantly by about 0.9, which reflects the same increase in pH in the mean values following the long dry spell that preceded the 2021 measurements.

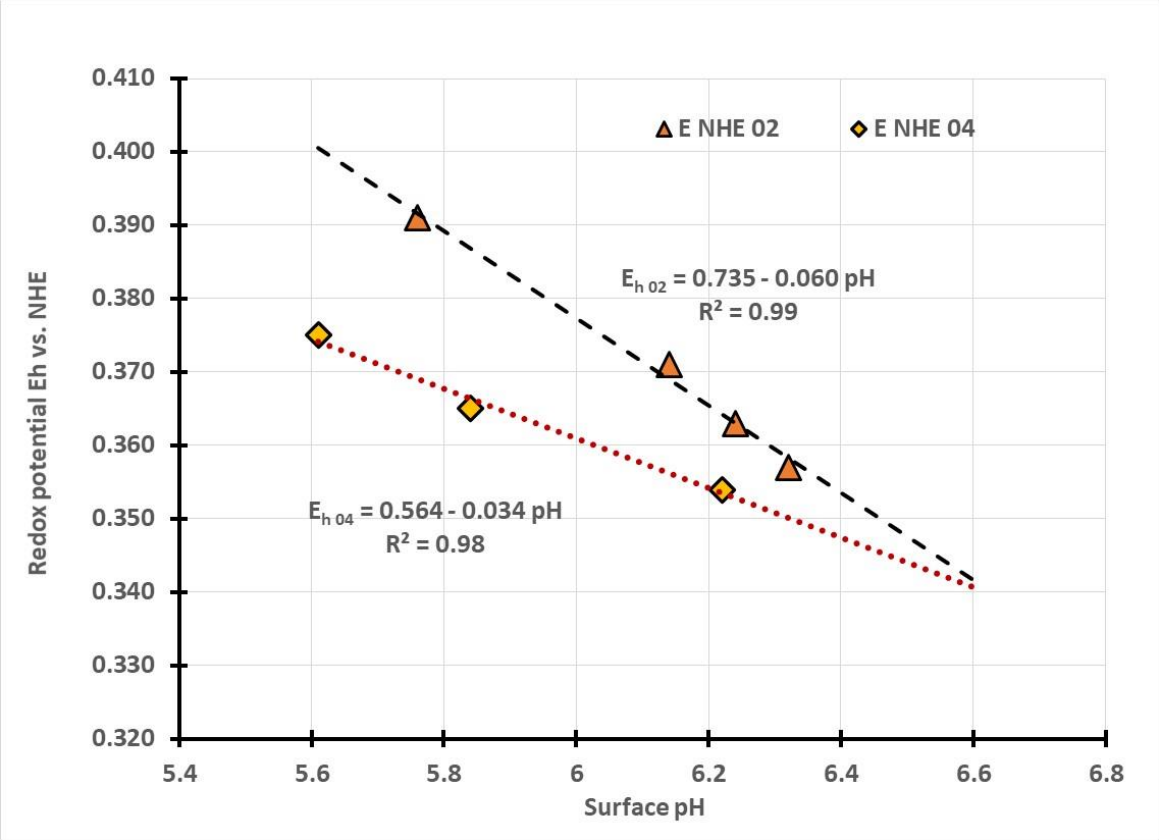

Figure 23: Pourbaix plot of the on-site E_h and pH data from 2021 for site 21

Table 16a: Statistical analysis of pH values on site 21 from 2017-2021

	2021	2020	2019	2018	2017
Mean	6.15	5.27	5.16	5.81	6.43
Standard Error	0.08	0.06	0.09	0.18	0.14
Median	6.23	5.31	5.21	5.7	6.44
Mode	6.46	5.49	5.21	n.a.	5.98
Standard Deviation	0.32	0.27	0.3	0.65	0.45
Range	0.99	1.08	0.97	2.1	1.5
Minimum	5.61	4.74	4.6	4.9	5.8
Maximum	6.6	5.82	5.6	6.9	7.3
Count	16	22	16	13	13

The mean E_h or redox potential for the site was much the same as it was in 2019-2021 which indicates that the dominant electroactive species are manganese minerals, as the amount of soluble

iron on this rock is very small and, in several years, the amount was below the detection limit of 5 parts per billion. Plots of the redox voltages across the sixteen locations on the rock showed a general slight increase of 0.2 mV per ppm increased chloride ion concentration. There were many data points where the trend was in the reverse direction, and this is where the increased chloride has produced enough alkalinity to be decreasing the solution activity of the manganese (manganous) ions.

Table 16b: Statistical analysis of redox potential at site 21: 2017-2021

	2021	2020	2019	2018
Mean	0.375	0.379	0.369	0.487
Standard Error	0.003	0.003	0.005	0.204
Median	0.375	0.379	0.369	0.489
Mode	0.365	0.378	n.a.	0.484
Standard Deviation	0.014	0.014	0.018	0.209
Range	0.043	0.071	0.066	0.229
Minimum	0.354	0.333	0.34	0.472
Maximum	0.397	0.404	0.406	0.499
Count	16	22	16	13

The impact of the increased salt surface concentration on rock 21 is also reflected in terms of increased acidity from the activity of halophytic bacteria, as seen in Figure 23, where the pH falls by approximately 0.002 pH/$[Cl]_{ppm}$. One grouping of data points in the graph were associated with the left-hand side of the rock, which has an intercept pH of 6.28 at zero chloride. The upper cohort had an intercept of 6.88 at zero chloride and this group came from data collected at the lower points on the rock where the sea salts were accumulating. The R^2 value for the left side of the rock was 0.83.

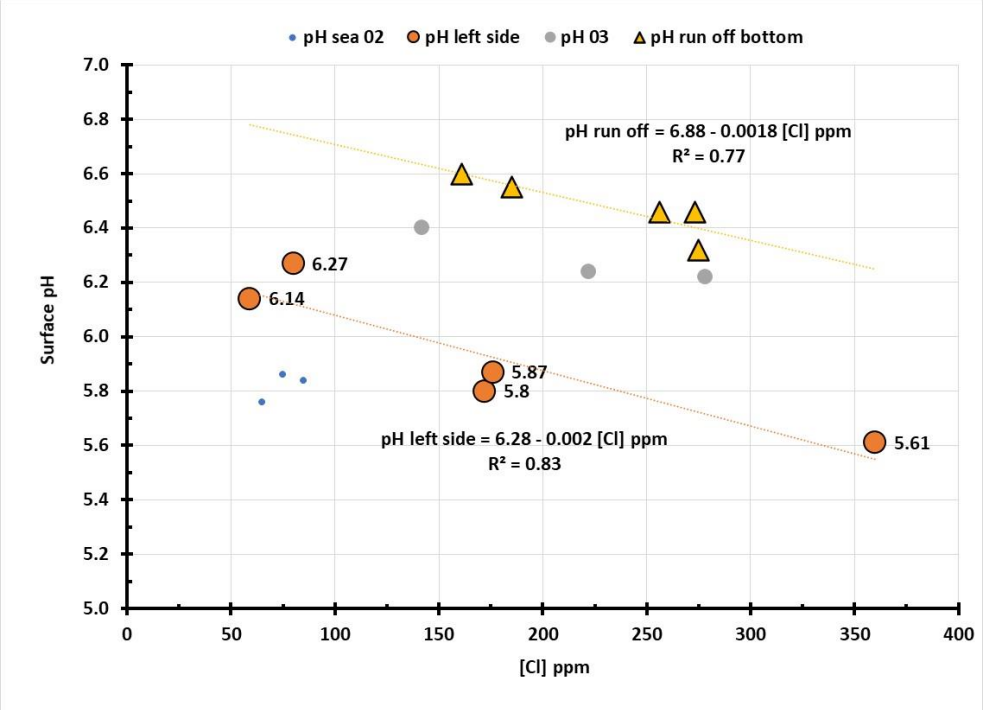

Figure 24: Plot of surface pH on site 21 during September 2021

The associated error in the regression line for assessment of the obligate chloride bacteria on the surface pH was within 2% of the intercept value of 6.28 ± 0.11 while the slope was -0.0020 ± 0.0005

{$^{pH}/_{[Cl]}$}, which is a 26% error. The microtopography of this site is critically important in understanding the movement of salts and the way in which they interact with surface minerals in and on the rock patina.

Table 16c: Statistical analysis of chloride ion activity at site 21: 2017-2021

	2021	2020	2019	2018	2017
Mean	179	43	95	20	143
Standard Error	23	7	20	4	14
Median	174	33	68	21	136
Mode	#N/A	22	25	n.a.	214
Standard Deviation	92	31	70	13	44
Range	301	140	225	46	126
Minimum	59	20	25	1	88
Maximum	360	160	250	47	214
Count	16	22	16	13	13

Summary of observations on site 7, Deep Gorge in October 2020

The long-term interactions of the Deep Gorge site (no 7) with the microenvironment in the Burrup has been monitored, on and off, since 2003 and is summarised in Figure 25. It is of interest to note that when the alkaline excursion possibly due to an accidental loss of ammonia at the Yara plant before the 2018 measurements and the following massive fall in mean pH in 2019 by a factor of δpH of 2.26 or a value of just over 180 times. This period was also associated with a higher amount of nitrate being found on the rock surfaces and at the time of our last report the significance of the changes was not fully comprehended. It is now believed that during the time between when the site was accidentally exposed to ammonia and when the next year's inspection took place, that nitrifying bacteria were able to convert the adsorbed ammonia into nitrate and so stimulate the microbial populations on the rock. An alternative explanation is that the increased nitrate was due to other NO_x emissions in the airshed.

Following the February 2020 cyclonic rain, during which 235 mm fell in two days, the pH moved to a more alkaline value of 5.75 i.e., the rainfall seems to be "resetting" the acidity decay clock. Since there were no major rainfall events in the 12-months preceding our measurements, the winds brought significant amounts of air borne sea salts to the region. Between 2020 and 2021 the mean surface chloride ion concentration increased almost ten-fold, and this pushed the mean pH values into the alkaline regions (see Table 17a and 17 c). Analysis of the changing pH on site 7 showed that there was a general trend towards more alkaline values, if the very high pH of 2018 and the very low mean pH of 2019 are ignored, for clearly historical reasons. The annual increase in pH for Deep Gorge is 0.067 pH for the period of 2004 to 2021. The linear regression that gave rise to equation 46 had an R^2 of 0.90 and the error was ± 1.43 in the intercept, which brought it close to zero. The slope of {$^{pH}/_{time,\ days}$} was 18.2 ± 3.4 x 10^{-5} pH/day.

$$pH_{\ site\ 7} = 0.000182\ t - 2.16 \quad \text{..... (46)}$$

To find that there was a long-term trend towards more alkaline values of the mean pH at site 7 was unexpected and so the sites will continue to be monitored.

Just as was observed on other sites in 2021, the mean pH (Table 17a) had increased during the long dry period by a modest amount of 0.33 or just over two times less acidic, with the mean chloride

increasing from 5 to 46 ppm in 2021 (Table 17c). Plots of the mean chloride (ppm) since monitoring for Yara began in 2017 shows a steady decrease of approximately 6 ppm per year, which leaves little buffering capacity on the rock surface and so this makes the pH data at site 7 more sensitive to changes in the chemical microenvironment.

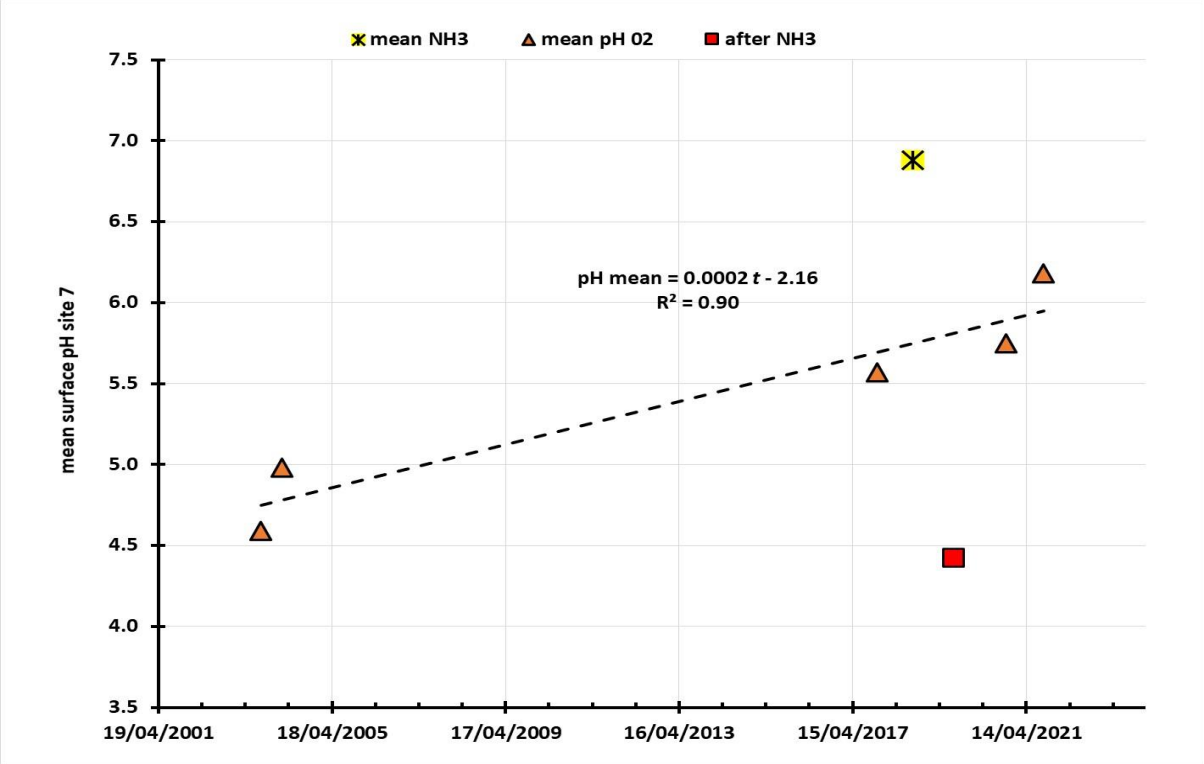

Figure 25: Plot of the mean surface pH on site 7 from 2003-2021

Part of the complexities of this site are reflected in the "see saw" shape of the pH time plots, but there are indications that the pH decreases with increasing chloride, which is contrary to other sites. This is consistent with localised activity of chloride obligate bacteria which are those microorganisms which need salt for their metabolic activities. Plots of the pH vs. chloride ion activity are summarised in equation 47 viz.,

$$^{\text{chloride}}\text{pH}_{\text{site 7}} = 6.62 - 0.019\,[\text{Cl}]_{\text{ppm}} \quad \text{..... (47)}$$

The regression equation had an R^2 value of 0.98 and the intercept error was ± 0.05 and the slope $\{^{pH}/_{[Cl]}\}$ was ± 0.001 pH/ppm chloride ion. One set of measurements showed no shift or change in pH as the chloride ion activity was increased from 32 to 130 ppm: the simple conclusion is that there are parts of the rock where the surface is not colonised by chloride obligate bacteria.

The Pourbaix plots for site 7 in 2021 showed only a single electrochemical step was associated with the surface chemistry, in which the ratio of protons to electrons was 1:2 i.e., the slope was -30mV per pH, according to the standard reaction scheme,

$$Mn(OH)^{+} + H_2O \rightarrow Mn(OH)_2^{2+} + H^{+} + 2\,e^{-},$$

in which there is a two-electron oxidation and simultaneous hydrolysis of the Mn4+ ion to the dihydroxy species. Inspection of the mean Eh data in Table 17 b shows that after the initial voltage drop between 2018 and 2019, the mean redox potential is steadily increasing towards more positive values and is now only 39 mV less anodic than when first measured. The cyclonic rain in February 2020 "neutralised" the developing acidity at site 7 and brought the pH back to 5.8 ± 0.4, which is essentially the same as when measured in 2017 – see Figure 25. The higher chloride on the surface confers a greater buffer capacity on the rock to resist acidity from either the chloride obligate bacteria or from acidic metabolites associated with reproduction in response to the additional nitrate

loading, which in 2012 had a mean value of 0.20 ±0.03 ppm.

Table 17a: Statistical analysis of pH on site 7, Deep Gorge 2017-2021

	2021	2020	2019	2018	2017
Mean	6.18	5.75	4.42	6.68	5.57
Standard Error	0.06	0.10	0.13	0.12	0.11
Median	6.24	5.73	4.52	6.67	5.53
Mode	6.50	n.a.	n.a.	7.02	5.9
Standard deviation	0.29	0.43	0.44	0.39	0.42
Range	0.92	1.92	1.67	1.14	1.49
Minimum	5.58	4.94	3.31	6.06	4.92
Maximum	6.50	6.86	4.98	7.2	6.41

Data from the 2018 measurements of the Eh and pH showed that the dominant electrochemical process involved the formation of significant amounts of the manganese equivalent of magnetite, namely Mn3O4 which is also reflected in the mean Eh value of 0.429 volts. The fall in mean Eh in the 2019 measurements saw the mechanism change, for the slope had decreased to 29 mV per pH as per the reaction scheme described above (Table 17b). As in previous monitoring years, it was noted that there was a strong correlation between higher Eh and increased chloride concentration, as shown by equation 48, which shows that the redox potential increases by 0.7mV per ppm of chloride,

$$^{site\ 7}Eh = 0.358 - 0.0007\ [Cl]_{ppm} \quad (48)$$

The R2 for the eight measurements was 0.83 provides a modest degree of confidence in the reality of the apparent connection with increased redox activity with increased chloride across the rock surfaces. The error in the intercept was ± 0.005 volts and the slope {'Eh/[Cl]} was ± 0.13 mV per ppm.

Table 17b: Statistical analysis of Eh on site 7, Deep Gorge 2017-2021

	2021	2020	2019	2018
Mean	0.390	0.379	0.368	0.429
Standard Error	0.003	0.003	0.006	0.008
Median	0.390	0.379	0.366	0.432
Mode	0.398	0.386	0.355	0.432
Standard deviation	0.011	0.014	0.02	0.025
Range	0.049	0.049	0.061	0.082
Minimum	0.356	0.142	0.339	0.38
Maximum	0.405	0.191	0.4	0.462

The rock on the reverse side of the kangaroo image at site 7,that was used for colour monitoring, was systematically assessed for surface pH, chloride, and redox potential. One of the measures of how the increased chloride ion activity observed in 2021 works on the pH is seen in Tables 17a & 17c where the pH range decreased from 1.92 in the post cyclone Damien environment to only 0.92 in the following year. This reduced pH range was due to the mean chloride which had increased from 5 to 46 ppm. Less sea salt reduces the buffer capacity to respond acidic metabolites. The exposed nature of the site is also reflected in the conformity of the pH values going across the rock, from left to right. In the upper most row the mean pH was 6.24 ± 0.39 while the second row had the same mean value of 6.25 ± 0.22 and in the bottom row, where moisture and micronutrients accumulate the mean pH

was down slightly to 6.06 ± 0.24. The chloride ion profile across the rock was only readily discerned in the upper row where the chloride activity increased by 0.75 ppm per cm (*d*) moved towards the right-side of the reference rock, as shown by equation 49 viz.,

$$[Cl] = 76.2 + 0.75\ d \qquad (49)$$

The regression equation no 47 had an R^2 value of 0.94 with a salt error in the left-hand side (intercept) of ± 6.2 ppm and a slope error of ± 0.14 ppm/centimetre. The chloride levels across the rock in the middle and the bottom row were constant.

Table 17c: Statistical analysis the chloride activity on site 7, Deep Gorge 2017-2021

	2021	2020	2019	2018	2017
Mean	46	4.8	8.6	18.6	21.5
Standard Error	8	0.6	1.1	2.5	3.7
Median	33	4.3	7.2	17.3	24
Mode	21	2.6	6.9	n.a.	30
Standard deviation	34	2.4	3.8	7.8	11.7
Range	109	8.6	13	28.8	27.8
Minimum	21	2.4	4.3	8.2	7.2
Maximum	13	11	17.3	37	35

All the chloride distribution data is consistent with rain coming in from the coast and washing the rocks during the cyclone. Similarly, the build-up of chlorides is clearly coming with movement of moist sea air from the right to the left of the reference rock.

Summary of observations on site 6, Water Tanks in 2021

Comments on the distribution of chloride salts on the measurement rock has previously been made and an illustration of the wind shadow area is seen in Figure 4. The rock immediately adjacent to and approximately 50 cm forward of the engraved rock at site 6 was systematically assessed for surface pH, chloride, and redox potential in 2021, 2020, 2019 and 2018 and for both pH and chloride in 2017. The pH data collected in 2020 significantly less acidic than in 2019 because of the impact of the rain from cyclone Damien. The additional buffering capacity of the increased sea salt deposition this year was significant, with a mean chloride concentration of 242 ± 84 ppm (Table 18c). The buffer impact is also seen in the range of pH (Table 18a) which was 1.89, with a maximum pH of 6.56 and a minimum of 4.67. The set of eighteen measurements of pH, chloride and redox potentials were made in three rows of five measurements at a spacing of approximately 18 cm between points.

Table 18a: Statistical analysis of pH data from 2017-2021 at site 6, Water Tanks

	2021	2020	2019	2018	2017
Mean	5.57	5.34	4.67	5.85	5.66
Standard Error	0.17	0.08	0.05	0.19	0.07
Median	5.26	5.41	4.64	6.11	5.76
Mode	#N/A	5.46	4.59	4.7	5.85
Standard Deviation	0.65	0.35	0.18	0.7	0.22
Range	1.89	1.42	0.58	1.7	0.57
Minimum	4.67	4.59	4.43	4.7	5.28
Maximum	6.56	6.01	5.01	6.4	5.85
Count	15	18	15	12	10

An unexpected revelation on site 6 took place when searching for a better (more representative) washing rock when in the afternoon sunlight the image of a great white shark was found engraved on the chosen reference rock (Figure 26).

Figure 26: Washing sample rock "b" at site 6 showing a great white shark

The redox or E_h data is shown in Table 18 b and the Pourbaix diagram for site 6 in 2021 showed that the dominant relationship between the pH and the redox potential was associated with the two-electron oxidation of a partially hydrolysed Mn^{2+} ion, as shown below in the common equation no 50. The Pourbaix diagram had a slope of 28 mV per pH and so the most likely reaction is seen in Equation 16 viz.

$$Mn(OH)^{+} + H_2O \rightarrow Mn(OH)_2^{2+} + H^{+} + 2e^{-} \quad \text{..... (50)}$$

The regression line for the E_h and pH for site six in 2021 had an R^2 of 0.96 and the associated errors were an intercept value of 0.545 ± 0.012 volts and a slope of – 26 ± 2 mV, which is consistent with equation 50. The data in Table 18b shows that this site is remarkably stable, in terms of the overall redox reaction potential of + 0.392 ± 0.004 volts vs. NHE. There were no soluble iron species present in the washings from either rock "a" or rock "b" and this is consistent with the increased pH for the region which drives the solubility of iron downwards to the point of being less than the detection limit of 5 parts per billion. Analysis of the E_h and chloride measurements on the large rock showed that there is a systematic increase in the redox potential on the site as the amount of surface chloride ions increases. The E_h value increases at the rate of + 0.29 ± 0.06 mV/ppm chloride, which is consistent with the expected manner of formation of weak chloride complexes enhancing the kinetics of the relevant redox couples that are being measured on the rock surface during the testing procedures.

When the pH data was plotted as a function of the chloride readings the pH gradually decreased with increasing chloride concentration at the rate of – 0.012 ± 0.003 pH per ppm of chloride, up to the maximum value of around 350 ppm. Beyond this value there was no systematic response of the pH to chloride ions in the 400-432 ppm range, with some parts of the rock showing indicators of the presence of chloride obligate bacteria and others were essentially sterile and reflected the pH to be

expected with high sea salt concentration values. The pH showed complex behaviour, which is described in a series of three equations, viz., equations 51-53.

$$^{site\ 6}\ pH_{\ bottom\ row} = 8.43 - 0.011\ [Cl]_{\ ppm} \quad \text{..... (51)}$$

$$^{site\ 6}\ pH_{\ rock\ shadow} = 7.92 - 0.011\ [Cl]_{\ ppm} \quad \text{..... (52)}$$

$$^{site\ 6}\ pH_{\ top\ row} = 7.24 - 0.013\ [Cl]_{\ ppm} \quad \text{..... (53)}$$

The R^2 values for equations 51-53 were 0.94, 0.99 and 0.92 respectively and the errors in the pH intercept values at zero ppm chloride were 7.24 ± 0.57 for equation 53, 7.92 ± 0.20 for equation 52 and 8.43 ± 0.37 for equation 51. The three intercept values were just statistically significant from each other. The three slopes were the same, which indicates a common mechanism, and the mean value of $\{^{pH}/_{[Cl]}\}$ was -0.012 ±0.001 pH/ppm chloride ion. An illustration of how the chloride activity varied across the rock is shown below in Figure 27. An overall summary of the changing chloride levels from 2017 to 2021 is given in Table 18c. It was noted that there is a direct correlation between the maximum pH recorded and the mean chloride ion on the rock surfaces. This is entirely consistent with the chlorides being associated with increased alkalinity from the seawater.

Table 18b: Statistical analysis Eh on site 6, Water tanks 2017-2021

	2021	2020	2019	2018
Mean	0.394	0.385	0.391	0.396
Standard Error	0.005	0.002	0.005	0.006
Median	0.390	0.386	0.39	0.403
Mode	0.390	0.385	n.a.	0.403
Standard Deviation	0.020	0.01	0.017	0.02
Range	0.067	0.045	0.05	0.068
Minimum	0.371	0.365	0.369	0.358
Maximum	0.438	0.41	0.419	0.426
Count	15	18	15	10

The only times that this correlation fell apart were in the 2018 and 2020 seasons when there was very little chloride on the rock surface following cyclone Damien in 2020 (29 ± 17 ppm) and in 2018 when there had been heavy rain which reduced the chloride activity to 2.3 ± 3.2 ppm.

Table 18c: Statistical analysis of chloride ion activity on site 6 (Water Tanks) 2017-2021

	2021	2020	2019	2018	2017
Mean	242	29	9.7	2.3	190.8
Standard Error	22	4	1.8	0.9	48.6
Median	210	23	8.5	1.2	164.5
Mode	260	22	n.a.	n.a.	n.a.
Standard Deviation	84	17	6.3	3.2	97.3
Range	278	60	21	11.3	218
Minimum	154	14	3	0.3	108
Maximum	432	74	24	12	326
Count	15	18	14	10	12

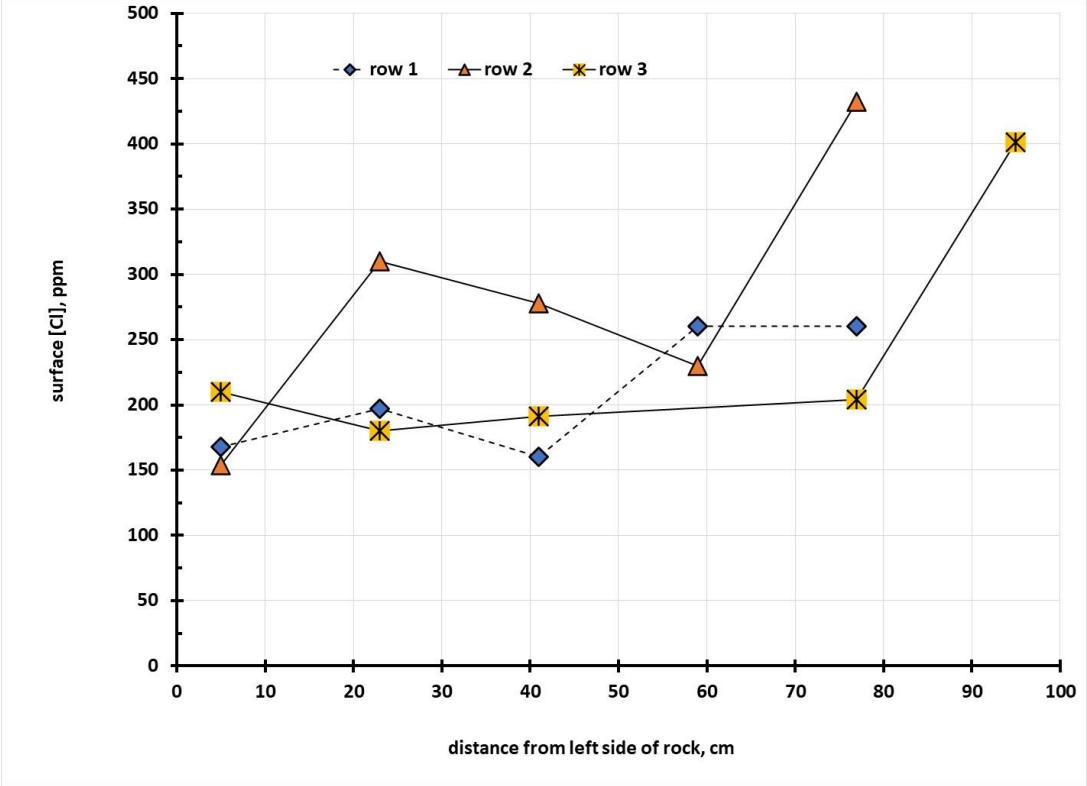

Figure 27: Chloride distribution in 2021 on site 6 showing impact of wind sheltering

It was found that there was no correlation between the observed range of pH with the amount of chloride on the rock surface, nor was there any linear relationship been the mean annual pH and the chlorinity of the surfaces.

Summary of observations on site 5, Burrup Road

In reviewing the in-situ corrosion data for site 5 it is useful to be able to view the measurement points on their precise locations, since there are coordinate specific responses that are open to interpretation when one can see the data maps. The collected pH, chloride and E_h data from 2017-2021 are summarised in Table 19a (pH), 19b (redox or E_h) and table 19c (chloride). The measurement points are shown in Figure 28. When the pH and E_h data were plotted on a Pourbaix diagram there were a series of parallel lines in which the overall redox equation was summarised as equation 54

$$Mn^{2+} + 2\ H_2O \rightarrow MnO_2 + 4\ H^+ + 2e^- \quad \text{..... (54)}$$

All the lines had the same -118 ± 3 mV/pH as would be expected for equation 54 but they had different intercept voltages, the extrapolation value to zero pH. For six data points which followed the left-hand margin of rock 5, the R^2 value was 0.96 and the intercept was 1.216 ± 0.079 volts, and the slope was – 127 ± 12 mV/pH. For the mid-line of the rock the R^2 was higher at 0.98 but the intercept was 1.069 ± 0.083, but this value lies within the range associated with the standard deviation of the slope of the left-hand side of the rock. In a similar fashion, the right-hand side of the rock had an intercept voltage which fell within the same range, but because the R^2 was only 0.74, the errors well exceed any differences in the voltage.

Thus site 5 can be seen to be associated with the oxidation of free manganous ions which was subjected to a two-electron oxidation step followed immediately with precipitation of manganese dioxide. The increased mean surface pH from 4.65 in 2020 to 6.30 was enough to bring about the change of mechanism, which had previously been associated with the 1:2 slope of oxidation of Mn(II) to Mn(IV) but from a starting point of the $Mn(OH)^+$ ion to produce the dihydroxy-manganese(IV) species $Mn(OH)_2^{2+}$ (see Table 19a). The reason for the dramatic shift in the mean pH

is seen in the data from Table 19c, in which the mean chloride went from 5.5 ± 4.2 after cyclone Damien to 60 ± 16 ppm in 2021, following the long dry spell.

Figure 28: Measurement locations for in-situ data on site 5 in 2021

The redox potential or E_h increased linearly from 0.364 volts with the chloride ion concentration at the rate of 0.6 ± 0.1 mV per ppm chloride and the values of E_h at zero chloride were typical of equilibria involving Mn(IV)/Mn(II) species. The increased pH across the site reduced the sensitivity of the E_h to chloride ions by a factor of two times. Inspection of the data in Table 18b shows that after the initial value of +0.467 in 2018, the progressive drop in the oxidizing voltage over successive years has been reversed and so the mean redox potential increased from +0.372 to + 0.408 during the transition from a Pourbaix slope of 1:2 with 1:1 in 2020 to 1:2 for 2018 indicates stabilisation of the higher oxidation states of manganese, with the move to greater alkalinity.

In previous reports it was noted that there was a progressive increase in the acidity of the measurement points across and up and down the reference rock 5, with the more acidic areas being at the foot of the rock where moisture and micronutrients combine to provide a more optimum environment for the respiration of aerobic bacteria. This site has been one of the most routinely acidic sites, with pH minima below 4 in 2018 and 2020. It was noted that one of the nearby reference washing rocks gave a soluble nitrate concentration of 0.3 ppm which in the past had led to more acidic surfaces, but the massive increase in the salt across the surface increased the minimum

pH from 3.87 in 2020 to 5.76 in 2020. Clearly the increased amount of sea salt has had a pronounced buffering effect on the acidity.

Table 19a: Statistical analysis of pH values on site 5 from 2017-2021

	2021	2020	2019	2018	2017
Mean	6.30	4.65	4.79	4.98	5.17
Standard Error	0.05	0.08	0.05	0.12	0.18
Median	6.34	4.72	4.72	5.02	5.17
Mode	#N/A	n.a.	4.72	4.87	n.a.
Standard Deviation	0.20	0.3	0.17	0.43	0.6
Range	0.79	1.18	0.49	1.61	1.68
Minimum	5.76	3.87	4.63	3.97	4.36
Maximum	6.55	5.05	5.12	5.58	5.17
Count	16	14	16	12	14

Table 19b: Statistical analysis of redox potential for site 5: 2017-2021

	2021	2020	2019	2018
Mean	0.408	0.372	0.390	0.467
Standard Error	0.003	0.002	0.01	0.003
Median	0.406	0.373	0.39	0.466
Mode	0.403	0.372	0.38	0.458
Standard Deviation	0.010	0.006	0.04	0.011
Range	0.038	0.019	0.131	0.032
Minimum	0.387	0.362	0.318	0.453
Maximum	0.425	0.381	0.449	0.485
Count	16	14	16	13

Table 19c: Statistical analysis of chloride concentrations site 5: 2017-2021

	2021	2020	2019	2018	2017
Mean	60	5.5	95	20	143
Standard Error	4	1.1	20	4	14
Median	60	3.9	68	21	136
Mode	64	n.a.	25	n.a.	214
Standard Deviation	16	4.2	70	13	44
Range	68	13.3	225	46	126
Minimum	33	1.5	25	1	88
Maximum	101	14.8	250	47	214
Count	16	14	16	13	14

The pH across the site fell with increasing chloride ion activity and so this indicates the presence of chloride obligate bacteria. Measurement sets down the left-hand side of the rock gave a regression

equation for the four points (equation 55) which had an R^2 of 0.99 and an intercept value of 6.98 ± 0.04 while the slope $\{^{pH}/_{[Cl]}\}$ was -0.0090 ± 0.0006, viz.,

$$pH_{[Cl]} = 6.98 - 0.0090\ [Cl]_{ppm} \quad \text{..... (55)}$$

Even though it is a small rock, measuring some 36 cm wide by 48 cm down, the surface does show off anisotropy in the distribution of the voltage, the chloride activity, and the pH, which are all interrelated. The average sensitivity of pH on the chloride ion concentration was -0.0082 ± 0.0009 pH/ppm chloride.

Summary of observations at CSIRO Site 4, near Withnell Bay Road

The CSIRO reference rock no 4 is located close to the Withnell Bay Road some 250 metres up the gully from the bisecting roadway. This rock was always viewed as a "canary" in terms of being that much closer to the point sources of anthropogenic pollutants such as NO_x and SO_x from the main NWSP on the opposite side of the road. However, the relative proximity to point emission sources does not consider the complex aerial distribution of waste products and the need for adsorption processes on the rock to make available this resource. The surface pH, chloride and E_h data was collected in the same manner as the other sites. The rock is large, and 20 sets of measurements were taken beginning at the upper left-hand side and moving in five steps across before moving down the rock face to the left and then stepping down to keep up a zig-zag sampling pattern. Owing to the diminishing size of the rock only four sampling points were taken towards the bottom or foot of the rock. The site is about 75° to the vertical. On the 9th of September 2021, the zephyr breeze at 2.3 km/hour. The rock was sampled every 18 linear centimetres.

Whereas the Pourbaix diagram in 2020 gave the same -120 mV/pH slope as was observed for site 5 in 2021, the changed conditions of chlorinity and pH altered the main equilibria to give a 1:1 ratio of protons to electrons and thus a slope of -59 mV/pH. The redox equation for this reaction is given in equation 56 viz.,

$$Mn^{2+} + 2\ H_2O \rightarrow MnO_2 + 2\ H^+ + 2\ e^- \quad \text{..... (56)}$$

As has been commonly noted in this 2021 seasonal report, the pH was more acidic as the sampling points moved down the rock face and the pH fell from 6.23 ± 0.10 at the top of the rock to 5.94 ± 0.17 at the foot, which is just statistically significant and very like other granophyre sites in the Burrup. The Pourbaix diagram for site 4 in 2021 is shown below in Figure 29 and the results of the regression analyses are shown in Table 20a, while the mean pH data over the monitoring period are shown in Table 19b, the mean redox data in Table 19c and the mean chloride data in Table 19d.

Table 20a: Pourbaix data for 2021 on CSIRO rock no 4

Location	Intercept	error volts	slope	slope error	R^2
lower	0.788	0.011	-0.064	0.002	0.99
row 2 & 3	0.783	0.107	-0.061	0.018	0.80
middle	0.750	0.078	-0.060	0.013	0.81

It is important to note that within experimental errors associated with the regression analyses that the reaction scheme has the same intercept, the same slope and therefore, the same overall electrochemical processes.

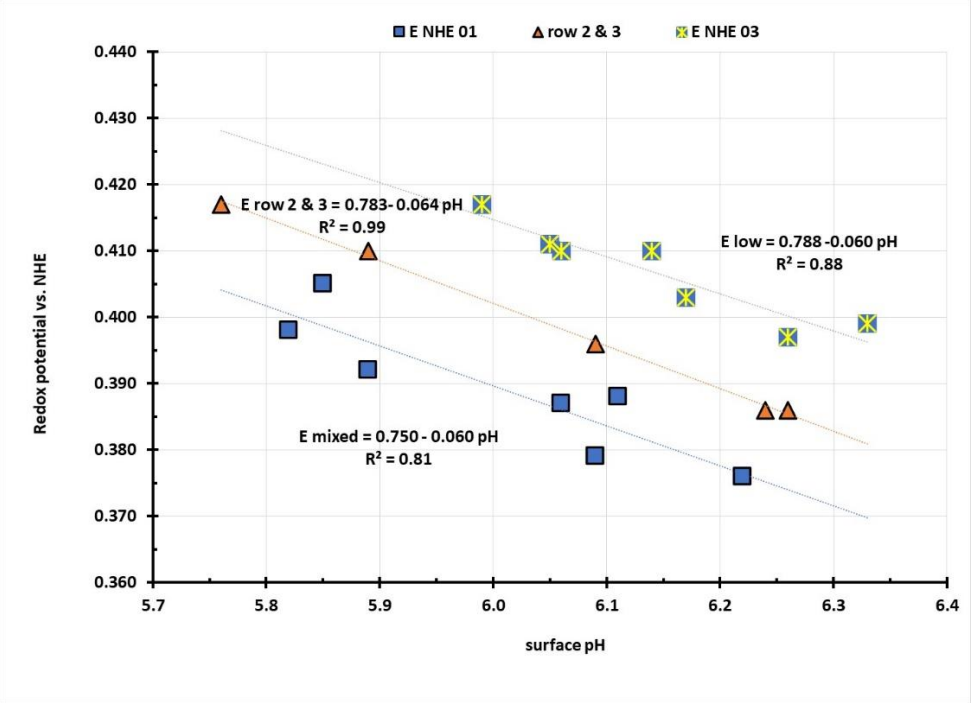

Figure 29: Pourbaix diagram for site 4, October 2021

The impact of the long dry spell, with no major rain events, in 2021 is readily seen in Table 19b where the mean pH has increased from 4.8 to 6.0 and, as noted above, this has brought about a different operational mechanism for the interaction of redox potentials and surface pH on this rock. With the increased saltiness (Table 20d) there is less of a range in the pH and the minimum has been moved from inherently acidic (4.33) to a much less aggressive microenvironmental pH (5.76). Some areas had a maximum of 76 ppm chloride, at which level there is significant capacity to adsorb acidic metabolites.

Table 20b: Statistical analysis of pH values on site 4 from 2017-2021

	2021	2020	2019	2018	2017
Mean	6.07	4.81	4.43	5.52	3.81
Standard Error	0.04	0.08	0.1	0.24	0.17
Median	6.09	4.72	4.48	5.34	4.05
Mode	6.26	4.62	4.48	5.34	4.05
Standard Deviation	0.16	0.35	0.35	0.92	0.52
Range	0.57	1.21	1.12	2.9	1.44
Minimum	5.76	4.33	3.83	4.38	2.98
Maximum	6.33	5.54	4.95	7.28	4.42
Count	20	18	15	12	9

The trend in redox potentials is like that found on site 5, which is many kilometres away, in that the E_h value initially fell by 93 mV between 2018 and 2019, then fell by another 15 mV (not significant) in 2020 but has now increased by 23 mV after the long dry spell. As has been observed on all the other Burrup sites, the redox potential was slightly sensitive to chloride ion activity as described by equation 57 viz.,

$$^{site\ 4}E_h = 0.357 - 0.0009\ [Cl]_{ppm} \quad \text{..... (57)}$$

For this relationship the R^2 was0.96 and the slope $\{^{Eh}/_{[Cl]}\}$ +0.00091 ± 0.00018 represents an 18% error while the intercept at zero chloride was 0.357 ± 0.007, which is only 2% of the value. Other sections of the rock surface showed similar increases in voltage with chloride ion activity, and they all fell within the standard deviation of the slope of the first group reported in equation 57.

Table 20c: Statistical analysis of redox potential site 4: 2018-2021

	2021	2020	2019	2018
Mean	0.400	0.377	0.392	0.485
Standard Error	0.003	0.003	0.004	0.003
Median	0.399	0.378	0.389	0.485
Mode	0.394	0.358	0.376	0.48
Standard Deviation	0.014	0.013	0.015	0.011
Range	0.046	0.037	0.037	0.046
Minimum	0.379	0.358	0.375	0.467
Maximum	0.425	0.395	0.412	0.513
Count	20	18	15	12

The pH was found to be dependent on chloride, falling by with a mean slope $\{^{pH}/_{[Cl]}\}$ of -0.0147 ± 0.0005 and the $^{zero\ Cl}$ pH intercept value was 6.83 ± 0.09. The high pH intercept value reflects the buffering capacity of the higher chloride ion concentration on the rock's surface. The apparent dominance of chloride obligate bacteria covered two thirds of the measurement points. For the sections of the double goanna site 4, there were one third of the data points that showed a reverse trend of the pH increasing with chloride ion concentration as shown in equation 58,

$$^{site\ 4}\ pH = 5.20 + 0.02\ [Cl]_{\ ppm} \quad \text{..... (58)}$$

For this data sub-set the R^2 value was much lower at 0.61 and there was only a 5% error in the intercept value of 5.21 ± 0.26 but a 36% error in the slope $\{^{pH}/_{[Cl]}\}$ of +0.022 ± 0.008 pH/$Cl_{\ ppm}$ and it is recommended that future studies by applied microbiologists assess the uniformity of microflora across the Burrup monitoring sites. This sub-group of data points was centred around the middle of the rock surfaces.

Table 20d: Statistical analysis of chloride concentration at site 4: 2018-2021

	2021	2020	2019	2018
Mean	38	11	4.4	2.2
Standard Error	3	1.3	0.5	0.5
Median	35	9	3.8	1.4
Mode	36	9	2.8	1.5
Standard Deviation	12	5.6	1.9	2.1
Range	52	31.2	5.9	6.6
Minimum	24	21.8	2.6	0.5
Maximum	76	6.2	8.5	7
Count	20	18	15	12

The monitoring data in 2020 had shown both halophytic bacteria and other sections of the rock where the pH increased with chloride concentration as an indicator of increased alkaline reserve of the deposited sea salts. For the middle sections of the rock, from the top to the bottom, there was a

reverse trend, shown by the regression equation 59, where the pH was seen to become increasingly acidic with increasing chloride ion activity.

$$pH_{\text{middle of rock}} = 6.24 - 0.11\,[Cl] \quad \text{.....(59)}$$

Inspection of figure 30 shows that there is a strong regression analysis with an R^2 value of 0.99 and the intercept $pH_{\text{zero Cl}}$ was 6.24 ±0.07 and the slope was -0.11± 0.006. The corresponding equation in the 2019 site assessment had a more acidic intercept value of 5.23 and a slightly steeper slope at -0.19 pH per ppm chloride. Decreasing pH with increasing chloride is an indicator of the activity of chloride obligate bacteria (Equation 59).

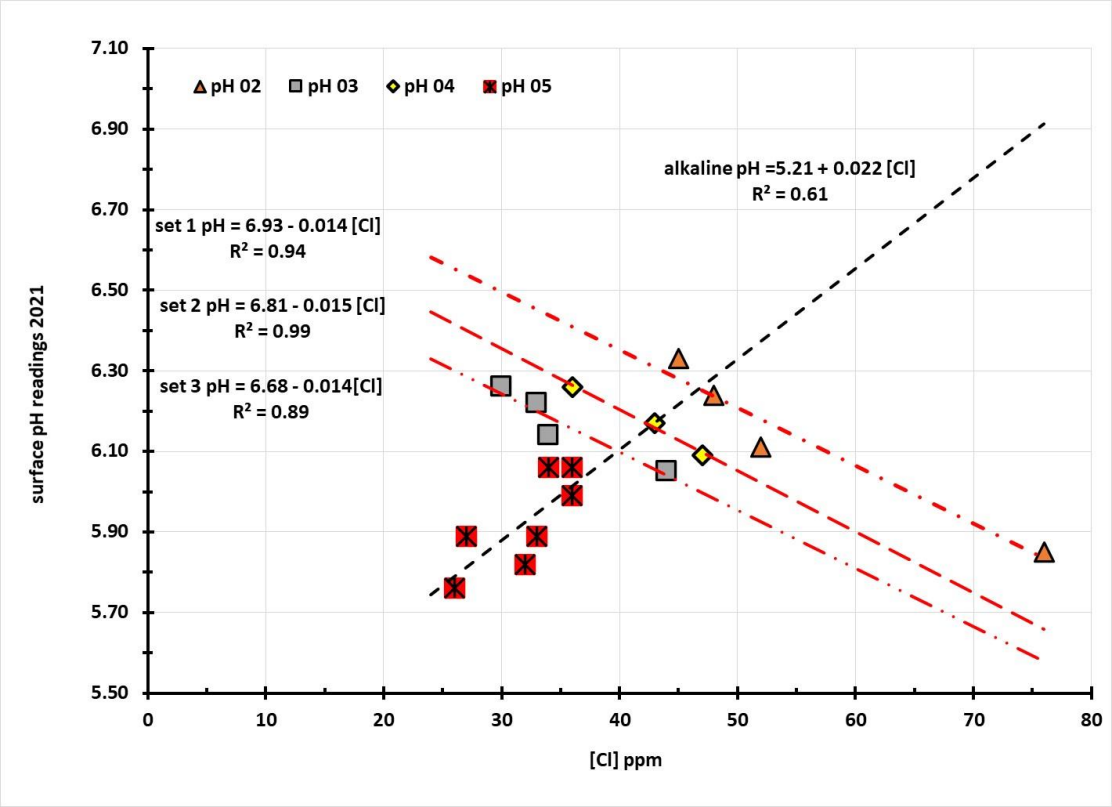

Figure 30: Plot of surface pH vs. chloride ppm in 2021 at site 4; mixed responses

The cyclonic rainfall event on the 6th of June 2018, before the measurements were taken on September 4, appears to have had a major impact on the rock surface, since the mean pH increased from 3.8 to 5.5, which represents a 50-fold reduction in acidity. Within a year the site pH had decreased to 4.4, over 12 times more acidic than in the previous year and this acidification trend was stopped through the intervention of cyclone Damien in February 2020, which resulted in the increased mean pH to 4.8 but it appears it was the lack of rain and the direction of prevailing winds that brought about the major shift towards alkaline values in 2021.

Environmental impact on the Climbing Man site 2003-2021

Owing to the nature of the main panel at the Climbing Man site, it is only practical to record the pH values, since other measurements require more physically demanding procedures, such as a second person holding a meter box and there is no room for their feet to stand. Thus, the surrogate rock a few metres to the left of the main panel has been used for measurements of the redox, pH and chloride data over the years. However, this unique situation is of great benefit as it allows for a direct comparison of the impact of the rock orientation on the adsorption of gaseous emissions and, indirectly, provides a measure of how rain events impact on the rock art sites. Owing to the singular cultural value of the main panel, measurements have been made on the pH of this site since 2003,

apart from the hiatus period between February 2004 and July 2017. The Fox report (Fox 2020) conducted statistical analysis of the changing pH values across the Burrup. His findings, inter alia, noted that for sloping rocks the pH was consistent across the rock surface but that there was an increase in acidity as the measurements progressed down the rock surface from the top towards the bottom. The long-term trends of the pH on both the main panel and the adjacent rock have been reported (above) in Figure 22. The 2021 pH data from the main panel are shown in Figure 31.

The top row (yellow background with stars) had the natural pH associated with weathered granophyre rock for the first 60 cm but as the right-hand side of the rock were approached, the pH fell from 6.0 to 5.4 at 80 cm to reach a lower value of 5.2 at the most distant point. The second row pH values (brown squares) was much more uniform for the first 80 cm before falling from 5.9 to 5.0 in the last 20 cm, which was the area that was mostly in shadow. In a similar fashion the third row was at a more alkaline starting position on the vertical face of the rock, but it moved to the same end point as the first row on the right-hand side of the rock. The mean pH of row 1 was 5.79 in the full sun and 5.28 in the shaded areas, indicating the important role of moisture in creating the right microenvironment for microbial activity. The same pattern of more acidic shaded areas was found on row 2 pH data, with the $^{row\ 2sunny}pH_{mean}$ 6.00 and the $^{shaded}pH_{mean}$ was 5.42, a shift of 0.58 pH to more acidic values. The corresponding bottom row values were 6.19 for the mean sunny sites to 5.17 for the most moist and shaded areas. This data confirms the bioavailability of micronutrients is a primary factor in determining the surface pH. The main panel showed a total range of 1.44 in pH from a minimum of 4.96 to a maximum of 6.40, as seen in Table 21a.

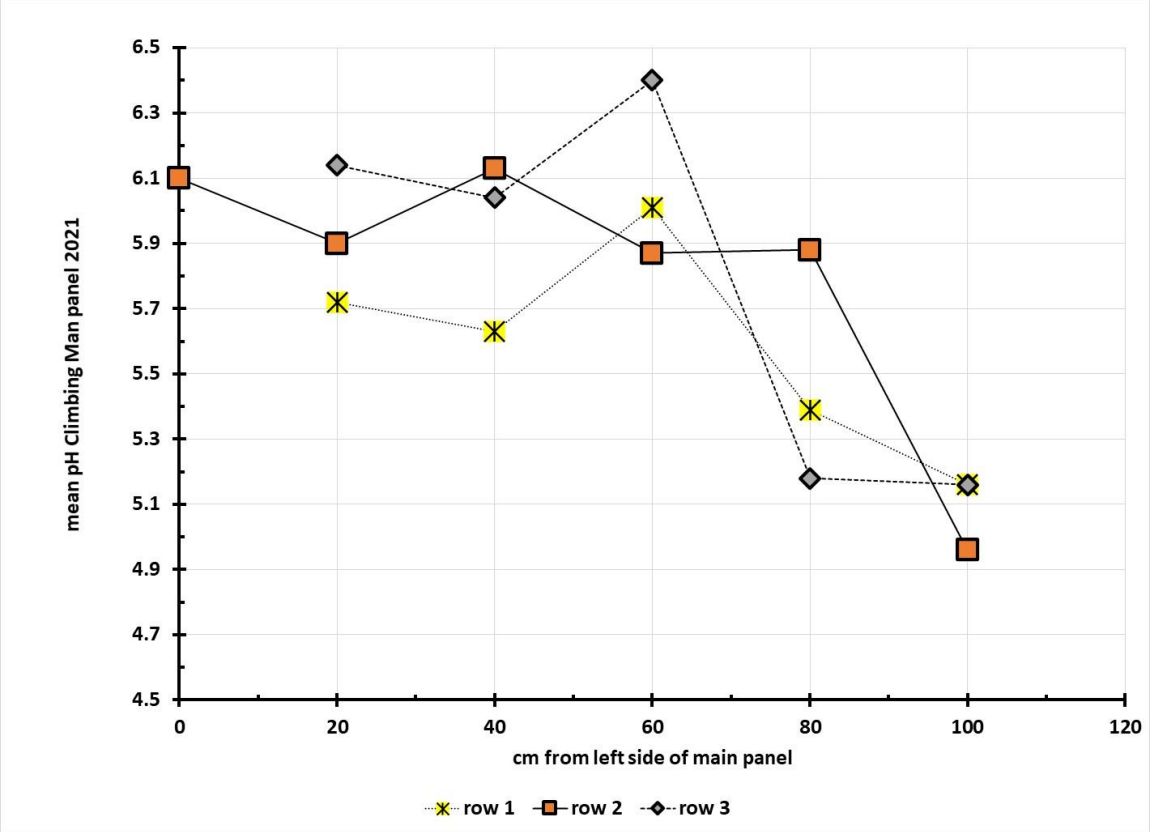

Figure 31: Surface pH of the Climbing Man in 2021 vs. distance from the left side

One of the most significant impacts of the change in angle in moving from the near vertical (5°) Climbing Man panel to the adjacent spilt rock (approximately 35°) the latter rock had a much greater capacity to adsorb moisture coming in from the ocean breezes. This is most strongly seen with a

mean 2021 chloride ion activity of 70 ppm, with a minimum of 42 and a maximum of 104 parts per million. The difference in angles is also reflected in the different mean pH values of 5.73± 0.43 for the main panel and 6.06 ± 0.20 for the split rock.

Observations on the Climbing Man split rock adjacent to the main panel

Given that only pH data could be safely recorded on the main panel on the Climbing Man, the detailed electrochemical measurements were conducted on the nearby "split rock" which is within three metres left of the main frieze. Plots of the E_h and pH data from this site gave Pourbaix diagrams which indicated that there was a single electrochemical reaction taking place on this site, but with a displacement on the voltage axis of 47 mV. The regression analysis gave equation 60

$$Mn^{+2} + 2\ H_2O \rightarrow Mn(OH)_2^{2+} + 2H^+ + 2\ e^- \quad \text{.....(60)}$$

The upper set of data had a mean intercept at zero pH of 0.805 ± 0.064 volts, with an R^2 of 0.89, hence the large scatter of 8% in the intercept value and a slope of -60 ± 10 mV/pH expected for a 1:1 proton and electron reaction. Most of the data points were from the right side of the rock while the others related to the left side. The lower line had the same slope of -54 ±8 mV/pH, which is experimentally indistinguishable from the upper set of data. The R^2 value was still very high at 0.94 and the intercept value for E_h was 0.753 ± 0.047, which is experimentally the same as the other value.

The varied chloride distribution across the split rock has previously been attested to and so it was not surprising to find increased redox potentials in response to increased chloride, equation 61 viz.,

$$^{\text{diagonal split rock}}\ E_h = 0.383 + 0.00068\ [Cl] \quad \text{.....(61)}$$

The regression analysis gave an R^2 of 0.97 and there was only a ± 5 mV error in the intercept value (1.3%) and the slope $\{^{Eh}/[Cl]\}$ had an error of ± 0.06 mV/ppm chloride, which amounted to only 10%. In the light of the above sensitivity observed in 2021 the differences in the intercept voltages from the Pourbaix plots are almost certain to be solely due to differences in the localised chloride ion activities.

The data in 2021 gleaned from the split rock showed that there were no statistically significant differences in the mean pH down the rock face, with row 1 being 5.99 ± 0.30, row two 6.12 ± 0.13 and the bottom row had a mean pH of 6.09 ± 0.09. This site runs counter to the general argument developed by Fox (2020). There was a systematic fall in the mean chloride doing down the rock, from row one being 81 ± 10, row two being 75 ± 20 ppm and the bottom row being 49 ± 11 ppm of chloride ion. It appears that during the wind driven salt deposition there was a counter current of wind reversing the distribution values of the chloride ions, like on site 22 with its complex chloride map showing the wind vortices. For all intents and purposes, the E_h was constant across the rows and down the rocks.

Table 21a: Statistical analysis of pH values on the Climbing Man split rock from 2017-2021

	2021	2020	2019	2018	2017
Mean	6.06	6.1	4.62	5.81	6.04
Standard Error	0.05	0.08	0.05	0.1	0.21
Median	6.09	6.13	4.59	5.93	6.05
Mode	6.27	6.21	n.a.	5.97	5.48
Standard Deviation	0.20	0.3	0.16	0.39	0.61
Range	0.69	1.18	0.56	1.27	1.68
Minimum	5.65	5.39	4.4	5.19	5.26
Maximum	6.34	6.57	4.96	6.46	6.94
Count	14	14	12	14	8

Plots of the pH profiles as a function of the chloride ion activity on the split rock showed a decreasing pH as the chloride ion concentration increased, in accordance with the regression equation no 62,

$$^{\text{split rock}}\text{pH} = 6.36 - 0.0075\ [\text{Cl}] \quad \text{.....(62)}$$

This regression equation had an R^2 of 0.96 and the intercept value 6.36 ± 0.06 pH is significantly more alkaline than typical values in 2020, when the low amount of surface chloride provided little buffering capacity for the rock surface to minimise the impact of acid-producing chloride obligate bacteria. The error in the slope was ± 0.0009 which amounted to only 12% in the value, giving a high degree of confidence in the fineness of the fit.

Table 21b: Statistical analysis of redox potential and chloride levels CM split: 2019-2021

	2021 E vs volt NHE	2020 E vs volt NHE	2021 Cl ppm	2020 Cl ppm	2019 Cl ppm
Mean	0.437	0.375	70	10.5	14.4
Standard Error	0.003	0.007	5	2.3	3.0
Median	0.436	0.374	71	7.1	12.2
Mode	0.434	0.378	65	n.a.	4.6
Standard Deviation	0.011	0.027	19	8.8	10.5
Range	0.037	0.109	62	31.1	35.5
Minimum	0.417	0.352	42	4.1	4.6
Maximum	0.454	0.461	104	35.2	40.1
Count	14	14	14	14	12

Colour measurements

Measurements conducted in September 2021

Colour measurements were conducted on sites 4, 5, 6, 7, 21, 22 and 23 using the Konica-Minolta Chromameter (KMC) with a set of 10 independent measurements on the background and engraved surfaces at the four designated reference points. Previous work in 2019 and 2018 had used 20 measurements but statistical analysis by Microfading Australia showed that this produced too many random errors, owing to the challenges of positioning the sensing head on areas characterised by high microtopography. The details of the colour measurements made in 2021 have been compared with those made in 2020, 2019, 2018 and in 2017. The advice received from Microfading Australia at the conclusion of their 2019 assessment changed the sampling protocol was changed to enable each rock area to be dusted with a dry paint brush to clear loose iron ore dust from the surface. Colour measurements on inhomogeneous surfaces is fraught with difficulty but by applying simple house cleaning protocols the sampling errors were minimised.

The initial analysis of the colour differences was conducted using the methodology outlined in the CSIRO September 2008 Report (CSIRO 2008) which involved using the CIE standard formula for colour difference by taking the square root of the differences between the L, a and b values recorded by the Konica Minolta Chromameter. The formula used for determining the colour difference was as noted below in Equation 63,

$$\Delta E_{97} = \{(L_b - L_e)^2 + (a_b - a_e)^2 + (b_b - b_e)^2\}^{½} \quad \text{..... (63)}$$

In Equation 60 the subscripts after the L, a and b values relate to the *b* for the background and *e* for the engraved surfaces. When comparing the colour data, it should be noted that the 2017 measurements were characterized by scatter due to the dust. Owing to the cyclonic rain that preceded the 2018 data collection there was much less dust on the rock surfaces. A moderate amount of surface dust was noted in 2019 and this issue was managed with a light “dusting” from a soft and very flexible natural bristle paint brush for the data collection, which had a smaller data scatter than the data points from 2019. Many of the sites that were assessed in September 2021 had

a moderate to light dusting of red dust from the pervasive iron minerals arising from ore transport and local traffic movement on dirt roads. Owing to uncertainties associated with the assessment of the colour difference readings on each of the six sites, both the original data and the calculated ΔE values were reviewed by Bruce Ford, Principal of www.microfading.com. This review was necessary as there have been major revisions by colour conservators regarding the evaluation of what are statistically reliable measurement of colour differences. Using the criterion that the MCDMt {total mean colour distance from the mean)/Delta E} > 0.5, the sites were assessed for colour difference between the background and the engraved areas as being compliant or not.

The primary colour difference data between the background and the engraved areas for 2021 is reported in Table 22 below. The data was collected with a measurement area of 8 mm. One major difference between the colour contrast data between 2020 and 2021 relates to 6, the Water Tanks. In 2020 three of the four measurement points had ΔE values less than one but in 2021 all four spots had ΔE values greater than 1 (Table 22). There appeared to be more systematic errors at site 7 than in previous years for the standard deviation of the four colour measurements was greater than 70% whereas it was closer to 50% variation in 2020. A matrix of all the 28 colour measurement points listed in Table 22 were plotted against the minimum pH values in 2021, as reported in the various chapters in previous discussion and the summarised results are shown in Figure 32.

Table 22: Colour differences for 2021 on four spots on each site ΔE (background – engraving)

$pH_{minimum}$		spot 1	spot 2	spot 3	spot 4
5.76	site 4	3.41	3.00	3.18	2.73
5.76	site 5	4.08	5.64	7.90	4.35
4.67	site 6	1.94	2.16	1.07	3.41
5.58	site 7	6.01	1.73	2.38	8.94
5.61	site 21	5.92	4.80	2.36	6.21
5.06	site 22	4.68	5.83	2.43	5.72
4.92	site 23	2.93	2.99	3.60	6.17

During the general discussions regarding the electrochemistry of the seven colour monitored sites in 2021 some major differences emerged between the data from the last two years. In 2020 sites 7 and 21 had two different Pourbaix slopes and site 5 had three values, ranging from 2 protons, to one per electron to one per two electrons. This indicated that there were several competing equilibria on the surface, with some areas of the rocks being more associated with oxidation of free Mn^{2+} ions and others associated with oxidation of the partially hydrolysed $Mn(OH)^{+}$ ion. On site 5 in 2020 there were several zones on the rock which indicated that oxidation of Mn(II) to Mn(IV) was taking place, with formation of the solid MnO_2 on the rock surface. This changing activity was seen as a reflection of the low salt concentration on the rock surface, following cyclone Damien, providing a chemical environment where it was possible to develop niche microenvironments that were significantly more acidic. By the time the 2021 measurements were conducted 11 months later, most of the rock surfaces had received very little natural washing and so they were characterised by much more alkaline surfaces, due to the increased buffering capacity because of the higher sea salt concentration. By way of contrast to the complexities of the redox equilibria observed in 2020, this more stable surface condition showed that there was only one equilibrium on each site.

The changes in colour contrast between the "clean" 2020 and the "salty" 2021 surfaces are summarised in Table 23. The data from 2020 shows greater colour contrast in the mean values for each of the seven sites and other than sites 6, 7 and 21 the scatter of the data is less.

Table 23: Comparison of the ΔE values on each spot between 2020 and 2021

2021 mean	2021 stdev	location	**2020 mean**	2020 stdev
3.1	0.3	site 4	**2.7**	1.9
5.5	1.7	site 5	**4.2**	1.8
2.1	1.0	site 6	**0.9**	0.4
4.8	3.4	site 7	**2.7**	1.3
4.8	1.8	site 21	**4.3**	1.0
4.7	1.6	site 22	**4.0**	1.5
3.9	1.5	site 23	**2.6**	1.1

In 2021 there were no instances of formation of Mn_3O_4 from the Mn(II) state but there was still the oxidation of Mn^{2+} to MnO_2, releasing two protons per electron, and this took place on site 5, which had the largest shift in the mean pH between the two years.

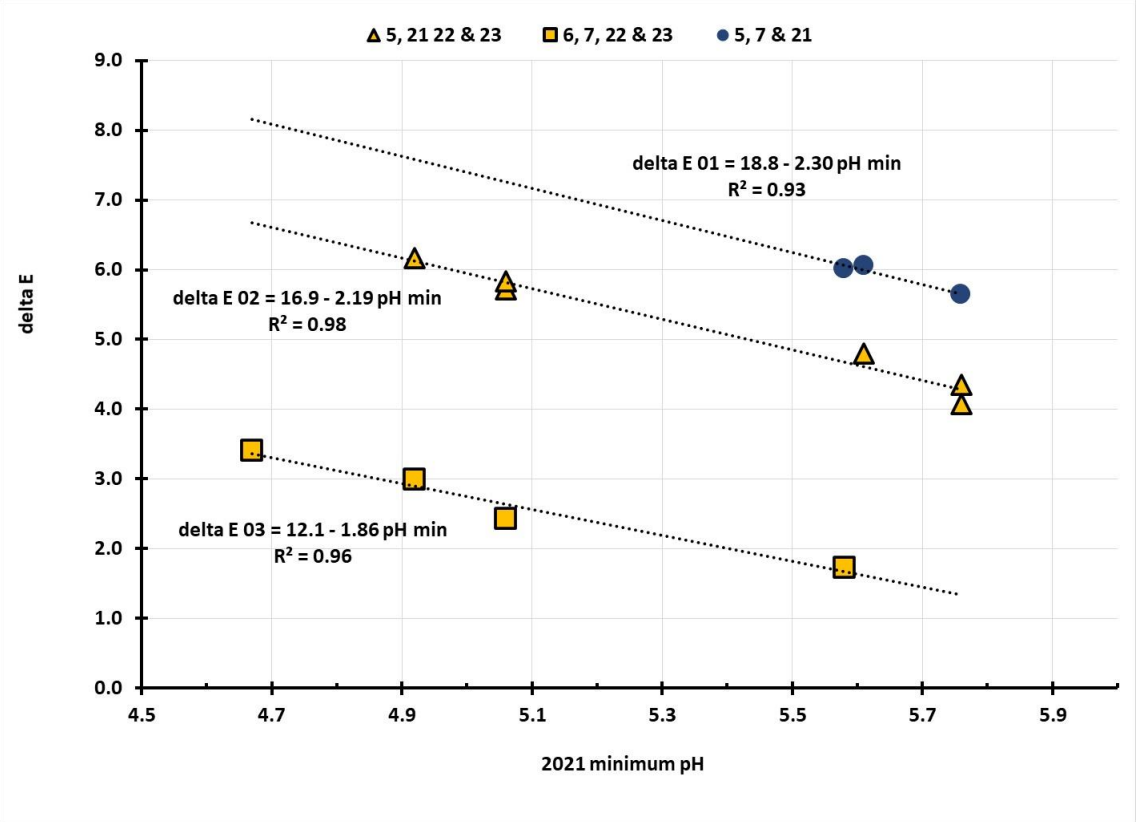

Figure 32: Plot of the contrast difference 2021 versus minimum pH

Data on how ΔE responded to the minimum pH (i.e., the most corrosive microenvironment) in 2020 had indicated that $\{^{\delta E}/_{pH\ min}\}$ increased by approximately 4 per unit increased acidity, since as the rock surfaces become more acidic the repatination processes (from natural weathering) of a thin layer of precipitated mineralisation is removed. The data in 2021 shown in Figure 32 shows that the slope $\{^{\delta E}/_{pH\ min}\}$ was 2.1 ± 0.2 increase in colour contrast per unit of increased acidity i.e., the response of

the colour contrast to increases in the minimum pH is about half that it was in 2020. This reduced sensitivity to changes in the pH are due to the higher mean values of the pH in 2021 and the associated increased buffering capacity of the surface.

Inspection of the data plots in Figure 32 indicates that for the ΔE_{03} vs. pH_{min} the four data points, which include areas on the granophyre rock site no 6, are getting close to the limit of human eye in perceiving a just noticeable fade, at the value of ΔE of 2.0, which illustrates the value of using the chromameter for monitoring the colour difference between the background and engraved areas. For casual visitors to the Burrup rock art monitoring sites, who rely solely on their recall of colour contrasts from years' past, this data provides a salutary lesson about capacity to discern colour change with the naked eye.

It is useful to get an idea of the challenges associated with measuring the colour contrasts on the reference points on the different rocks. This is illustrated by the two granophyre rocks at site 6 and at site 5. The data in Table 22 shows that the ΔE values vary from 1.1 to 3.4 (Figure 33) and at site 5 (Burrup Road) the contrast is seen (Figure 34) to be much stronger with ΔE values varying from 4.1 to 7.9, which in 2020 at spot 3 had a value of 5.8. It is possible that the cause of the lower colour contrast at site 6 (Water Tanks) is due to the much older engraving on that location than the cormorant at site 5, off up the hill from Burrup Road.

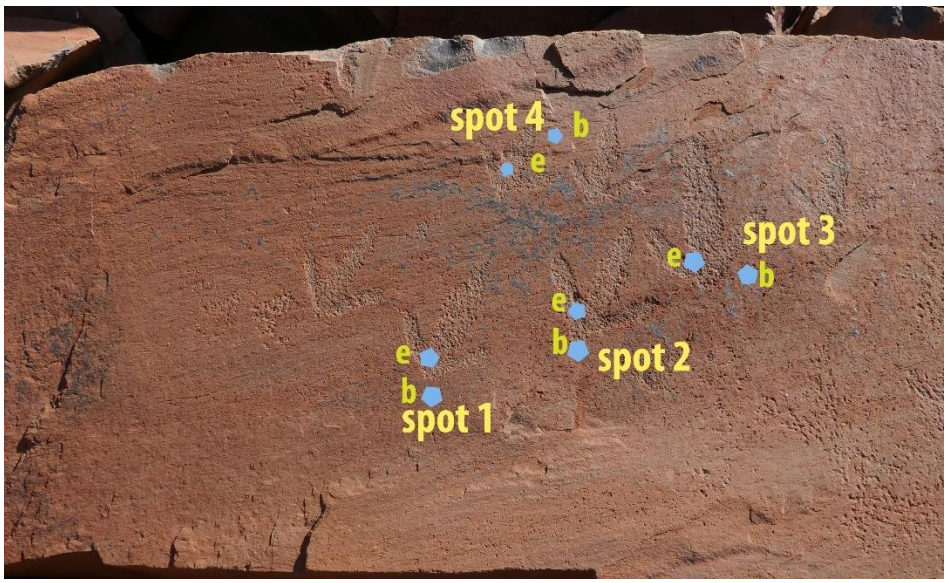

Figure 33: Reference rock no 6 (Water Tanks) with spot locations showing background and engraved areas

Another significant difference between the "fresh" 2020 data and the "salty" 2021 is that there are no clear trends of ΔE with the mean pH of the site values. For sites 5, 7 and 21 there was no systematic change in the colour contrast with the mean pH. For sites 4 and 22 (as a group) and for sites 6 & 23 (a second group) the colour contrast increased as the mean pH moved towards more acidic values. However, there it is not possible to compare these data points and their dependence on pH as there were only two sites in each group. Put in the simplest of terms, a much more readily interpretable set of ΔE colour change data, as measured by the Minolta Chromameter, is obtained when the colour differences are plotted as a function of the minimum pH observed for each site.

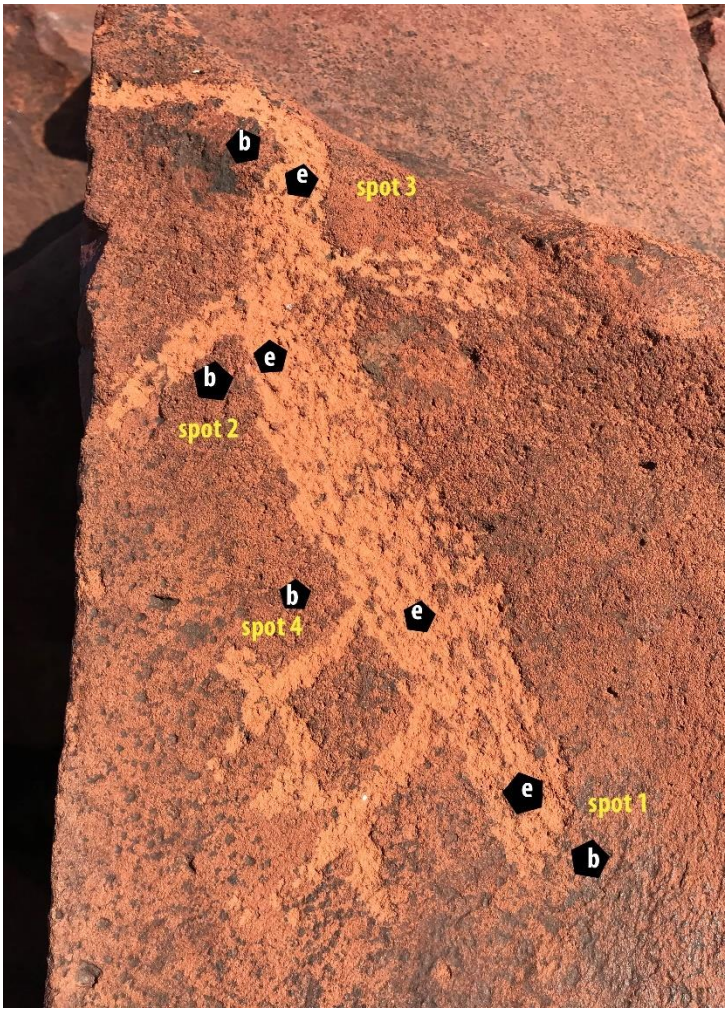

Figure 34: Site 5 showing locations of the sampling points at Burrup Road

Colour differences across the sites between the years 2017-2021.

A series of calculations by Microfading Australia (Ford 2021) were conducted in which the data was statistically analysed to see if the mean colour differences between the background and the engraving at each reference point on the monitored rocks was meaningful. If the answer was YES, then that data set is reported in Table 25 in **BOLD BLACK** font. If the differences are not statistically reliable, then they are listed in **BOLD RED**. The statistical method considers the internal variability in the sets of ten (10) colour measurements taken on each reference point. The microtopography of the rocks naturally makes collection of reproducible spectra a challenge, but one that does clearly reap dividends, as shown by the previous discussion where the colour difference values of ΔE have been shown to correlate well with the minimum pH recorded on each site. When the cut off parameter of the mean colour difference divided by the ΔE value was above 0.5 or in that region, the commentary in Table 24 is noted **BOLD GREEN** as ~, for being possibly yes and possibly no. The basic diagram of colour space is shown in Figure 35 below.

It has not been previously alluded to, but it is instructive to review not just the individual colour measurements on each of the seven monitored sites, but to look at it as a whole grouping of data across the Burrup. The results are summarised in Table 24 and the $L^*a^*b^*$ values for all the background readings show a remarkable uniformity across the sites, with the standard deviations of the readings amounting to 12 ± 1% of the three variables. This is significant in that it shows the common colour of the parent weathered rock surfaces. When the engraved values are compared the

is a greater scatter of data, particularly in the a* {red (+) to green (-)}, where the standard deviation of the mean amounts to 19% of the value. It should be noted that this is not an inherent problem for the group since the engravings are believed to be significantly different in their age and so the reformation of the original iron-rich patina would be expected to show measurable colour differences. It is also interesting to note that the b* values {yellow(+) to blue(-)} show a similar extent of variation as in the background values.

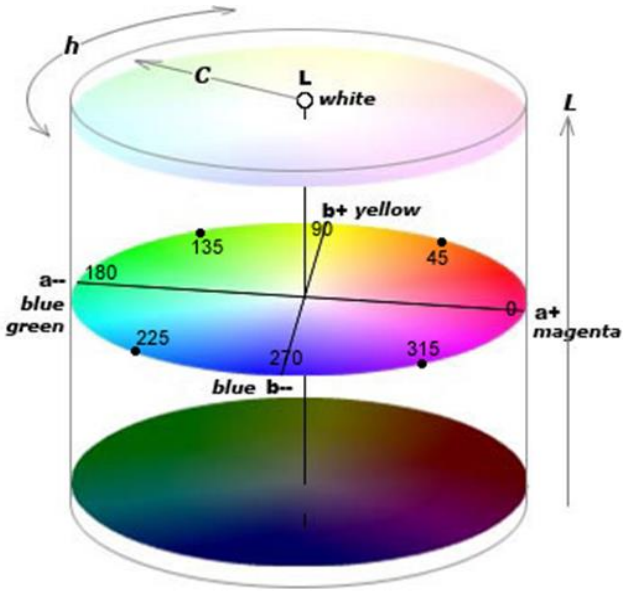

L* a* b* and L C h are different ways of describing the same shift in CIELAB space

L* = Lightness
a* = red-green axis
b* = yellow-blue axis

C = vividness (chroma)
h = hue angle anticlockwise from red (0)

Figure 35: CIELAB space diagram illustrating the values of L*, a* and b*

Table 24: Statistical analysis of the 2021 colour measurements

	L*	a*	b*
Background - mean	**32.07**	**12.65**	**14.43**
std dev mean background	3.38	1.57	1.71
Engraving	**35.89**	**14.15**	**18.32**
stdev engraving	2.95	2.72	2.41
Δ (Engraving-Background)	**3.82**	**1.50**	**3.89**
stdev delta	2.31	1.89	2.52

When the formula for calculating the colour difference between the background and engraved 28 monitoring points in the Yara survey cohort, the mean colour difference is 5.7, which is well above the average value of 2.0 for the human eye to be able to discern colour changes.

Having access to all the colour data for the Yara historic monitoring period from 2017-2021, Australian Microfading noted that there was a remarkable uniformity within each site for the $L^*a^*b^*$ data sets from the engraved surfaces, with the exception being the information collected in 2020. For this year alone there was a diminution of the L^* or lightness values by 3.24 so the rocks in that year appeared to be darker. In a similar fashion, the a^* values were less red by 4.26 and the b^* values were also less yellow with a fall in the chroma of 6.46, so the net colour change of ΔE had a value of 5.05. At present there is no specific position as to why the 2020 year was so different, but it is tempting to reflect that the general cleanliness of the rock surfaces, with minimal buffering from sea salts, had created a different microenvironment and that the microflora had responded. The loss of redness and the lowering of the yellowness all indicates that there was removal of some of the repatination layer.

The most reliable measure of the changes in the colour of the rocks with the mean surface pH was found for the combination of the pH data collected in 2018, which had the Deep Gorge site (no 7) as an outlier due to the accidental release of ammonia. This site was still an outlier when the mean pH data from 2020 was considered and the odd solution behaviour of site 22, which appeared to have been subject to a heavy localised rainfall event (it is quite near to the coast) made the site lie below the regression line associated with the four other sites, so this relationship was dismissed as the pH did not seem to be representative. A plot of the way in which ΔE changed with the mean pH is seen in Figure 36 and in equation 64.

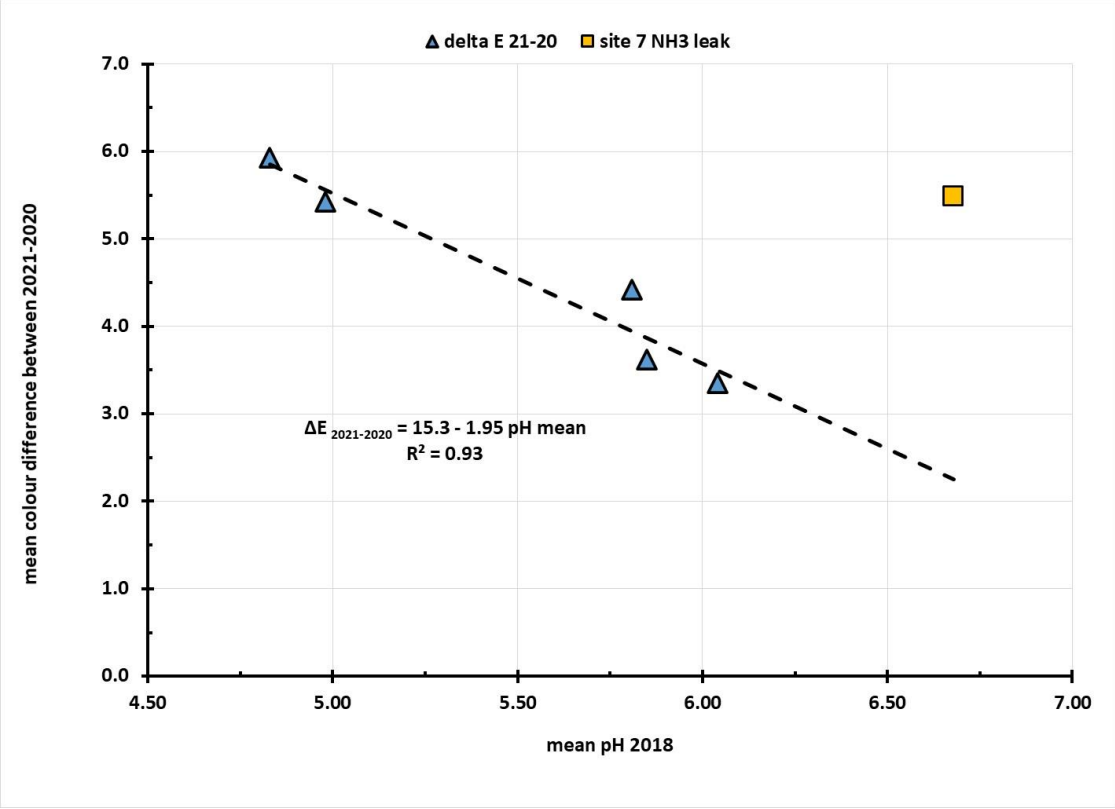

Figure 36: Plot of ΔE for the colour difference between 2021 and 2020 vs mean pH $_{2018}$

$$\Delta E_{2020\text{-}2019} = 15.3 - {}^{mean}\,pH_{2018} \quad \text{.....(64)}$$

The regression analysis for equation 60 had a high R^2 value of 0.93 and the intercept value was 15.3 ± 1.7 (an 11%) variation and the pH dependence $\{^{\Delta E\ 2020\text{-}2019}/_{pH\ mean\ 2018)}\}$ was -1.95 ± 0.30 or a variation of 15%. Thus, the colour contrast decreases linearly as the mean pH increases. This observation is

consistent with the way in which the redox processes change with seasonal variations in microbial activity, which controls the pH along with the deposition of sea salts from prevailing winds.

Table 25: Colour differences (background and engraving) and significance 2017-2021

site	ΔE00 2017	ΔE00 2018	ΔE00 2019	ΔE00 2020	ΔE00 2021
S5 spot1	**5.83**	**5.31**	**4.84**	**4**	**4.08**
S5 spot2	**6.7**	**5.81**	**6.66**	**5.77**	**5.64**
S5 spot3	**7.61**	4.81	**9.86**	**6.38**	**7.90**
S5 spot4	**4.15**	**6.45**	**5.78**	**2.14**	**4.35**
S6 spot1	**1.51**	**2.04**	**1.91**	**0.72**	**1.94**
S6 spot2	**1.02**	**2.15**	**0.88**	**0.71**	**2.16**
S6 spot3	**1.86**	**2.8**	**1.54**	**0.45**	**1.07**
S6 spot4	**3.1**	**2.33**	**1.83**	**1.3**	**3.41**
S7 spot1	**6.75**	**2.51**	**3.56**	**4.25**	**6.01**
S7 spot2	**3.01**	**2.47**	**3.3**	**3.44**	**1.73**
S7 spot3	**3.84**	**5.67**	**5.14**	**1.53**	**2.38**
S7 spot4	**4.6**	5.5	**4.4**	1.53	**8.94**
S21 spot1	**5.34**	**7.99**	**4.62**	**4.27**	**5.92**
S21 spot2	3	**3.86**	5.44	**4.12**	**4.80**
S21 spot3	**5.23**	4.15	3.97	**4.76**	**2.36**
S21 spot4	**3.88**	6.63	5.53	**6.33**	**6.21**
S22 spot1	**6.63**	2.56	1.02	**6.49**	**4.68**
S22 spot2	**2.43**	1.16	2.8	**3.07**	**5.83**
S22 spot3	**4.61**	3.12	2.71	**4.15**	**2.43**
S22 spot4	**3.91**	3.98	5.32	**3.63**	**5.72**
S23 spot1	**2.17**	3.47	**3.32**	**2.01**	**2.93**
S23 spot2	**2.52**	**4.31**	**1.34**	**3.34**	**2.99**
S23 spot3	**6.97**	**3.48**	**1.05**	**3.39**	**3.60**
S23 spot4	**2.65**	3.28	**4.65**	**1.43**	**6.17**
S4 spot 1			**3.56**	**5.28**	**3.41**
S 4 spot 2			**1.91**	**0.3**	**3.00**
S 4 spot 3			**1.6**	**2.96**	**3.18**
S 4 spot 4			**1.04**	**2.33**	**2.73**

Conclusion

The analysis of the relationship between the pH and the concentrations of metal ions reporting to the wash solutions enabled the mechanism controlling the release of manganese containing minerals to the wash solutions to be determined. From a combination of the Pourbaix diagrams and the regression analyses of the voltages at zero pH, the formal redox voltages of the electroactive species are normally obtained. An unexpected feature of the analyses in 2021 was the presence of measurable amounts of iron on five of the seven sites, only sites 7 and 22 (both gabbro rocks) had no soluble iron on them. The mean concentration of iron was $1.30 \pm 0.03 \times 10^{-7}$ M which was higher than the mean concentration of manganese which was 0.35×10^{-7} M, which is contrary to normal expectations of manganese ions being more soluble than the corresponding iron moieties. Owing to the much higher salt concentrations on the rock surfaces than following cyclone Damien, the changed order of solubilities can be understood in terms of the chemistry of the formation of chloride complexes with iron compared with manganese.

One of the limitations of Pourbaix style analysis of the relationship between the redox potential and the pH is that it is not possible to distinguish between the -59 mV. Slope associated with one proton released per electron. This is summarised below for the general transition metal oxidative hydrolysis shown in equation 65, since the reaction is the same for both manganese and iron viz.,

$$M(OH)^{+} + H_2O \rightarrow M(OH)_2^{+} + H^{+} + e^{-1} \quad \text{..... (65)}$$

Similarly, the slope alone is not sufficient to differentiate between the general reaction shown in equation 66,

$$2\ M(OH)^{+} + H_2O \rightarrow M(OH)_2^{+} + M(OH)^{2+} + H^{+} + 2e^{-1} \quad \text{..... (66)}$$

A provisional assignment as to the dominant redox couple is shown in the Pourbaix data for 2021 shown in Appendix I. The engraved cormorant image on site 5, above the Burrup Road near the Yara air monitoring station adjacent to the Pluto main flare tower, showed the $\{E_h/pH\}$ slope of -120 mV/ pH which is associated with oxidation of Mn^{2+} to Mn(IV) and precipitation of MnO_2 as the black-brown manganese dioxide.

In the aftermath of cyclone Damien in 2020 there were several sites where the Pourbaix diagrams showed mixed electrochemical pathways i.e., there were two slopes found for the measurements on the E_h-pH diagram. By way of contrast in 2021, when there had been a long period of no major rain event, each site showed uniform electrochemical behaviour and showed a single unifying reaction scheme. Based on the intercept voltages at the extrapolated pH=0 points, it was possible to assign the -60 mV/pH slope to iron on site 4 and at the Climbing Man split rock. For sites 21, 22 and 23, which had the same -60 mV slope, the electrochemically active species appears to be dominated by manganese. The same analysis approach was able to assign all the $\{E_h/pH\}$ -30 mV/pH slopes to manganese couples.

The increased alkalinity on the monitoring rock art sites has reduced the dependence of calcium solubility, based on the p{Ca} vs pH plots, to give a fractional slope i.e., less than a 1:1 dependence in line with the systematic trends observed in the years where the impact of rain events has been largely absent. The practical implications of these observations are simply that the bulk of the calcium in the washings is coming from the adsorbed sea salts. Where local variations occur this is due to the higher calcium content of the parent gabbro rocks, which have been previously analysed by CSIRO. Major effect of the increased sea salts are interdependent, for not only does this affect the mean pH it also reduces the impact of microflora consumption of the adsorbed nitrate ions. Because sea salts contain calcium carbonate, the production of acidic metabolites results in converting some of the carbonate to bicarbonate ions (i.e., CO_3^{2-} to HCO_3^{-}) which is part of a weak acid-weak base conjugate system it buffers the changes in acidity. This is because the pH is proportional to the logarithm of the ratio of carbonate to bicarbonate. The data from 2020 showed a mixed impact of rains from cyclone Damien, but in several cases the freshly washed rock surfaces

acted as ideal sites for conversion, through adsorption, of anthropogenic NO_x to nitrate ions which then became available to the microflora. With little or no sea salts to act as a pH buffer, a relatively small concentration of acidic metabolites has a major impact on the way in which the mean pH changes with soluble nitrate concentration.

The data on mean pH showed that the rock adjacent to the Climbing Man had the same value as in 2020 at 6.1 and it had previously been the least acidic of the eight monitored sites. After a year of little to no rain events the pH at site 6 (the Water Tanks) was slightly more alkaline by 0.23 pH due to increased salt concentration on the rock, but this is well within the range of surface pH on each measured rock, as was site 7 (Deep Gorge) which had an increase from pH 5.8 to 6.2, which is likely a reflection of the increased buffering capacity of the salty rock surface. Sites 21, 22 and 23 showed δpH values of +0.84 ± 0.08 or a seven-fold decrease in surface acidity. The decrease in acidity for sites 4, 5 and the Climbing Man had a mean δpH of +1.4 ± 0.21 or a 25-fold decrease in acidity. In summary, at the end of September 2021 all the rock art sites were at the natural pH of weathered gabbro and granophyre rock in the Burrup (pH 5.7 ± 0.2) such as at sites 21, 22 and 23, or in a much more alkaline condition, owing to the accumulation of sea salts on the rock surfaces. The other sites had a mean ^{2021}pH value of 6.2 ± 0.2 compared with the same locations in 2020 where the mean ^{2020}pH was 4.8 ±0.4 or a general reduction in acidity by twenty-five times.

For the six sites examined in and around the Yara facility there is a decreased amount of sulphate ions than cannot be explained by the increased presence of sea salts. The mean sulphate in 2017 was 5.2 ± 3.0 which decreased to a value of 1.2 ± 0.7 ppm in 2018. However, in 2019 it had increased to 4.5 ± 64 ppm before falling to 1.5 ± 2.2 ppm in 2020. Following the dry spell, the mean value for the moderate concentration of sulphate in the washing solutions for 2021 was 0.8 ± 0.4 ppm, which is not statistically significantly different to the average data from the previous year. The mean sulphate level at sites 6a, 21b and 23b was 15.0 ± 5.5 ppm but these sites are also associated with high chloride ion concentration due to deposition of sea salts, as was borne out by the normal range of $\{^{Cl}/_{SO4}\}$ of 2.9 ± 0.8. Sites 4b and 22a washing rocks had lower sulphate and hence higher chloride to sulphate ratios and these rocks had microfossils on their surface, which would have lowered the sulphate available to the wash solutions.

Analysis of the variations of the minimum pH in 2021 and the sulphate concentration showed up complex behaviour that was due to the creation of different microenvironments on the rock surfaces due to the accumulation of sea salts. For the high chloride sites the ^{minimum} pH $_{2021\ salty}$ fell by 0.088 per ppm of sulphate while for the less salty areas, where there is reduced buffer capacity on the rock surface, the ^{minimum} pH $_{2021\ normal}$ fell by 0.46 per ppm $\{SO_4^{2-}]$ with values of ≤ 2.2 ppm sulphate. For nine rock surfaces, the mean pH of 5.68 ± 0.08 at a mean $[SO_4^{2-}]$ concentration of 1.0 ± 0.6 ppm where the pH is essentially independent of the sulphate ion concentration. This indicates that for sites 4, 5, 7, 21a, and the Climbing Man reference rocks may not be colonised by organisms that can metabolise sulphate ions. A hallmark of the 2021 measurements has been the ability to discern systematic differences in how granophyre and gabbro rocks respond to nitrate ion concentration in the wash solutions. The plots of mean pH for the granophyre rocks had a more alkaline intercept $^{zero\ NO3}$ pH $_{mean}$ of 6.75 ± 0.12 compared with the gabbro rocks at 6.41 ± 0.04, which is statistically significant. It was also found that the nitrate dependence (slope) of the rocks in 2021 were much smaller than in 2020 because of the higher sea salt surface concentrations and their associated increased pH buffer capacity. When the $\{pH/_{[NO3]}\}$ slopes are the same it is a strong indication that the degradation mechanisms are the same. For the granophyre rocks in 2021 the slope of the mean pH with nitrate was -1.94 ± 0.28 which is experimentally the same as for the gabbro rocks at -1.92 ± 0.19 which effectively confirms that the principal form of degradation relates to acid assisted dissolution of microscopic amounts of the rock patina.

Over the last five years of monitoring the colour contrast between the background and engraved areas on four spots on each of the seven monitoring rocks for Yara Pilbara Nitrates has provided a unique insight into the biodynamic nature of the rock surfaces in the Burrup. By using the same chromameter as the CSIRO had done for their extended colour monitoring there is now an unquestionable rich archive of colour information which can now be better interpreted, since the impact of the changes in redox reactions on the surfaces, changes in the surface pH measurements and in the chloride ion surface activity are now much better understood.

During the general discussions regarding the electrochemistry of the seven colour monitored sites in 2021 it became clear that there was much more uniformity on the rocks themselves, since a single electrochemical process defined the connections between E_h and pH. This in turn meant that there was greater consistency in colour measurement in 2021 compared with 2020. By the time the 2021 measurements were conducted 11 months later, most of the rock surfaces had received very little natural washing and so they were characterised by much more alkaline surfaces, due to the increased buffering capacity because of the higher sea salt concentration. In 2021 there were no instances of formation of the dark coloured Mn_3O_4 but there was still the oxidation to MnO_2 which took place on site 5, which had the largest shift in the mean pH between the two years.

For 2021 the changes in ΔE with the minimum pH were half the sensitivity as in 2020 as the slope $\{^{\delta E}/_{pH\ min}\}$ was - 2.1 ± 0.2 increase in colour contrast per pH unit change and this is due to the increased buffer capacity on the salty rock surfaces which minimise the chemical alteration of the repatination layers on the engravings. Evidence of the direct connection between ΔE and the mean pH was not unequivocal which is why our focus has been on the changes in the minimum pH and how it has affected the colour contrast. The historic colour data for all the background readings show a remarkable uniformity across the sites, with the standard deviations of the readings amounting to 12 ± 1% of the three colour parameters. This is significant in that it shows the common colour of the parent weathered rock surfaces. When the engraved values are compared there is a greater scatter of data, particularly in the a^* {red (+) to green (-)}, where the standard deviation of the mean amounts to 19% of the value. It should be noted that this is not an inherent problem since the engravings are believed to be significantly different in their age and so the reformation of the original iron-rich patina would be expected to show measurable colour differences. It is also interesting to note that the b^* values {yellow(+) to blue(-)} show a similar extent of variation as in the background values.

During the review of all the data collected over the past five years on the way in which the colour changed with pH, the best response of ΔE to the mean pH was found by looking at the colour changes between 2021 and 2020 and acidity data collected in 2018, which had the Deep Gorge site (no 7) as an outlier due to the accidental release of ammonia. Thus, the colour contrast decreases linearly as the mean pH increases – this observation is consistent with the way in which the redox processes change with seasonal variations in microbial activity, which controls the pH along with the deposition of sea salts from prevailing winds. The conclusion of this colour study is that the work should continue so that the dynamics of changing colour contrast can be determined. There is unequivocal evidence that the changes in colour contrast are affected by the changes in the mean and in the minimum pH observed on the rock art sites at the reference positions. For casual visitors to the Burrup rock art monitoring sites, who rely solely on their recall of colour contrasts from years' past, this data provides a salutary lesson about capacity to discern colour change with the naked eye.

END of REPORT

REFERENCES

Arthur, I, 2004, Report on the identification of yeasts and moulds from rocks in the Burrup, Mycology, Department of Health Laboratories, Western Australia, Unpublished report, 1-6.

Burford, E P, Fomina, M and Gadd, G M, 2003, Fungal involvement in bioweathering and biotransformation of rocks and minerals, *Mineralogical Magazine* 67 (6), 1127–1155.

Clark, R, 2004, Identification of surface minerals in weathered rocks from the Burrup peninsula, unpublished report to the Burrup Rock Art Monitoring Scientific Committee, November 2004, 1–18.

Ford, B., 2020, Report to Heritage Conservation Solutions on analysis of colour differences between engraved and background sites in the Burrup, unpublished report November 2020, pp 1-24.

Fox, D., 2020, Statistical Modelling of Rock Surface pH Data from the Burrup Peninsula, Western Australia 2003 – 2019, Unpublished report to GBH Solutions by Environmetrics Australia, September 2020 p 1-93.

Gadd, G M, 2004, 'Mycotransformation of organic and inorganic substrates', *Mycologist*, 18 (2), 60–70.

Lau, D, Ramanaidou E., Furman, S., Hacket A., Caccetta M., Wells M., McDonald B., 2008, *Burrup Peninsula Aboriginal Petroglyphs: Colour Change and Spectral Mineralogy 2004–2007*, CSIRO Materials Science and Engineering, Clayton, Victoria, Australia, 1-44.

King, J, 2003, Report on the identification of bacteria, yeasts, moulds, and fungi in the Burrup, unpublished report, Department of Agriculture, Perth, Western Australia.

MacLeod, I D, 2003, A micro-environmental study of rocks on the Burrup: effects of water and nutrients on pH and microflora, unpublished report, Western Australian Museum, 1–66.

MacLeod, I.D., 2017, Report to the Murujuga Aboriginal Corporation; Impact of industrial emissions on the pH and Eh of engraved rock art on the Burrup peninsula", Unpublished report of Heritage Conservation Solutions, pp 1-17.

MacLeod, I.D, 2019, Collecting in-situ data in the field and laboratory: artefact corrosion and conservation, Japanese Institute for Anatolian Archaeology, http://www.jiaa-kaman.org/en/consymposium_2019.html, pp 1-18

Markley T., Wells M., Ramanaidou E., Lau D., and Alexander D., 2015, Burrup Peninsula Aboriginal Petroglyphs: Colour Change & Spectral Mineralogy 2004–2014, CSIRO report, EP1410003 October 2015, 1-189.

North, N A, 1982, Corrosion products on marine iron, *Studies in Conservation* 27, 75–83.

Pourbaix, M., 1974, *Atlas of electrochemical equilibria in aqueous solutions,* National Association of Corrosion Engineers, Houston, Texas USA pp 1-644.

Ramanaidou E., Walton G., and Winchester D., 2017, Extreme Weathering Experiments on the Burrup Peninsula / Murujuga Weathered gabbros and granophyres, EP172193 May 2017, 1-62.

APPENDIX I: MacLeod publications on rock art conservation

Refereed journal articles

Haydock, P. & MacLeod, I.D. (1987) “The use of micro-meteorological studies as an aid to the conservation of aboriginal rock art”. *ICOM Committee for Conservation*, Sydney, September 1987, p 1149-1153.

MacLeod, I.D. (1991) "Microclimate modelling in old museum buildings". *Historic Environment-Conservation in Context: Artefact and Place,* 8(1&2), p 37-41

Ford, B., MacLeod, I.D., and Haydock, P., (1994) "Rock art pigments from the Kimberley region of Western Australia: identification of the minerals and conversion mechanisms", *Studies in Conservation* 39, p 57-69.

MacLeod, I.D., Haydock, P., Tulloch, D. & Ford, B. (1995) "Effects of microbiological activity on the conservation of aboriginal rock art" *AICCM Bulletin* 21(1), 3-10

MacLeod, I.D., Haydock, P & Charton, E., (1996) "Avian guano and its effects on the preservation of rock paintings" *Preservation of Rock Art 1995 AURA Occasional Papers 9*, Ed. Andrew Thorn & Jacques Brunet p 60-64.

MacLeod, I.D., Haydock P. and Ford, B. (1997) “Conservation Management of West Kimberley Rock Art: Microclimate studies and Decay Mechanisms” *Kimberley Society Occasional Paper No 1. Aboriginal Rock Art of the Kimberley* Ed K.F. Kenneally, M.R. Lewis., M. Donaldson and C. Clement, Kimberley Society Inc, Perth, Western Australia. pp 65-69.

MacLeod, I.D., (2000) “Rock art conservation and management: the past, present and future options”, *Reviews in Conservation,* 1, pp 32-45.

MacLeod, I.D., and Haydock, P., (2002) “Microclimate modelling for prediction of environmental conditions within rock art shelters”, Preprints for ICOM-CC Triennial Meeting, Rio de Janeiro, Brazil September 2002, Vol II, 571-577.

MacLeod, I.D. (2005) “The effects of moisture, micronutrient supplies and microbiological activity on the surface pH of rocks in the Burrup peninsula”, Preprints for ICOM-CC Triennial Meeting, Den Haag, The Netherlands, September 2005, Vol II 386-393

Black, J., MacLeod I.D., and Smith, B., (2017), Theoretical effects of industrial emissions on colour change at rock art sites on Burrup Peninsula, *J Archaeological Science*: *Reports* 12, 457-462.

MacLeod, I.D., and W. Fish. (2021) Determining decay mechanisms on engraved rock art sites using pH, chloride ion and redox measurements with an assessment of the impact of cyclones, sea salt and nitrate ions on acidity. In *Transcending Boundaries: Integrated Approaches to Conservation. ICOM-CC 19th Triennial Conference Preprints, Beijing, 17–21 May 2021,* ed. J. Bridgland. Paris: International Council of Museums.

Unpublished Reports

MacLeod, I.D., Haydock, P. and Ford, B (1991)- "Conservation research into the preservation of rock paintings in the West Kimberley region of Western Australia", Report to the Western Australian Heritage Committee, pp 1-89

MacLeod, I.D., Haydock, P & Charton, E., (1992) "The effects of avian guano on the preservation at *Walga Rock*". Report to the Australian Institute of Aboriginal and Torres Strait Islanders Studies, Canberra, pp 1-45.

MacLeod, I.D., Haydock, P and Ford, B (1994) *Conservation research into the preservation of rock paintings in the West Kimberley Region of Western Australia: Wet Season Report*. Report to the Heritage Council of WA, March 1994, pp-143.

MacLeod, I.D. and Haydock, P., (1996) *Research into the Conservation or rock paintings in the West Kimberley: Microclimate data analysis* Report to AIATSIS, May 1996, pp 1-132

Ford, B., Officer, K. and MacLeod, I.D., (1999) *A study of lichen invasion of Nursery Swamp II, Aboriginal Rock Art Site, Namadji National Park, Australian Capital Territory, Final Report May 1999*, Australian Capital Territory National Parks Association, Canberra 1999, pp. 1-28.

MacLeod, I.D., (2003) "The microenvironment of rocks on the Burrup: analysis of the relationships between nutrient supplies, surface pH and microflora – preliminary report, Report to the Minister of Culture and the Arts, pp 1-55.

MacLeod, I.D., (2017), "Report to the Murujuga Aboriginal Corporation; Impact of industrial emissions on the pH and Eh of engraved rock art on the Burrup peninsula", pp 1-17.

MacLeod, I.D., (2018), "Conservation analysis at the Yara monitoring sites 2018"

MacLeod, I.D., (2019) "Conservation analysis at the Yara monitoring sites 2019"

MacLeod, I.D., (2020 "Conservation analysis at the Yara monitoring sites 2020"

APPENDIX II: Electrochemical analysis of reactions from Pourbaix diagrams 2021

$Mn^{2+} + 2\ H_2O \rightarrow MnO_2 + 4\ H^+ + 2\ e^-$, slope - 120 mV/pH

Location	Pourbaix slope	Intercept	R^2	Metal
Site 5	-0.120 ± 0.008	1.142 ± 0.104	0.96	**Mn**

$Mn^{+2} + 2H_2O \rightarrow Mn(OH)_2^{2+} + 2\ H^+ + 2\ e^-$ slope - 60 mV/pH

Site 4	-0.060 ± 0.002	0.774 ± 0.020	0.98	**Fe**
Site 21	-0.056 ± 0.003	0.719 ±0.021	0.98	**Mn**
Site 22	-0.055 ±0.006	0.706 ±0.035	0.96	**Mn**
Site 23	-0.058 ± 0.005	0.708 ± 0.029	0.99	**Mn**
Climbing Man	-0.057 ± 0.004	0.753 ± 0.047	0.94	**Fe**

$Mn(OH)^+ + H_2O \rightarrow Mn(OH)_2^{2+} + H^+ + 2\ e^-$ slope - 30 mV/pH

Site 6	-0.026 ± 0.002	0.545 ± 0.012	0.96	**Mn**
Site 7	-0.035 ± 0.003	0.608 ± 0.009	0.98	**Mn**
Site 21	-0.034 ± 0.004	0.564 ± 0.023	0.98	**Mn**

APPENDIX III: Chemical analysis of the wash solutions from the CSIRO monitoring sites September 2021.

Concentrations are in mg/L other than electrical conductivity which is in mS/m

Client Id	Site 4a	Site 4b	Site 5a	Site 5b	Site 6a	Site 6b	Site 7a	Site 7b
Al	0.0130		0.0120	0.0120				
As								
B	0.0080				0.0050			
Ba	0.0038	0.0008	0.0021	0.0017	0.0010	0.0010	0.0012	0.0009
Ca	**0.70**	**0.30**	**0.40**	**1.30**	**0.40**	**0.30**	**0.60**	**0.30**
Cd								
Cl	**3.30**	**2.80**	**4.60**	**1.50**	**49.00**	**2.50**	**2.70**	**1.40**
Co	0.0001							
Cr								
Cu	0.0005	0.0006	0.0012	0.0012	0.0047	0.0022	0.0015	0.0020
ECond	**2.40**	**2.00**	**2.50**	**2.00**	**23.20**	**1.40**	**1.70**	**1.20**
Fe	0.0160		0.0150	0.0050				
K	**0.30**	**0.40**	**0.40**	**0.40**	**0.60**	**0.10**	**0.70**	**0.30**
Mg	**0.10**		**0.20**		**0.20**	**0.10**	**0.20**	
Mn	0.0100	0.0014	0.0016	0.0016	0.0016	0.0014	0.0024	0.0017
NO_2								
NO_3	**0.50**	**0.14**	**0.30**	**0.13**	**1.10**	**0.08**	**0.22**	**0.18**
Na	**3.00**	**0.80**	**2.70**	**1.50**	**1.90**	**1.10**	**2.00**	**0.80**
Ni								
Oxalate								
Pb		0.0001			0.0001			
S	**0.60**		**0.30**	**0.20**	**0.30**	**0.20**	**0.40**	**0.10**
SO_4	**1.30**	**0.30**	**1.00**	**0.80**	**20.20**	**1.10**	**1.00**	**0.60**
V	0.0001							
Zn	0.0060	0.0050	0.0040	0.0030	0.0110	0.0030	0.0060	0.0040
Ni								
Oxalate								
Pb			0.0002		0.0005	0.0001		
S	**0.2**	**0.1**	**0.5**	**0.2**	**0.7**	**0.4**	**0.5**	**1.1**
SO4	**0.2**	**0.3**	**0.5**	**0.4**	**1.5**	**0.8**	**1.2**	**2.8**
V		0.0002						
Zn	0.013	0.011	0.028	0.01	0.012	0.012	0.008	0.007

Appendix III continued

Client Id	Site 21a	Site 21b	Site 22a	Site 22b	Site 23a	Site 23b	Climbing man, a	Climbing man b
Al							0.0110	
As								
B		0.0070	0.0050				0.0060	
Ba	0.0029	0.0088	0.0013	0.0016	0.0012	0.0018	0.0027	0.0011
Ca	1	2.2	0.3	0.5	0.4	0.8	1.4	0.4
Cd								
Cl	5.4	32	1.3	1.3	1.3	51	9.3	0.8
Co								
Cr								
Cu	0.0014	0.0008	0.0075	0.0029	0.0091	0.0067	0.0044	0.0027
ECond	2.9	13.8	1	0.9	1	24.2	4.7	0.7
Fe	0.0060	0.0050				0.0050	0.0060	
K	0.4	0.6	1.7	0.5	0.3	0.4	0.5	0.5
Mg	0.2	1.1	0.2	0.1		0.2	0.2	
Mn	0.0021	0.0020	0.0019	0.0019	0.0027	0.0030	0.0033	0.0014
NO_2								
NO_3	0.22	0.27	0.26	0.23		0.65	0.31	0.08
Na	4.3	9.1	2.3	1.6	1.6	2.3	1.5	1.2
Ni								
Oxalate								
Pb								0.0001
S	0.9	2.5	0.1	0.3	0.3	0.4	0.4	0.1
SO_4	1.6	9.3	0.2	0.4	0.5	15.6	2.2	0.3
V								
Zn	0.0090	0.0110	0.0260	0.0060	0.0100	0.0090	0.0040	0.0070

APPENDIX IV: Surface pH measurements 2003-2004 in the Burrup

	17-Jun-03	28-Aug-03	23-Feb-04
Location		pH	pH
Dampier W1		5.03	4.90
Dampier W1		4.85	4.82
Dampier W1		5.14	4.77
Dampier W1		5.13	5.18
Dampier W1		4.61	4.47
Dampier W1		4.95	4.59
Dampier W1		4.37	4.80
Dampier W1		4.10	4.88
Dampier W1		4.49	4.76
Dampier W1			4.71
Dampier W1			4.64
Dampier W1 mean		**4.74**	**4.77**
Dampier W1 st. dev.		**0.37**	**0.19**

Dampier W2		4.30	4.41	
Dampier W2		4.34	4.32	
Dampier W2		4.96	4.61	
Dampier W2		4.80	4.63	
Dampier W2		4.86	4.40	
Dampier W2		4.72	4.27	
Dampier W2		4.78	4.16	
Dampier W2		4.94	4.78	
Dampier W2		4.82	4.50	
Dampier W2		4.33	4.68	
Dampier W2 mean		**4.7**	**4.5**	
Dampier W2 st. dev.		**0.3**	**0.2**	
				27-Feb-04
Burrup SW1		4.70	4.43	4.63
Burrup SW1		4.69	5.33	4.76
Burrup SW1		4.94	4.52	4.97
Burrup SW1		4.49	4.89	4.79
Burrup SW1		4.96	4.68	4.78
Burrup SW1		4.16	4.60	4.92
Burrup SW1		4.42	4.92	3.89
Burrup SW1		4.66	4.98	4.94
Burrup SW1			5.01	4.94
Burrup SW1			4.65	5.02
Burrup SW1 mean		**4.63**	**4.80**	**4.76**
Burrup SW1 st. dev.		**0.27**	**0.27**	**0.33**

27-Feb-04

Burrup SW2		5.39	4.88	4.87
Burrup SW2		5.32	4.49	4.68
Burrup SW2		4.64	4.82	4.83
Burrup SW2		4.44	4.83	5.16
Burrup SW2		4.60	4.72	4.83
Burrup SW2		5.43	4.69	4.80
Burrup SW2		5.00	4.65	4.98
Burrup SW2		5.40	4.72	5.00
Burrup SW2		5.38	4.63	5.19
Burrup SW2			4.59	5.24
Burrup SW2 mean		**5.07**	**4.70**	**4.96**
Burrup SW2 st. dev.		**0.40**	**0.12**	**0.19**

27-Feb-04

King Bay 1		4.89	4.61	4.91
King Bay 1		4.37	5.34	4.73
King Bay 1		5.27	5.15	4.46
King Bay 1		4.98	4.69	4.79
King Bay 1		5.41	4.39	4.64
King Bay 1		5.30	4.70	4.98
King Bay 1		4.85	5.02	4.80
King Bay 1		4.94	5.00	4.87
King Bay 1		6.04	5.12	4.93
King Bay 1		5.33	4.93	4.88
King Bay 1		5.36		4.91
King Bay 1		5.17		
King Bay 1 mean		**5.16**	**4.90**	**4.81**
King Bay 1 st. dev.		**0.41**	**0.29**	**0.15**

27-Feb-04

King Bay 2		5.27	4.85	4.61
King Bay 2		5.24	4.89	4.75
King Bay 2		5.27	4.89	4.80
King Bay 2		5.41	4.74	4.95
King Bay 2		5.31	5.29	4.86
King Bay 2		4.59	4.77	5.30
King Bay 2		4.88	5.22	4.78
King Bay 2		3.82	5.41	4.76
King Bay 2		5.05	4.93	5.02
King Bay 2		4.91	5.17	3.54
King Bay 2		5.48		5.02
King Bay 2		5.44		4.78
King Bay 2 mean		**5.06**	**5.02**	**4.76**
King Bay 2 st. dev.		**0.5**	**0.2**	**0.42**

Withnell Bay		5.15	5.02
Withnell Bay		4.95	5.01

Withnell Bay		5.18	5.27
Withnell Bay		4.95	4.97
Withnell Bay		4.98	4.73
Withnell Bay		4.79	5.19
Withnell Bay		4.47	4.82
Withnell Bay		4.70	5.50
Withnell Bay		4.85	5.04
Withnell Bay		4.46	4.55
Withnell Bay		4.91	5.01
Withnell Bay mean		**4.85**	**5.01**
Withnell Bay st. dev.		**0.24**	**0.26**

Withnell Bay 2		4.92	5.76
Withnell Bay 2		4.73	5.28
Withnell Bay 2		4.26	5.52
Withnell Bay 2		4.45	5.52
Withnell Bay 2		4.89	5.24
Withnell Bay 2		4.97	5.26
Withnell Bay 2		4.78	5.44
Withnell Bay 2		4.83	5.26
Withnell Bay 2		4.93	5.50
Withnell Bay 2		4.66	5.68
Withnell Bay 2 mean		**4.74**	**5.45**
Withnell Bay 2 st. dev.		**0.23**	**0.18**

North Withnell Bay 1		4.48	4.66
North Withnell Bay 1		4.59	4.80
North Withnell Bay 1		4.17	4.85
North Withnell Bay 1		4.86	4.62
North Withnell Bay 1		4.37	4.66
North Withnell Bay 1		4.54	4.75
North Withnell Bay 1		4.29	4.76
North Withnell Bay 1		4.51	5.03
North Withnell Bay 1			5.16
North Withnell Bay 1			4.89
North Withnell Bay 1			
North Withnell Bay 1			
North Withnell Bay 1			
North Withnell Bay 1 mean		**4.48**	**4.82**
North Withnell Bay 1 st. dev.		**0.21**	**0.17**

North Withnell Bay 2		4.77	4.65
North Withnell Bay 2		4.74	3.45 soil area

North Withnell Bay 2		4.66	4.87
North Withnell Bay 2		4.31	4.79
North Withnell Bay 2		4.83	5.09
North Withnell Bay 2		4.65	4.76
North Withnell Bay 2		4.58	4.88
North Withnell Bay 2		4.50	5.13
North Withnell Bay 2		4.63	5.05
North Withnell Bay 2			4.73
North Withnell Bay 2			5.03
North Withnell Bay 2 mean, no soil		4.63	4.90
North Withnell Bay 2 st. dev. no soil		0.15	0.17
North Withnell Bay 2 mean			**4.9**
North Withnell Bay 2 st. dev.			**0.2**

Deep Gorge 1		4.91	4.71
Deep Gorge 1		4.54	5.06
Deep Gorge 1		4.87	4.74
Deep Gorge 1		4.72	4.87
Deep Gorge 1		4.89	4.90
Deep Gorge 1		4.10	5.14
Deep Gorge 1		4.32	4.98
Deep Gorge 1		4.06	4.80
Deep Gorge 1		5.19	4.80
Deep Gorge 1		4.17	5.07
Deep Gorge 1		4.14	
Deep Gorge 1 mean		**4.54**	**4.91**
Deep Gorge 1 st. dev.		**0.40**	**0.15**

Deep Gorge 2		4.59	4.69
Deep Gorge 2		4.93	4.97
Deep Gorge 2		4.46	5.45
Deep Gorge 2		4.63	5.31
Deep Gorge 2		4.57	5.20
Deep Gorge 2		4.79	5.04
Deep Gorge 2		4.71	5.16
Deep Gorge 2		4.36	5.12
Deep Gorge 2		4.70	5.31
Deep Gorge 2			3.85
Deep Gorge 2			
Deep Gorge 2 mean		**4.64**	**5.01**
Deep Gorge 2 st. dev.		**0.17**	**0.46**

Deep Gorge 3			5.19
Deep Gorge 3			4.91
Deep Gorge 3			5.06
Deep Gorge 3			4.73
Deep Gorge 3			4.78
Deep Gorge 3			4.91
Deep Gorge 3			5.39
Deep Gorge 3			5.27
Deep Gorge 3			5.23
Deep Gorge 3			5.10
Deep Gorge 3 mean			**5.06**
Deep Gorge 3 st. dev.			**0.22**

Climbing Man Gully 1		5.37	4.96
Climbing Man Gully 1		5.53	4.80
Climbing Man Gully 1		5.39	5.03
Climbing Man Gully 1		4.84	4.78
Climbing Man Gully 1		5.41	4.97
Climbing Man Gully 1		4.83	4.63
Climbing Man Gully 1		4.81	4.93
Climbing Man Gully 1		5.70	5.03
Climbing Man Gully 1		3.04	5.37
Climbing Man Gully 1		5.55	4.22
Climbing Man Gully 1		5.42	5.53
Climbing Man Gully 1		4.62	4.26
Climbing Man Gully 1			4.58
Climbing Man Gully 1 mean		**5.0**	**4.9**
Climbing Man Gully 1 st. dev.		**0.7**	**0.4**
Climbing Man Gully 1 mean (-acid spot)		5.22	
Climbing Man Gully 1 st. dev. (-acid spot)		0.37	

Climbing Man Gully 1-1		5.05	4.92
Climbing Man Gully 1-1		4.85	5.00
Climbing Man Gully 1-1		5.03	3.95
Climbing Man Gully 1-1		5.97	4.45
Climbing Man Gully 1-1		5.78	3.94
Climbing Man Gully 1-1		5.46	3.83
Climbing Man Gully 1-1		5.79	3.97
Climbing Man Gully 1-1		5.45	3.68
Climbing Man Gully 1-1		5.23	4.94
Climbing Man Gully 1-1		5.31	3.85
Climbing Man Gully 1-1 mean		**5.39**	**4.25**
Climbing Man Gully 1-1 st. dev.		**0.37**	**0.52**

June 03 Adjacent to Climbing Man	3.74		4.86

Feb 04 Climbing Man itself	4.31		4.85
Feb 04 Climbing Man itself	4.54		3.91
Feb 04 Climbing Man itself	4.19		3.61
Feb 04 Climbing Man itself	4.1		4.87
Feb 04 Climbing Man itself	4.27		3.75
Feb 04 Climbing Man itself	4.78		4.86
Feb 04 Climbing Man itself	4.55		4.82
Feb 04 Climbing Man itself	3.58		4.68
Feb 04 Climbing Man itself			5.13
Feb 04 Climbing Man itself			4.68
Feb 04 Climbing Man itself mean	**4.23**		**4.55**
Feb 04 Climbing Man itself st. dev.	**0.39**		**0.53**

Climbing Man gully 2B			5.19
Climbing Man gully 2B			5.04
Climbing Man gully 2B			5.23
Climbing Man gully 2B			5.28
Climbing Man gully 2B			5.21
Climbing Man gully 2B			5.06
Climbing Man gully 2B			5.35
Climbing Man gully 2B			5.43
Climbing Man gully 2B			5.29
Climbing Man gully 2B			5.53
Climbing Man gully 2B mean			**5.26**
Climbing Man gully 2B st. dev.			**0.15**

Compound, off site up hill		4.88	3.81
Compound, off site up hill		4.49	5.06
Compound, off site up hill		4.76	4.94
Compound, off site up hill		4.33	4.76
Compound, off site up hill		5.17	5.67
Compound, off site up hill		4.17	4.65
Compound, off site up hill		4.16	3.88
Compound, off site up hill		4.73	3.86
Compound, off site up hill		4.61	4.59
Compound, off site up hill		4.67	4.40
Compound, off site up hill		4.64	
Compound, off site, uphill, mean		**4.60**	**4.56**
Compound, off site, uphill st. dev.		**0.30**	**0.60**

Compound off site, 2			3.85
Compound off site, 2			4.62
Compound off site, 2			3.82
Compound off site, 2			4.66
Compound off site, 2			4.58
Compound off site, 2			4.91
Compound off site, 2			4.51
Compound off site, 2			4.52
Compound off site, 2			4.83
Compound off site, 2			3.94
Compound off site, 2 mean			**4.42**
Compound off site, 2 st. dev.			**0.40**

Rock 3	4.67		4.46
Rock 3	4.76		4.79
Rock 3			4.63
Rock 3			5.03
Rock 3			4.40
Rock 3			4.16
Rock 3			4.71
Rock 3			4.69
Rock 3			4.82
Rock 3			4.54
Rock 3 mean	**4.72**		**4.62**
Rock 3 st. dev.	**0.06**		**0.25**

Rock 86	4.56	4.71	4.98
Rock 86	4.67	4.72	4.95
Rock 86	4.46	4.62	5.09
Rock 86	4.63	5.04	5.08
Rock 86	5.57	4.89	4.86
Rock 86	5.3	4.96	5.10
Rock 86	5.12	5.22	4.90
Rock 86		4.99	4.92
Rock 86		4.96	4.64
Rock 86		5.05	5.21
Rock 86			5.05
Rock 86 mean	**4.90**	**4.92**	**4.98**
Rock 86 st. dev.	**0.43**	**0.18**	**0.15**

Rock 97	5.21		4.87
Rock 97	5.26		5.30
Rock 97	5.74		5.11
Rock 97			5.03
Rock 97			6.06
Rock 97			5.68
Rock 97			5.34
Rock 97			5.41
Rock 97			5.67
Rock 97			5.00
Rock 97 mean	**5.40**		**5.35**
Rock 97 st. dev.	**0.29**		**0.37**

Rock 162	4.92	4.72	4.88
Rock 162	5.87	4.63	4.82
Rock 162	5.29	4.86	4.81
Rock 162		4.73	4.88
Rock 162		4.68	5.21
Rock 162		4.50	5.41
Rock 162		4.54	5.12
Rock 162		4.68	5.14
Rock 162		4.71	5.21
Rock 162			5.06
Rock 162 mean	**5.36**	**4.67**	**5.05**
Rock 162 st. dev.	**0.48**	**0.11**	**0.20**

Rock 938		3.97	5.83
Rock 938		4.38	5.12
Rock 938		4.75	5.06
Rock 938		5.15	4.83
Rock 938		4.87	5.45
Rock 938		4.57	4.56
Rock 938		4.64	5.75
Rock 938		5.20	4.35
Rock 938		4.50	4.47
Rock 938		4.80	3.98
Rock 938		5.00	
Rock 938		4.85	
Rock 938		5.63	
Rock 938		**4.7**	
Rock 938		**5.4**	
Rock 938 mean		**4.82**	**4.94**
Rock 938 st. dev.		**0.41**	**0.61**

Rock 1681	5.63	4.57	4.14
Rock 1681	5.36	4.43	5.18
Rock 1681	5.53	4.38	4.93
Rock 1681	5.59	4.17	4.40
Rock 1681	5.28	4.29	4.88
Rock 1681	5.45	4.43	4.8
Rock 1681	5.40	4.21	4.93
Rock 1681	4.86	4.76	4.73
Rock 1681	5.34	4.32	4.85
Rock 1681	4.90	4.10	4.63
Rock 1681	5.64	4.15	
Rock 1681	5.67	3.92	
Rock 1681	4.74	3.86	
Rock 1681	5.81	3.85	
Rock 1681 mean	**5.37**	**4.25**	**4.75**
Rock 1681 st. dev.	**0.33**	**0.26**	**0.30**

Gidley Island 1			25-Feb-04
Gidley Island 1			10:00
Gidley Island 1			4.45
Gidley Island 1			4.81
Gidley Island 1			5.09
Gidley Island 1			4.96
Gidley Island 1			5.06
Gidley Island 1			4.93
Gidley Island 1			4.86
Gidley Island 1			5.08
Gidley Island 1			4.63
Gidley Island 1 mean			**4.17**
Gidley Island 1 st. dev.			**1.67**

Gidley Island 2			25-Feb-04
Gidley Island 2			10:30
Gidley Island 2			4.73
Gidley Island 2			4.52
Gidley Island 2			4.68
Gidley Island 2			4.67
Gidley Island 2			5.24
Gidley Island 2			4.94
Gidley Island 2			4.65
Gidley Island 2			4.78
Gidley Island 2			4.76
Gidley Island 2			5.00
Gidley Island 2			4.57
Gidley Island 2 mean			**4.78**
Gidley Island 2 st. dev.			**0.21**

Gidley Island 3			25-Feb-04
Gidley Island 3			11:00
Gidley Island 3			4.61
Gidley Island 3			5.54
Gidley Island 3			4.70
Gidley Island 3			5.10
Gidley Island 3			4.50
Gidley Island 3			4.92
Gidley Island 3			5.25
Gidley Island 3			5.26
Gidley Island 3			5.50
Gidley Island 3			4.21
Gidley Island 3 mean			**4.96**
Gidley Island 3 st. dev.			**0.45**

Dolphin Island 1			25-Feb-04
Dolphin Island 1			12:10
Dolphin Island 1			4.93
Dolphin Island 1			4.85
Dolphin Island 1			4.72
Dolphin Island 1			4.63
Dolphin Island 1			4.61
Dolphin Island 1			5.05
Dolphin Island 1			4.86
Dolphin Island 1			4.71
Dolphin Island 1			5.08
Dolphin Island 1			4.95
Dolphin Island 1			4.52
Dolphin Island 1 mean			**4.81**
Dolphin Island 1 st. dev.			**0.19**

Dolphin Island 2			25-Feb-04
Dolphin Island 2			12:35
Dolphin Island 2			5.14
Dolphin Island 2			4.91
Dolphin Island 2			4.89
Dolphin Island 2			3.68
Dolphin Island 2			3.74
Dolphin Island 2			5.04
Dolphin Island 2			4.85
Dolphin Island 2			5.07
Dolphin Island 2			4.79
Dolphin Island 2			5.04
Dolphin Island 2			4.72
Dolphin Island 2			0.54
Dolphin Island 2			
Dolphin Island 2 mean			**4.97**
Dolphin Island 2 st. dev.			**0.12**

Dolphin Island 3			25-Feb-04
Dolphin Island 3			12:55
Dolphin Island 3			5.22
Dolphin Island 3			5.32
Dolphin Island 3			5.15
Dolphin Island 3			5.66
Dolphin Island 3			5.07
Dolphin Island 3			4.65
Dolphin Island 3			3.87
Dolphin Island 3			4.81
Dolphin Island 3			5.25
Dolphin Island 3			5.07
Dolphin Island 3			5.22
Dolphin Island 3 mean			**5.03**
Dolphin Island 3 st. dev.			**0.46**